
# NAVAL POSTGRADUATE SCHOOL

**MONTEREY, CALIFORNIA**

# THESIS

**COMPARATIVE ANALYSES OF MULTI-PULSE PHASE CONTROLLED RECTIFIERS IN CONTINUOUS CONDUCTION MODE WITH A TWO-POLE LC OUTPUT FILTER FOR SURFACE SHIP DC APPLICATIONS**

by

Kurt A. Young

March 2013

| | |
|---|---|
| Thesis Advisor: | Robert W. Ashton |
| Second Reader: | Andrew A. Parker |

**Approved for public release; distribution is unlimited**

THIS PAGE INTENTIONALLY LEFT BLANK

| REPORT DOCUMENTATION PAGE | | | Form Approved OMB No. 0704–0188 |
|---|---|---|---|



| 1. AGENCY USE ONLY *(Leave blank)* | 2. REPORT DATE<br>March 2013 | 3. REPORT TYPE AND DATES COVERED<br>Master's Thesis |
|---|---|---|

| 4. TITLE AND SUBTITLE<br>COMPARATIVE ANALYSES OF MULTI-PULSE PHASE CONTROLLED RECTIFIERS IN CONTINUOUS CONDUCTION MODE WITH A TWO-POLE LC OUTPUT FILTER FOR SURFACE SHIP DC APPLICATIONS | 5. FUNDING NUMBERS |
|---|---|
| 6. AUTHOR(S) Kurt A. Young | |
| 7. PERFORMING ORGANIZATION NAME(S) AND ADDRESS(ES)<br>Naval Postgraduate School<br>Monterey, CA 93943–5000 | 8. PERFORMING ORGANIZATION REPORT NUMBER |
| 9. SPONSORING /MONITORING AGENCY NAME(S) AND ADDRESS(ES)<br>N/A | 10. SPONSORING/MONITORING AGENCY REPORT NUMBER |

**11. SUPPLEMENTARY NOTES** The views expressed in this thesis are those of the author and do not reflect the official policy or position of the Department of Defense or the U.S. Government. IRB Protocol number ___N/A_____.

| 12a. DISTRIBUTION / AVAILABILITY STATEMENT<br>Approved for public release; distribution is unlimited | 12b. DISTRIBUTION CODE<br>A |
|---|---|

**13. ABSTRACT (maximum 200 words)**

The Navy of tomorrow will require a robust and reconfigurable power system capable of supplying power not only to large high power propulsion loads but to growing combat system loads like high power radar and pulse loads such as rail guns and free-electron lasers. A critical component in such a system is the phase controlled rectifier. As such, the issues associated with the inclusion of a power electronics rectifier need to be addressed. These issues include input Alternating Current (AC) interface requirements, the output Direct Current (DC) load profile, and overall stability in the presence of non-linear loads. Understanding these issues and determining the means of assuring compatibility with a Navy all-electric ship is the focus of this thesis.

By using a Simulink® model of a variable parameter load, several multiple-pulse count, high power rectifiers were exercised. The Simulink® results were compared to the linearized small signal transfer function analysis results.

These experiments led to the conclusion that increasing the pulse count and output filtering reduces the input interface current distortion. However, there are tradeoffs in terms of complexity and size of the passive components, and optimization based on source and load specifications is required.

| 14. SUBJECT TERMS Phase Controlled Rectifier, Multiple Pulse Count, Non-Linear Loads | 15. NUMBER OF PAGES<br>145 |
|---|---|
| | 16. PRICE CODE |

| 17. SECURITY CLASSIFICATION OF REPORT | 18. SECURITY CLASSIFICATION OF THIS PAGE | 19. SECURITY CLASSIFICATION OF ABSTRACT | 20. LIMITATION OF ABSTRACT |
|---|---|---|---|
| Unclassified | Unclassified | Unclassified | UU |

NSN 7540–01–280–5500 Standard Form 298 (Rev. 2–89)
Prescribed by ANSI Std. 239–18

THIS PAGE INTENTIONALLY LEFT BLANK

**Approved for public release; distribution is unlimited**

# COMPARATIVE ANALYSES OF MULTI-PULSE PHASE CONTROLLED RECTIFIERS IN CONTINUOUS CONDUCTION MODE WITH A TWO-POLE LC OUTPUT FILTER FOR SURFACE SHIP DC APPLICATIONS

Kurt A. Young
Lieutenant Commander, United States Navy
B.S., University of Wisconsin-Platteville, 2000

Submitted in partial fulfillment of the
requirements for the degree of

**MASTER OF SCIENCE IN ELECTRICAL ENGINEERING**

from the

**NAVAL POSTGRADUATE SCHOOL**
**March 2013**

Author: Kurt A. Young

Approved by: Robert W. Ashton
Thesis Advisor

Andrew A. Parker
Second Reader

R. Clark Robertson
Chair, Department of Electrical and Computer Engineering

THIS PAGE INTENTIONALLY LEFT BLANK

## ABSTRACT

The Navy of tomorrow will require a robust and reconfigurable power system capable of supplying power not only to large high power propulsion loads but to growing combat system loads like high power radar and pulse loads such as rail guns and free-electron lasers. A critical component in such a system is the phase controlled rectifier. As such, the issues associated with the inclusion of a power electronics rectifier need to be addressed. These issues include input Alternating Current (AC) interface requirements, the output Direct Current (DC) load profile, and overall stability in the presence of non-linear loads. Understanding these issues and determining the means of assuring compatibility with a Navy all-electric ship is the focus of this thesis.

By using a Simulink® model of a variable parameter load, several multiple-pulse count, high power rectifiers were exercised. The Simulink® results were compared to the linearized small signal transfer function analysis results.

These experiments led to the conclusion that increasing the pulse count and output filtering reduces the input interface current distortion. However, there are tradeoffs in terms of complexity and size of the passive components, and optimization based on source and load specifications is required.

THIS PAGE INTENTIONALLY LEFT BLANK

# TABLE OF CONTENTS

THIS PAGE INTENTIONALLY LEFT BLANK

# LIST OF FIGURES

THIS PAGE INTENTIONALLY LEFT BLANK

# LIST OF TABLES

THIS PAGE INTENTIONALLY LEFT BLANK

# LIST OF ACRONYMS AND ABBREVIATIONS

| | |
|---|---|
| AC | Alternating Current |
| CCM | Continuous Conduction Mode |
| DC | Direct Current |
| *LC* | Inductor-Capacitor |
| RMS | Root Mean Square |
| SCR | Silicon Controlled Rectifier |
| THD | Total Harmonic Distortion |

THIS PAGE INTENTIONALLY LEFT BLANK

# EXECUTIVE SUMMARY

The Navy of tomorrow will require a robust and reconfigurable power system capable of supplying power not only to large high power propulsion loads but to growing combat system loads like high power radar and pulse loads such as rail guns and free-electron lasers. A critical component in such a system is the phase controlled rectifier. As such, the issues associated with the inclusion of a power electronics rectifier need to be addressed. These issues include input Alternating Current (AC) interface requirements, the output Direct Current (DC) load profile, and overall stability in the presence of non-linear loads. Understanding these issues and determining the means of assuring compatibility with a Navy all-electric ship is the focus of this thesis.

The objective of this thesis was to investigate differences between multi-pulse phase controlled rectifiers in continuous conduction mode (CCM) with a two-pole inductor-capacitor (*LC*) output filter. A 6-pulse phase controlled rectifier with a two-pole *LC* output filter is shown in Figure 1. This circuit is the basic building block module for higher pulse count systems as it is easily stackable.

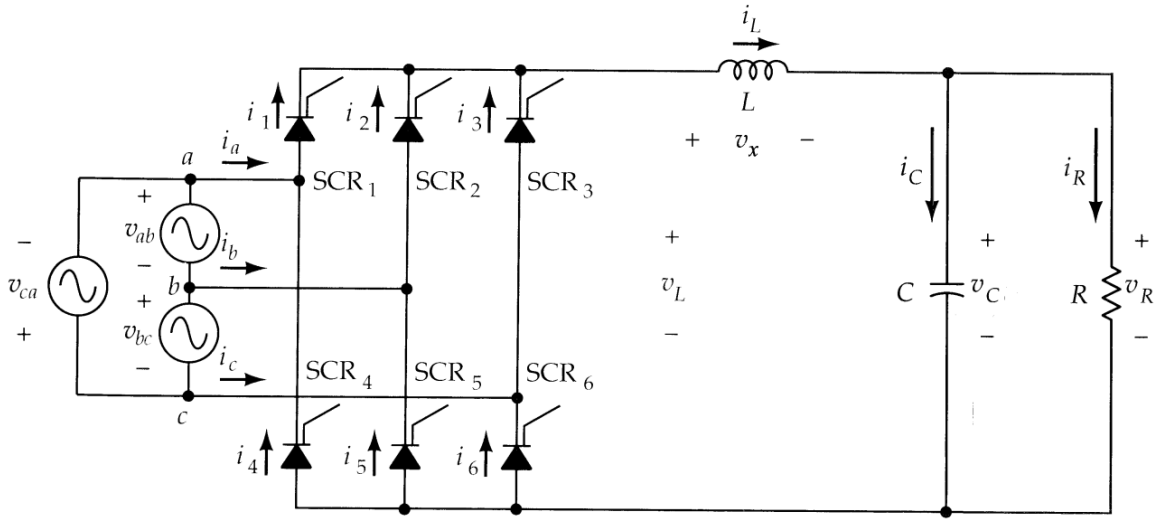


Figure 1. Circuit diagram of a controlled three-phase rectifier with a two-pole *LC* output filter. From [1].

The key differences that were evaluated between these multi-pulse controlled rectifiers were the critical inductance $L_{crit}$ (the inductance which is required to maintain the rectifier in CCM), the peak-to-peak ripple voltage as a percentage of the average output voltage $\%V_{C(pp/avg)}$ (also commonly known as the DC output voltage ripple), and the total harmonic distortion in phase A of the line current $\%THD_i$ .

The determination of $L_{crit}$ was made by applying standard circuit analysis techniques, first to the 6-pulse controlled rectifier circuit of Figure 1, and then by extending the analysis to a p-pulse controlled rectifier. A plot of $L_{crit}$ versus the firing angle $\alpha$ is shown for a 6-, 12-, 18-, 24-, and 96-pulse controlled rectifier in Figure 2. From Figure 2, it is clear that $L_{crit}$ is lower for higher pulse count controlled rectifiers than for lower pulse

count controlled rectifiers; the reduction in $L_{crit}$ is reduced by successively increasing pulse count.

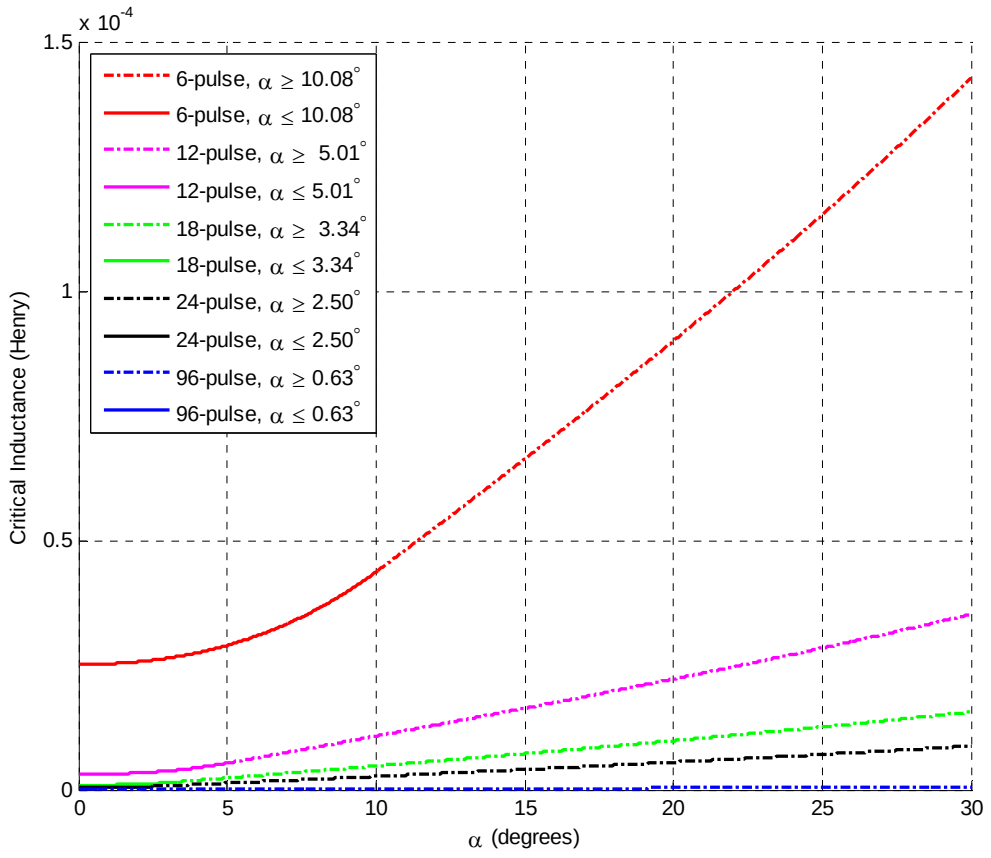


Figure 2. Critical inductance plot for controlled p-pulse rectifiers with unity resistance operating at 60 Hz.

The determination of $\%V_{C(pp/avg)}$ was also made by applying standard circuit analysis techniques to the 6-pulse controlled rectifier circuit of Figure 1 and extrapolating the results to a p-pulse controlled rectifier. However, slight approximations were introduced in the impedance of the load and the determination of the capacitor peak-to-peak ripple voltage. A plot of $\%V_{C(pp/avg)}$ versus the firing

angle $\alpha$ is shown for a 6-, 12-, 18-, 24-, and 96-pulse controlled rectifier in Figure 3. From Figure 3, it is clear that $\%V_{C(pp/avg)}$ is lower for higher pulse count controlled rectifiers than for lower pulse count controlled rectifiers; the reduction in $\%V_{C(pp/avg)}$ is dramatically reduced by successively increasing pulse count.

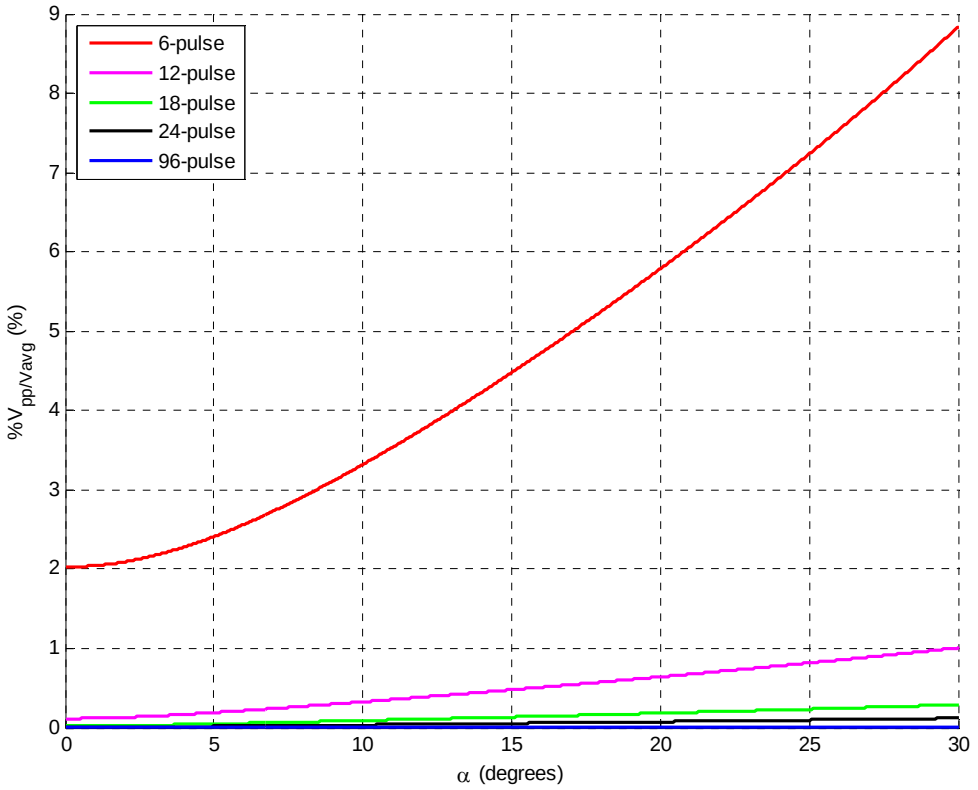


Figure 3. Capacitor peak-to-peak ripple voltage as a percentage of the average output voltage for a 6-, 12-, 18-, 24-, and 96-pulse controlled rectifier with a two-pole *LC* output filter.

The calculation of $\%THD_i$ was performed via simulation using Simulink® on four p-pulse controlled rectifiers with the same predefined passive components. A plot of $\%THD_i$

versus the firing angle $\alpha$ for the simulated 6-, 12-, 18-, and 24-pulse controlled rectifiers is shown in Figure 4. From Figure 4, it is clear that $\%THD_i$ is lower for higher pulse count controlled rectifiers than for lower pulse count controlled rectifiers; the reduction in $\%THD_i$ is greatly reduced by successively increasing pulse count.

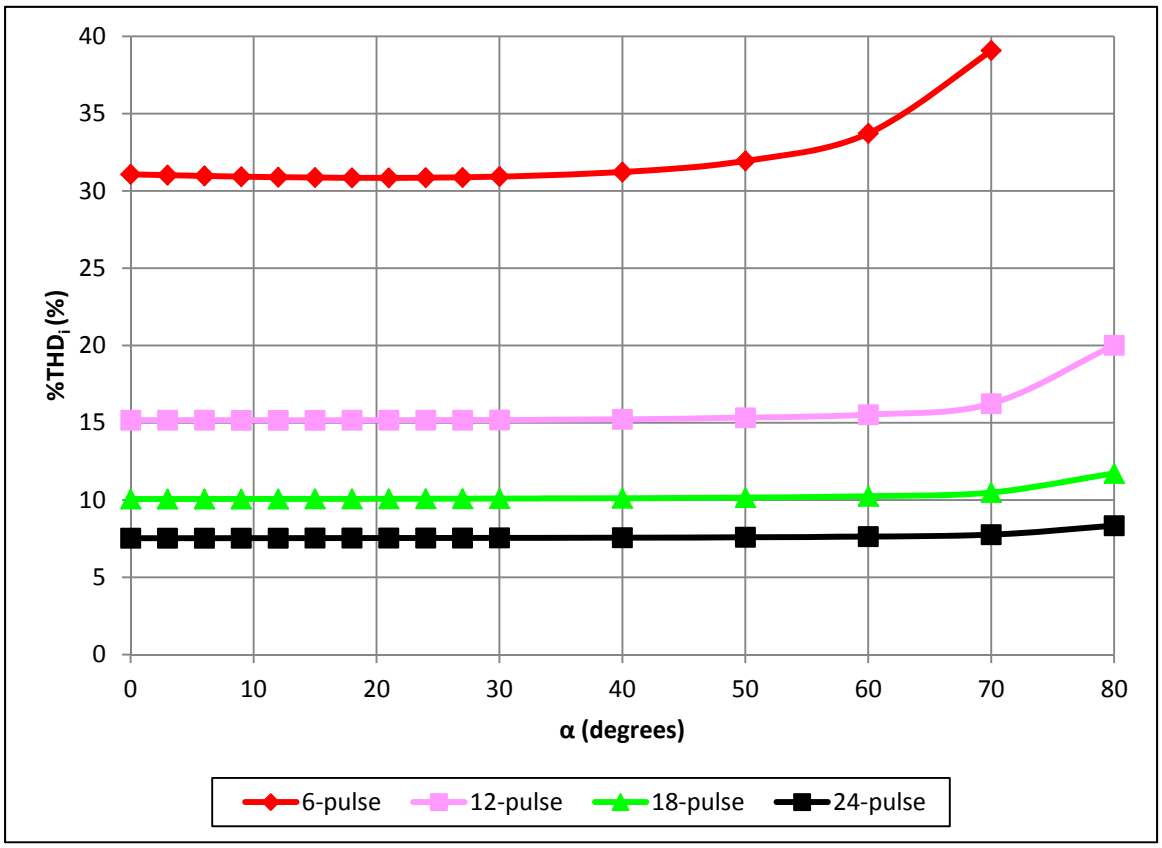


Figure 4. Percent total harmonic distortion in $i_{ap}$ versus $\alpha$ for p–pulse controlled rectifiers with a two-pole *LC* output filter.

All of these results led to the main conclusion that increasing the pulse count is beneficial in that it reduces $L_{crit}$, $\%V_{C(pp/avg)}$, and $\%THD_i$. However, in reality, tradeoffs must be considered in terms of pulse count versus complexity and size of the power electronic and passive components.

## LIST OF REFERENCES

[1] R. W. Ashton, Notes for EC3150 (Solid State Power Conversion), Naval Postgraduate School, unpublished, 2012.

# ACKNOWLEDGMENTS

Without a doubt, this thesis is one of the most difficult undertakings I have ever accomplished in my life. While the work was my own, I could never have hoped to have completed it without the help of many people. First, I would like to thank my thesis advisor, Dr. Robert Ashton. He presented me with a thesis topic the likes of which I had worked on as an undergraduate student, but never fully understood nor could get to completely function properly. Undaunted, I accepted this project, inspired and hungry to discover and learn every detail about it that I could in my short time at Naval Postgraduate School (even so, I am sure I only scratched the surface). His help in finding many of the errors I had made in the countless derivations and equations presented in this thesis was invaluable. Also, I would like to thank Mr. Andrew Parker for his role as a second reader of this work.

I would like to thank my wife, Carolyn, and my children, Anthony and Ashley, for understanding and enduring the sacrifice this project has caused. Additionally, I always appreciated the encouragement and pride in me from my mother- and father-in-law, Sue and Tom Scaffidi (God rest his soul), and my mom, Eugenia Cray.

I could not have done this without the friendship and camaraderie from some of the fine people I have met here who I hope to stay in touch with and remain friends with for the rest of my life, especially John Krbec and Karma and Aida Simons and Ryan, Nikki, and Gwyneth Kelly. I also wish to express my thanks and extend fair winds and

following seas to Ben and Michelle Pimentel, Tim Policar, Will Fleming, Jennifer Sanders, Kaylene and Brandon Carter, Ashley and Carson McAbbe, and Alex, Julie, and Nathan Rios.

Finally, I would like to thank the Engineering Duty Officer (EDO) community for selecting me for lateral transfer and believing that I was a worthwhile investment in light of having already received one Navy-funded master’s degree. The EDO community prides itself on being the technical leaders of the Navy and therefore requires that its members obtain technical master’s degrees from NPS or the Massachusetts Institute of Technology. To you I say mission accomplished, and I will not let you down!

# I. INTRODUCTION

## A. BACKGROUND

A multi-pulse phase controlled rectifier is a type of alternating current (AC) to direct current (DC) converter. This means that it takes an AC voltage source (typically a sinusoid) and changes it into a DC voltage. In reality, the output will be a higher frequency AC waveform with a greatly reduced peak-to-peak voltage that has an average DC value. The term multi-pulse usually applies to three-phase systems and has to do with the fact that there are multiple arch-shaped pulses corresponding to the peak regions of all of the different phase combinations of the source voltages that are seen by the rectifying circuit elements. By using transformers to create phase shifts in the source voltages and connecting these rectifiers together in different fashions, rectifiers with very high pulse counts can be made. A controlled rectifier means that the DC output voltage can be controlled or adjusted in value, whereas an uncontrolled rectifier will produce a fixed DC output.

A recent and growing trend toward an all-electric ship and the development of integrated power systems has caused the role of these types of rectifiers to become even more important. Due to the ever-increasing shipboard power requirements to support such items as rail-guns, free-electron lasers, high power radars, and electromagnetic aircraft launch systems, the Navy has a tremendous need for rugged and reliable high power conversion modules in the megawatt range [1].

In addition to the problem of how to meet all of the power demands caused by these new types of loads is the fact that the power electronics (the phase controlled rectifiers) supplying these loads are non-linear. Non-linear loads produce unwanted harmonic distortion as a by-product which can negatively affect all directly connected electrical equipment. The phase controlled rectifiers must be capable of keeping the produced harmonics to an acceptable level [2].

## B. OBJECTIVES

The differences between multi-pulse phase controlled rectifiers in continuous conduction mode (CCM) with a two-pole inductor-capacitor (*LC*) output filter are investigated in this research. The differences that are specifically investigated are how the critical inductance, DC output voltage ripple, and total harmonic distortion (THD) are affected by having differing pulse counts.

## C. RELATED/PREVIOUS WORK

In [3] and [4], many of the equations for the critical inductance of a 6-pulse controlled rectifier with a two-pole *LC* output filter are developed and presented. However, they do not develop equations beyond those for a 6-pulse converter. Similarly, the discussion regarding DC output voltage ripple was limited to that of a 6-pulse converter in [3] and [4]. However, there has been much work and literature presented on the reduction of THD by increasing pulse count. In [5], a 24-pulse count rectifier topology is achieved from a single three-phase source using a novel interconnection of conventional single and three-phase

transformers to effectively produce four three-phase systems. In [6], an 18-pulse rectifier based on using a differential delta autotransformer to achieve the necessary phase shifts is presented for aerospace applications. In [7], a pulse doubling technique for a 36-pulse converter is accomplished via two paralleled 18-pulse converters using a delta/polygon-connected transformer. In order to double the number of pulses from 36 to 72, a tapped interphase transformer with two additional diodes is added at the output of the rectifier. In [8], the same authors present a similar pulse doubling technique in a 12-pulse converter which uses two paralleled 6-pulse converters connected through a star-wired transformer. A tapped interphase reactor is connected at the output to double the pulses from 12 to 24. An interesting design is presented in [9] by way of a parallel-connected controlled 18-pulse rectifier. Under reduced loading conditions, the firing angle increases, which results in higher THD and lower system efficiency. To combat this effect, the authors propose a dynamic control scheme which involves simultaneous and/or selective control of the firing angle and converter pulse count. For pulse count control, an appropriate 6-pulse rectifier or pair of 6-pulse rectifiers is disabled or enabled depending on the current loading.

## D. THESIS ORGANIZATION

Background material on single-phase rectifiers, starting with uncontrolled diode rectifiers and concluding with controlled rectifiers, is provided in Chapter II. Critical inductance calculations are developed, first for a 6-pulse controlled rectifier, then for a p-pulse controlled

rectifier, in Chapter III. The expressions and equations for the DC output voltage ripple, are developed in Chapter IV, first for a p-pulse controlled rectifier with a purely resistive load, then for a p-pulse controlled rectifier with a two-pole *LC* output filter. The general concepts of harmonics and THD are presented in Chapter V, as well as how they can be reduced by increasing pulse count. Simulink® simulations of a 6-, 12-, 18-, and 24-pulse controlled rectifier with a two-pole *LC* output filter are provided in Chapter VI. Conclusions and recommendations for future work are discussed in Chapter VII.

# II. SINGLE-PHASE RECTIFIERS

## A. UNCONTROLLED SINGLE-PHASE RECTIFIERS

### 1. Uncontrolled Single-Phase Half-Wave Rectifier

Before being able to fully discuss what a multi-pulse phase controlled rectifier in CCM with a two-pole *LC* output filter is, it is useful to begin with a far simpler rectifier circuit commonly known as a half-wave rectifier. One such half-wave rectifier circuit is illustrated in Figure 1, where a sinusoidal voltage source is applied to a resistive load through an ideal diode. The diode behaves like a check-valve, only allowing positive AC current to pass through to the resistor. During the negative portion of the source voltage waveform, the diode blocks the current flow, resulting in no voltage drop across the load. Profiles of the source voltage, load voltage, and current are shown in Figure 2. From Figure 2, it is clear how the circuit of Figure 1 earned its common name, due to half of the source voltage input waveform being applied to the resistive load [3], [4].

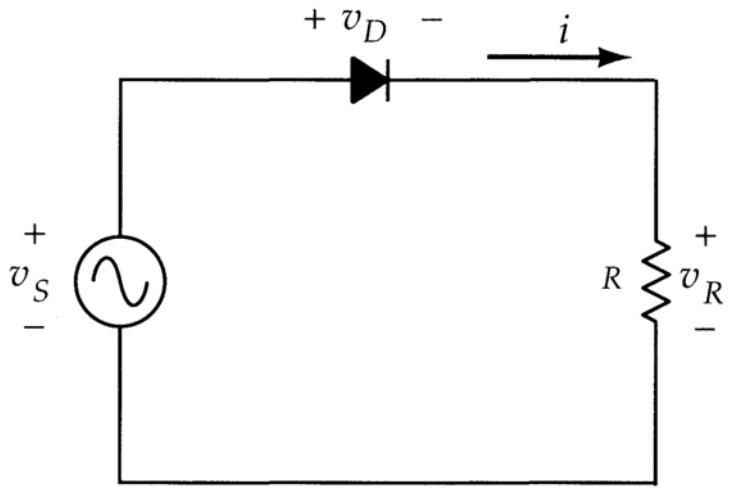


Figure 1. Uncontrolled half-wave rectifier circuit with an ideal diode and a resistive load. From [3].

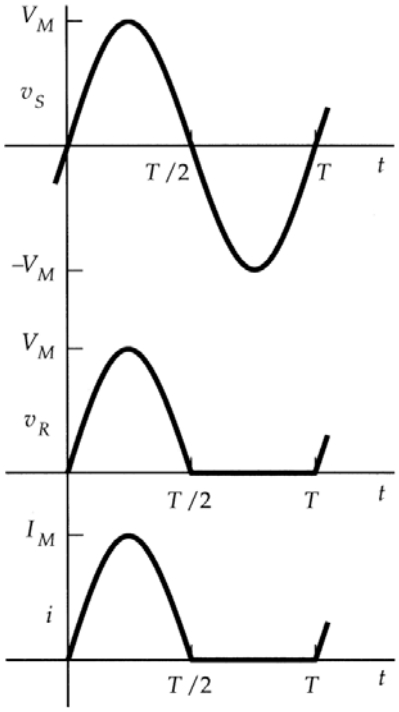


Figure 2. Source voltage, resistor voltage, and current waveform profiles for an uncontrolled half-wave rectifier circuit. From [3].

## 2. Uncontrolled Single-Phase Full-Wave Rectifier

A full-wave rectifier is the next logical progression beyond a half-wave rectifier. A simple full-wave rectifier (sometimes called a bridge rectifier) with a resistive load is shown in Figure 3.

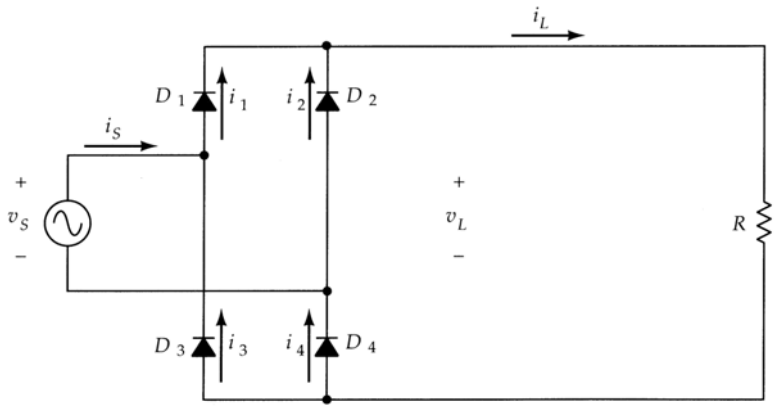


Figure 3. Uncontrolled full-wave rectifier circuit with ideal diodes and a resistive load. From [3].

In this circuit, the source voltage and load resistor are identical to those of the half-wave rectifier case. In the full-wave rectifier circuit, in addition to the current that flows during the positive portion of the source voltage waveform, current will also flow during the negative portion due to the second pair of diodes. During the positive portion of the source voltage waveform, diodes $D_1$ and $D_4$ are "on" while diodes $D_2$ and $D_3$ are "off," and current will flow in the direction indicated by the load current $i_L$. During the negative portion of the source voltage waveform, diodes $D_1$ and $D_4$ are "off" while diodes $D_2$ and $D_3$ are "on." Notice that the direction of $i_L$ is unchanged. This unidirectional current results in a

positive load voltage drop during both the positive and negative portions of the source voltage waveform. Profiles of the source voltage, source current, load voltage, and load current as described are illustrated in Figure 4 [3], [4].

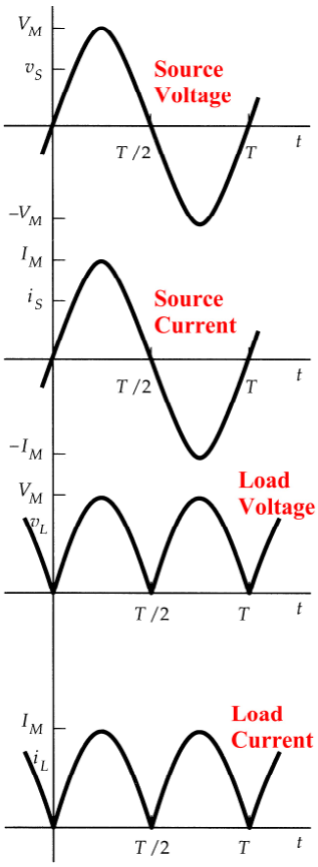


Figure 4. Source voltage, source current, load voltage, and load current waveform profiles for an uncontrolled full-wave rectifier circuit. After [3].

## B. CONTROLLED SINGLE-PHASE RECTIFIERS

### 1. Controlled Single-Phase Half-Wave Rectifier

If the diode from the circuit of Figure 1 is replaced with a thyristor or silicon controlled rectifier (SCR), the result is a controlled half-wave rectifier of Figure 5. The

SCR behaves similarly to a diode in that it is a one-way device and will block current flow in the negative direction. However, it will not conduct in the forward direction until an appropriate trigger signal has been applied to its gate [10]. In reality, there will be a short delay before the SCR turns “on” even after it has been adequately triggered; but for the purpose of explanation, the SCR in Figure 5 can be considered ideal and will turn “on” immediately when triggered. The angle at which the SCR is triggered is commonly called the firing angle $\alpha$. If the SCR in Figure 5 is triggered at time $t_1$, which is equal to $\alpha / \omega$ (where $\omega$ is the radian frequency), the resistor voltage and current will be as shown in Figure 6 [3], [4].

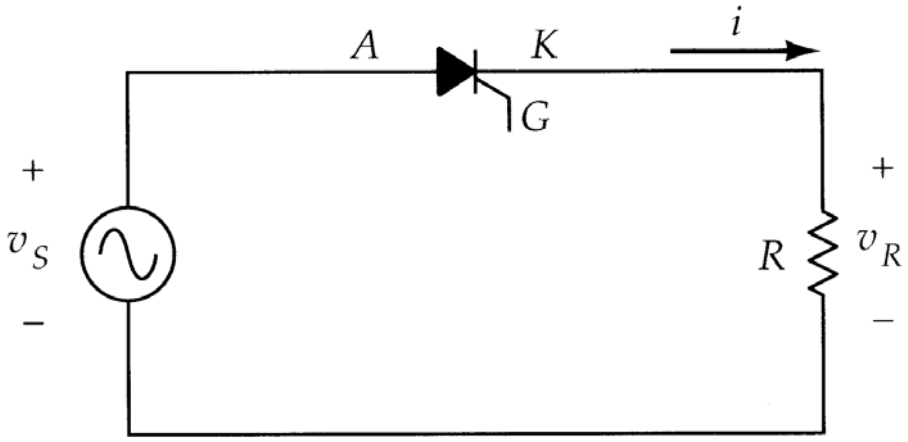


Figure 5. Controlled half-wave rectifier circuit with an ideal SCR and a resistive load. From [3].

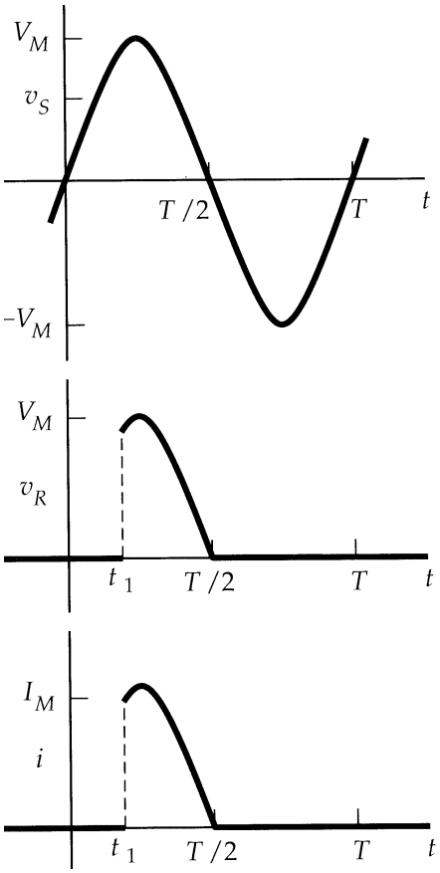


Figure 6. Source voltage, load voltage, and load current waveform profiles for a controlled half-wave rectifier circuit triggered at time $t_1$. From [3].

## 2. Controlled Single-Phase Full-Wave Rectifier

By replacing the diodes in Figure 3 with SCRs, a controlled full-wave rectifier is created as shown in Figure 7. SCRs are gated in pairs with the firing angle $\alpha$ again corresponding to time $t_1 = \alpha / \omega$. During the positive portion of the source voltage waveform, all SCRs are initially "off" until $SCR_1$ and $SCR_4$ are gated "on" while $SCR_2$ and $SCR_3$ remain "off" due to being reverse biased. During the negative portion of the source voltage waveform, the opposite situation occurs and all SCRs are "off" until $SCR_2$ and $SCR_3$ are gated "on" while $SCR_1$ and $SCR_4$ remain

reverse biased and “off.” The resulting current yields zero voltage drop across the load resistor during the time the SCRs are “off” and a positive load voltage drop during both the positive and negative portions of the source voltage waveform when the appropriate SCRs have been gated “on.” Profiles of the source voltage, source current, load voltage, and load current as just described are illustrated in Figure 8 [3], [4].

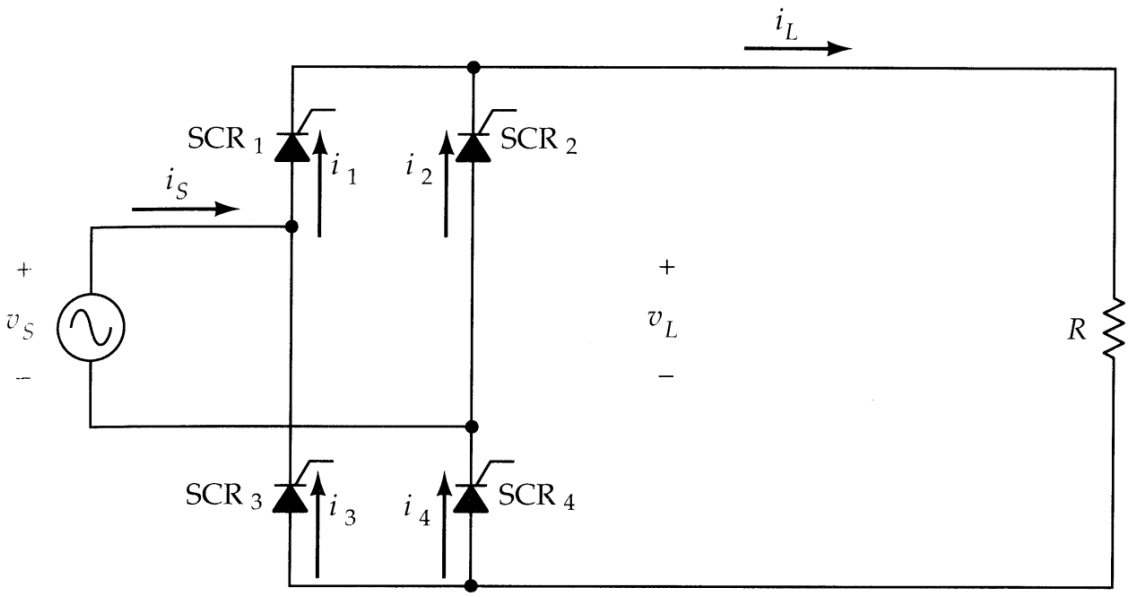


Figure 7. Controlled full-wave rectifier circuit with ideal SCRs and a resistive load. From [3].

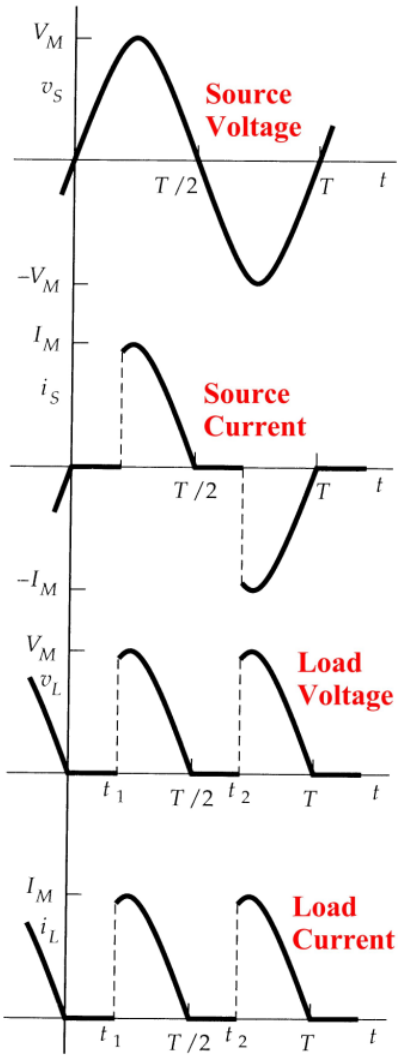


Figure 8. Source voltage, source current, load voltage, and load current waveform profiles for a controlled full-wave rectifier circuit triggered at time $t_1$. $t_2 = t_1 + T/2$. After [3].

# III. CRITICAL INDUCTANCE

A controlled three-phase rectifier with a two-pole *LC* output filter is depicted in the bridge configuration of Figure 9. In this configuration, the number of pulses is twice the number of phases, hence, three-phase becomes synonymous with 6-pulse [11]. One very useful circuit element parameter for these types of rectifiers is the value of the inductor necessary to maintain the circuit operating in CCM. This particular value of inductance is called the critical inductance $L_{crit}$. For nominal circuit operation, the instantaneous inductor current is required to always be positive, which is the definition of CCM, and the capacitor is required to be very large such that the instantaneous capacitor voltage is approximately equal to the average capacitor voltage $v_C(t) \cong V_{C(avg)}$ [3], [4]. While it does require lengthy equations and calculations, we can solve for $L_{crit}$, as will be shown in the continuing sections.

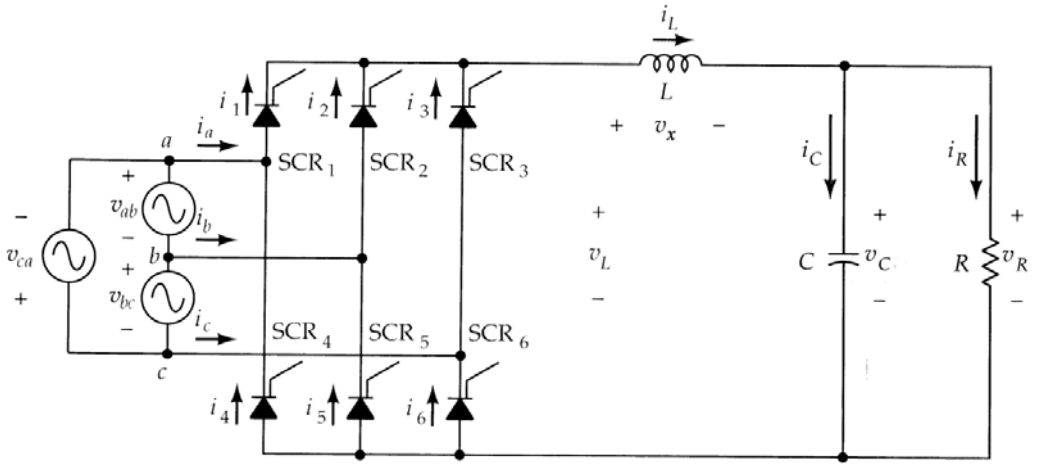


Figure 9. Circuit diagram of a controlled three-phase rectifier with a two-pole *LC* output filter. From [4].

## A. AVERAGE LOAD VOLTAGE CALCULATION

To aid in understanding the relationship between the voltage sources for a three-phase circuit such as the one shown in Figure 9, the three line-to-line source voltages are plotted in Figure 10. While each voltage waveform possesses the same magnitude, they are offset from each other by 120°.

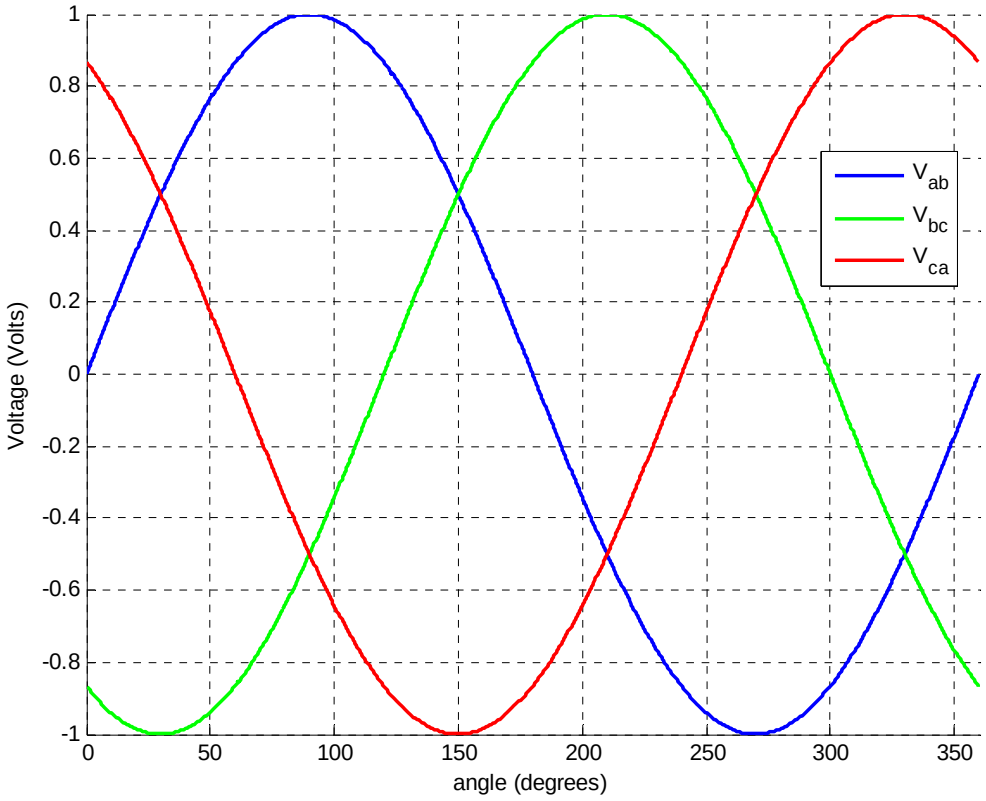


Figure 10. Line-to-line source voltage waveforms $V_{ab}$, $V_{bc}$, and $V_{ca}$ with unity magnitudes for a hypothetical three-phase circuit.

In addition to the three line-to-line source voltages as indicated by the polarities in Figure 9, there are three more line-to-line voltages that exist by looking at them

from the opposite polarities. These additional voltage waveforms, along with the originals, are plotted in Figure 11.

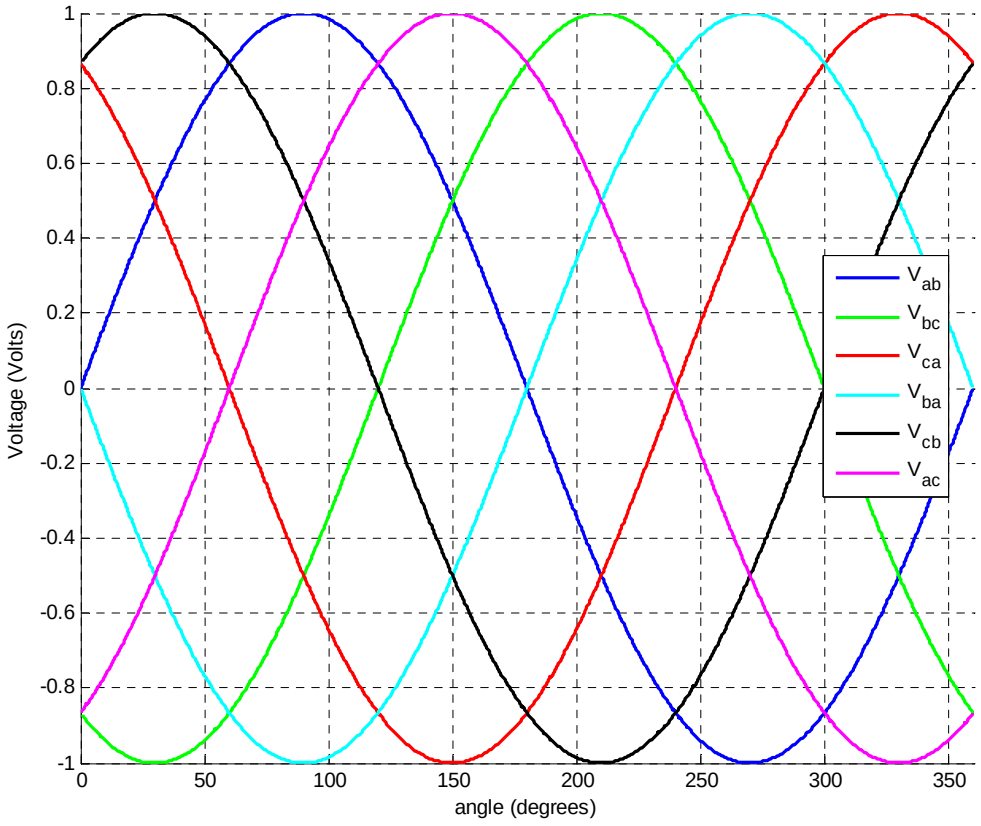


Figure 11. Line-to-line voltage waveforms $V_{cb}$, $V_{ab}$, $V_{ac}$, $V_{bc}$, $V_{ba}$, and $V_{ca}$ with unity magnitudes for a hypothetical three-phase circuit.

From Figure 9 and [3] and [4], the average capacitor voltage $V_{C(avg)}$ is given by

$$V_{C(avg)} = \frac{6}{2\pi} \int_{\alpha+60^\circ}^{\alpha+120^\circ} V_m \sin\gamma d\gamma \,, \qquad (1)$$

where $V_m$ is the peak value of the line-to-line voltage. The six in the numerator is due to the fact that there are six voltage pulses over one period for a three-phase rectifier, as illustrated in Figure 11. The integration limits are solved for by first dividing one period of 360° by six pulses to obtain a pulse-width of 60°. Dividing this pulse-width by two and adding and subtracting it with 90° yields the upper and lower limit firing angle offsets for the upper and lower integration limits. By integrating (1), we get

$$V_{C(avg)} = \left[ -\frac{3V_m}{\pi} \cos\gamma \right]_{\gamma=\alpha+60°}^{\gamma=\alpha+120°}. \tag{2}$$

Evaluating (2), we obtain

$$V_{C(avg)} = -\frac{3V_m}{\pi}\left[\cos(\alpha+120°) - \cos(\alpha+60°)\right], \tag{3}$$

which, by applying the trigonometric identity, $\cos(a+b) = \cos(a)\cos(b) - \sin(a)\sin(b)$, becomes

$$V_{(avg)} = -\frac{3V_m}{\pi}\left\{\begin{array}{l}\cos(\alpha)\cos(120°) - \sin(\alpha)\sin(120°) \\ -\left[\cos(\alpha)\cos(60°) - \sin(\alpha)\sin(60°)\right]\end{array}\right\}, \tag{4}$$

which ultimately simplifies to

$$V_{C(avg)} = \frac{3V_m}{\pi}\cos\alpha. \tag{5}$$

## B. PROCEDURE TO SOLVE FOR THE BOUNDARY ANGLE $\alpha_b$ AS THE TRANSITION POINT BETWEEN SUB-MODES OF CCM

In the circuit of Figure 9 there exists a firing angle $\alpha_b$ such that the instantaneous source voltage is equal to the average capacitor voltage $|v_s(\alpha)| = V_{C(avg)}$. Therefore, for an

instantaneous source voltage $v_s(t)$ given as $v_s(t) = V_m \sin(\omega t)$ and an average capacitor voltage previously solved for in (5), we have the equality

$$V_m \sin(\omega t_1) = \frac{3V_m}{\pi} \cos \alpha_b \quad . \tag{6}$$

By substituting $\omega t_1 = \alpha_b + 60°$, we have

$$V_m \sin(\alpha_b + 60°) = \frac{3V_m}{\pi} \cos \alpha_b \quad . \tag{7}$$

By applying the trigonometric identity $\sin(a+b) = \sin(a)\cos(b) + \cos(a)\sin(b)$, we produce

$$V_m \left[ \sin(\alpha_b)\cos(60°) + \cos(\alpha_b)\sin(60°) \right] = \frac{3V_m}{\pi} \cos \alpha_b , \tag{8}$$

which can be rewritten as

$$\frac{1}{2} \left[ \sin \alpha_b + \sqrt{3} \cos \alpha_b \right] = \frac{3}{\pi} \cos \alpha_b \quad . \tag{9}$$

Grouping similar terms yields

$$\sin \alpha_b = \left( \frac{6}{\pi} - \sqrt{3} \right) \cos \alpha_b , \tag{10}$$

which can then be reduced, leaving

$$\tan \alpha_b = \left( \frac{6}{\pi} - \sqrt{3} \right), \tag{11}$$

which can be solved for $\alpha_b$ to two decimal places as [3], [4]

$$\alpha_b = 10.08° \, . \tag{12}$$

## C. PROCEDURE TO SOLVE FOR THE CRITICAL INDUCTANCE FOR A FIRING ANGLE > 10.08°

With a continuous inductor current and for firing angles greater than 10.08°, the absolute value of the instantaneous source voltage is greater than the average capacitor voltage at the point of commutation, given by $\alpha + 60° = \omega t_1$. Therefore, the slope of the inductor current at the point of commutation is always greater than zero, and it can be said that the voltage source is always electrically connected to the load via the SCR bridge network. In Figure 12, the waveform profiles of the instantaneous load voltage, average load voltage, and instantaneous inductor current for the circuit of Figure 9 are provided. In order to establish a well-defined boundary condition for the proceeding calculations, we let $L = L_{crit}$ so that $i_L(t_1) = i_L(t_2) = 0$ every one-sixth period of the source voltage, resulting in operation on the boundary between continuous and discontinuous modes (also known as being barely continuous), as shown in Figure 12.

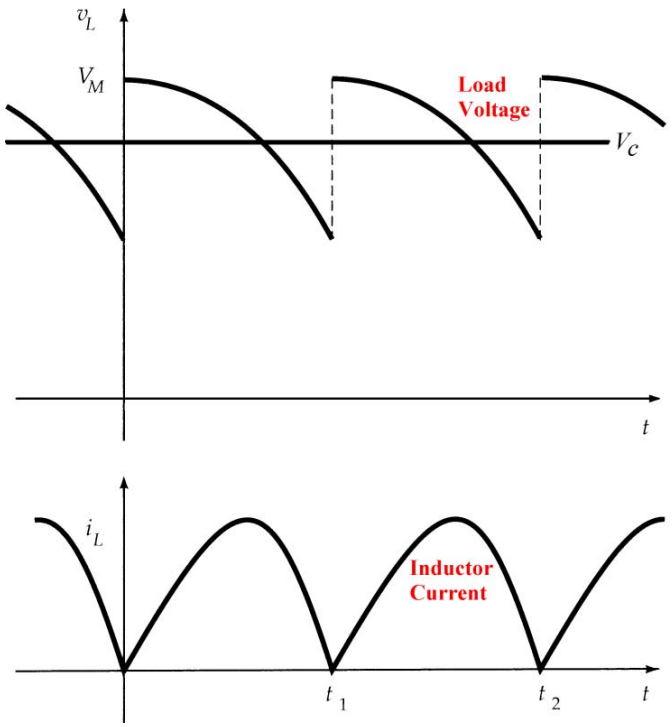


Figure 12. Load voltage, average load voltage, and inductor current waveform profiles for a controlled three-phase rectifier with a two-pole *LC* output filter with a firing angle greater than 10.08°. After [3].

From Kirchhoff's Voltage Law (KVL), we have

$$v_s(t) = v_x(t) + V_{C(avg)}, \tag{13}$$

where $v_s(t)$ is the source voltage given by $v_s(t) = V_m \sin(\omega t)$.

Substituting (5) for $V_{C(avg)}$ and $L\frac{di_L(t)}{dt}$ for $v_x(t)$, we get

$$V_m \sin(\omega t) = L\frac{di_L(t)}{dt} + \frac{3V_m}{\pi}\cos\alpha \quad . \tag{14}$$

Rearranging (14), we get

$$\frac{di_L(t)}{dt} = \frac{V_m}{L}\left(\sin(\omega t) - \frac{3}{\pi}\cos\alpha\right). \tag{15}$$

To solve for $i_L(t)$, it is necessary to set up the integral of (15), leading to

$$i_L(t) = \frac{V_m}{L}\int_{t_1}^{t}\left[\sin(\omega t) - \frac{3}{\pi}\cos\alpha\right]dt\,, \tag{16}$$

which, when integrated, results in

$$i_L(t) = \frac{V_m}{L}\left[\frac{-\cos(\omega t)}{\omega} - \frac{3t\cos\alpha}{\pi}\right]_{t_1}^{t}. \tag{17}$$

Upon evaluating (17) and factoring out $1/\omega$, we get

$$i_L(t) = \frac{V_m}{\omega L}\left[-\cos(\omega t) - \frac{3\omega t\cos\alpha}{\pi} - \left(-\cos(\omega t_1) - \frac{3\omega t_1\cos\alpha}{\pi}\right)\right]. \tag{18}$$

Rearranging (18), we get

$$i_L(t) = \frac{V_m}{\omega L}\left[\cos(\omega t_1) - \cos(\omega t) + \left(\frac{3}{\pi}\right)(\omega t_1 - \omega t)\cos\alpha\right]. \tag{19}$$

By substituting $\omega t_1 = \alpha + 60°$ in (19), we get

$$i_L(t) = \frac{V_m}{\omega L}\left[\cos(\alpha + 60°) - \cos(\omega t) + \left(\frac{3}{\pi}\right)\left(\frac{\alpha\pi}{180} + \frac{\pi}{3} - \omega t\right)\cos\alpha\right]. \tag{20}$$

It is now necessary to calculate the average load current $I_{avg}$, given by

$$I_{avg} = \frac{1}{T}\int_{0}^{T} i_L(t)dt\,. \tag{21}$$

Substituting (20) into (21), we get

$$I_{avg} = \frac{6V_m}{2\pi\omega L}\int_{\alpha+60°}^{\alpha+120°}\left[\cos(\alpha + 60°) - \cos(\omega t) + \frac{3}{\pi}\left(\frac{\alpha\pi}{180} + \frac{\pi}{3} - \omega t\right)\cos\alpha\right]d(\omega t)\,. \tag{22}$$

Integrating and evaluating the integral given by (22) in one step would be very cumbersome, so it is broken up into three parts. Let

$$X_1 = \cos\left(\alpha + 60°\right) \int_{\alpha+60°}^{\alpha+120°} d(\omega t), \tag{23}$$

$$X_2 = \int_{\alpha+60°}^{\alpha+120°} \left[-\cos(\omega t)\right] d(\omega t), \tag{24}$$

and

$$X_3 = \frac{3\cos\alpha}{\pi} \int_{\alpha+60°}^{\alpha+120°} \left[\frac{\alpha\pi}{180} + \frac{\pi}{3} - \omega t\right] d(\omega t). \tag{25}$$

Starting with $X_1$ and integrating (23), we get

$$X_1 = \left[\omega t \cos\left(\alpha + 60°\right)\right]_{\omega t=\alpha+60°}^{\omega t=\alpha+120°}, \tag{26}$$

which, when evaluated, becomes

$$X_1 = \frac{\pi}{3}\cos\left(\alpha + 60°\right). \tag{27}$$

By applying the trigonometric identity $\cos(a+b) = \cos\left(a\right)\cos\left(b\right) - \sin\left(a\right)\sin\left(b\right)$ to (27), we get

$$X_1 = \frac{\pi}{3}\left[\cos\left(\alpha\right)\cos\left(60°\right) - \sin\left(\alpha\right)\sin\left(60°\right)\right], \tag{28}$$

which can be rewritten as

$$X_1 = \frac{\pi}{6}\left[\cos\left(\alpha\right) - \sqrt{3}\sin\left(\alpha\right)\right]. \tag{29}$$

Continuing with $X_2$ and integrating (24), we get

$$X_2 = \left[-\sin(\omega t)\right]_{\omega t=\alpha+60°}^{\omega t=\alpha+120°}, \tag{30}$$

which, when evaluated, becomes

$$X_2 = \sin(\alpha + 60°) - \sin(\alpha + 120°)\ . \tag{31}$$

By applying the trigonometric identity $\sin(a+b) = \sin(a)\cos(b) + \cos(a)\sin(b)$ to (31), we get

$$\begin{aligned} X_2 &= \sin(\alpha)\cos(60°) + \cos(\alpha)\sin(60°) \\ &-\left[\sin(\alpha)\cos(120°) + \cos(\alpha)\sin(120°)\right], \end{aligned} \tag{32}$$

which simplifies to

$$X_2 = \sin\alpha\ . \tag{33}$$

Finishing with $X_3$ and integrating (25), we get

$$X_3 = \left(\frac{3\cos\alpha}{\pi}\right)\left[\left(\frac{\alpha\pi}{180} + \frac{\pi}{3}\right)\omega t - \frac{(\omega t)^2}{2}\right]_{\omega t=\alpha+60°}^{\omega t=\alpha+120°}, \tag{34}$$

which, when evaluated, becomes

$$X_3 = \left(\frac{3\cos\alpha}{\pi}\right)\left[\left(\frac{\alpha\pi}{180} + \frac{\pi}{3}\right)\left(\frac{\pi}{3}\right) - \frac{1}{2}\left\{\left(\frac{\alpha\pi}{180} + \frac{2\pi}{3}\right)^2 - \left(\frac{\alpha\pi}{180} + \frac{\pi}{3}\right)^2\right\}\right]. \tag{35}$$

Simplifying (35), we get the result

$$X_3 = -\frac{\pi\cos\alpha}{6}\ . \tag{36}$$

Inserting the resultant expressions from (29), (33), and (36) back into (22), we have

$$I_{avg} = \frac{6V_m}{2\pi\omega L}\left\{\frac{\pi}{6}\left[\cos(\alpha) - \sqrt{3}\sin(\alpha)\right] + \sin\alpha - \frac{\pi\cos\alpha}{6}\right\}, \tag{37}$$

which, when simplified, produces

$$I_{avg} = \frac{3V_m\sin\alpha}{\pi\omega L}\left(1 - \frac{\pi\sqrt{3}}{6}\right). \tag{38}$$

Because we have already solved for $V_{C(avg)}$ in (5), we have another expression for $I_{avg}$ using Ohm's Law, as

$$I_{avg} = \frac{3V_m}{\pi R}\cos\alpha \,. \tag{39}$$

By substituting (39) into (38), we can solve for $L_{crit}$ as [3], [4]

$$L_{crit} = \frac{R\tan\alpha}{\omega}\left(1 - \frac{\pi\sqrt{3}}{6}\right). \tag{40}$$

## D. PROCEDURE TO SOLVE FOR THE CRITICAL INDUCTANCE FOR A FIRING ANGLE < 10.08°

With a continuous inductor current and for firing angles less than 10.08°, the absolute value of the instantaneous source voltage is less than the average capacitor voltage at the point of commutation. Therefore, the slope of the inductor current at the point of commutation is always less than zero. Unlike the previous sub-mode in which the minimum inductor current occurred at the firing point, for this sub-mode, the minimum inductor current occurs at an angle $\theta_3 = \omega t_3$ (where $\theta = \theta_3 - 60°$ referenced to $\alpha$), as shown in Figure 13.

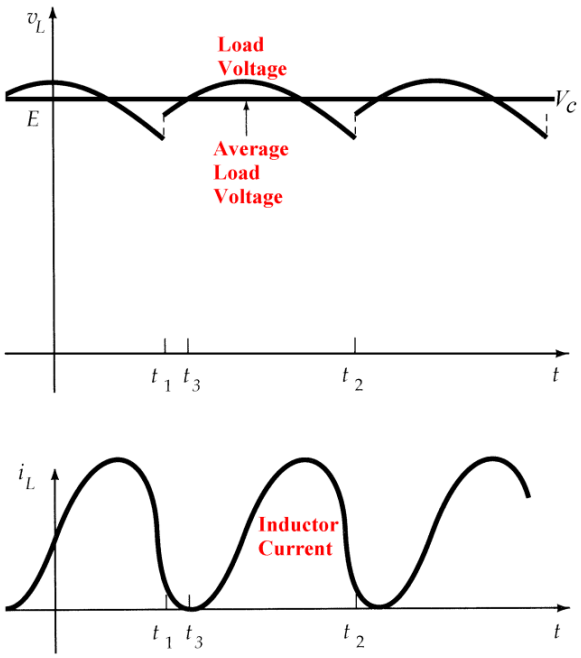


Figure 13. Load voltage, average load voltage, and inductor current waveform profiles for a controlled three-phase rectifier with a two-pole *LC* output filter with a firing angle less than 10.08°. After [3].

Once again, we can say that the voltage source is always electrically connected to the load via the SCR bridge network, and the conducting SCRs are able to ride-through the minimum current point at $t_3$. At $t_3$, the average capacitor voltage is equal to the instantaneous source voltage and the slope of the inductor current is zero. Therefore, for an instantaneous source voltage $v_s(t)$ given as $v_s(t) = V_m \sin(\omega t_3)$ and an average capacitor voltage previously solved for in (5), we have the equality

$$V_m \sin(\omega t_3) = \frac{3V_m}{\pi} \cos\alpha \ . \qquad (41)$$

By substituting $\omega t_3 = \theta + 60°$, we have

$$V_m \sin\left(\theta + 60°\right) = \frac{3V_m}{\pi}\cos\alpha\,, \tag{42}$$

which can be solved for $\theta$ as

$$\theta = \sin^{-1}\left(\frac{3}{\pi}\cos\alpha\right) - 60°\,. \tag{43}$$

For $t > t_3$, the instantaneous source voltage is greater than the average capacitor voltage, and the inductor current begins to increase. By triggering the SCRs at $\alpha_b$ as previously determined in (12), an additional verification can be made at the boundary between sub-modes. For the instantaneous source voltage $v_s(t) = V_m \sin(\omega t_3)$ and an average capacitor voltage as previously solved for in (5) (but with $\alpha_b$ now substituted for $\alpha$), we have the equality

$$V_m \sin\left(\omega t_3\right) = \frac{3V_m}{\pi}\cos\alpha_b\,. \tag{44}$$

By substituting $\omega t_3 = \theta_b + 60°$, we have

$$V_m \sin\left(\theta_b + 60°\right) = \frac{3V_m}{\pi}\cos\alpha_b\,, \tag{45}$$

which can be solved for $\theta_b$ as

$$\theta_b = \sin^{-1}\left(\frac{3}{\pi}\cos\alpha_b\right) - 60°\,. \tag{46}$$

At $\alpha_b = 10.08°$, $\theta_b = 10.08°$. In order to once again establish a well-defined boundary condition for the subsequent calculations, we let $L = L_{crit}$ so that $i_L(t_3) = 0$ every half-period of each phase of the source voltage, again resulting in operation on the boundary between continuous and discontinuous modes, as illustrated in Figure 13. We begin

once again with the KVL equation as given in (13), with the same expressions for $v_s(t)$, $v_x(t)$, and $V_{C(avg)}$, working through identical equations given by (14) and (15), and arrive at

$$i_L(t) = \frac{V_m}{L}\int_{t3}^{t}\left[\sin(\omega t) - \frac{3}{\pi}\cos\alpha\right]dt \quad . \tag{47}$$

After integration, we have

$$i_L(t) = \frac{V_m}{L}\left[\frac{-\cos(\omega t)}{\omega} - \frac{3t\cos\alpha}{\pi}\right]_{t_3}^{t}, \tag{48}$$

and after evaluating (48) and factoring out $1/\omega$, we get the result

$$i_L(t) = \frac{V_m}{\omega L}\left[-\cos(\omega t) - \frac{3\omega t\cos\alpha}{\pi} - \left(-\cos(\omega t_3) - \frac{3\omega t_3\cos\alpha}{\pi}\right)\right]. \tag{49}$$

Rearranging (49), we get

$$i_L(t) = \frac{V_m}{\omega L}\left[\cos(\omega t_3) - \cos(\omega t) + \left(\frac{3}{\pi}\right)(\omega t_3 - \omega t)\cos\alpha\right]. \tag{50}$$

By substituting $\omega t_3 = \theta + 60°$ into (50), we get

$$i_L(t) = \frac{V_m}{\omega L}\left[\cos(\theta + 60°) - \cos(\omega t) + \left(\frac{3}{\pi}\right)\left(\frac{\theta\pi}{180} + \frac{\pi}{3} - \omega t\right)\cos\alpha\right]. \tag{51}$$

Once again, we calculate the average load current using (21). By substituting (51) into (21), we get

$$I_{avg} = \frac{6V_m}{2\pi\omega L}\int_{\alpha+60°}^{\alpha+120°}\left[\cos(\theta + 60°) - \cos(\omega t) + \frac{3}{\pi}\left(\frac{\theta\pi}{180} + \frac{\pi}{3} - \omega t\right)\cos\alpha\right]d(\omega t) \quad . \tag{52}$$

Integrating and evaluating the integral given by (52) in one step would once again be very cumbersome, so it is separated into three parts. Let

$$X_1 = \cos(\theta + 60°) \int_{\alpha+60°}^{\alpha+120°} d(\omega t)\,, \tag{53}$$

$X_2 = X_2$ from (24), and

$$X_3 = \frac{3\cos\alpha}{\pi} \int_{\alpha+60°}^{\alpha+120°} \left[\frac{\theta\pi}{180} + \frac{\pi}{3} - \omega t\right] d(\omega t)\,. \tag{54}$$

Starting with $X_1$ and integrating (53), we get

$$X_1 = \left[\omega t \cos(\theta + 60°)\right]_{\omega t=\alpha+60°}^{\omega t=\alpha+120°}\,, \tag{55}$$

which, when evaluated, becomes

$$X_1 = \frac{\pi}{3}\cos(\theta + 60°)\,. \tag{56}$$

Since $X_2$ is identical to the previous $X_2$, the result is provided from (33). Finishing with $X_3$ and integrating (54), we get

$$X_3 = \left(\frac{3\cos\alpha}{\pi}\right)\left[\left(\frac{\theta\pi}{180} + \frac{\pi}{3}\right)\omega t - \frac{(\omega t)^2}{2}\right]_{\omega t=\alpha+60°}^{\omega t=\alpha+120°}\,, \tag{57}$$

which, when evaluated, becomes

$$X_3 = \left(\frac{3\cos\alpha}{\pi}\right)\left[\left(\frac{\theta\pi}{180} + \frac{\pi}{3}\right)\left(\frac{\pi}{3}\right) - \frac{1}{2}\left\{\left(\frac{\alpha\pi}{180} + \frac{2\pi}{3}\right)^2 - \left(\frac{\alpha\pi}{180} + \frac{\pi}{3}\right)^2\right\}\right]. \tag{58}$$

Simplifying (58), we get

$$X_3 = \left(\frac{\pi}{180}\right)(\theta - \alpha - 30°)\cos\alpha\,. \tag{59}$$

Inserting the resultant expressions from (56), (33), and (59) back into (52), we have

$$I_{avg} = \frac{3V_m}{\pi\omega L}\left[\frac{\pi}{3}\cos(\theta+60°)+\sin\alpha+\left(\frac{\pi}{180}\right)(\theta-\alpha-30°)\cos\alpha\right]. \qquad (60)$$

Using (39) once again, we can substitute it into (60) and solve for $L_{crit}$ as

$$L_{crit} = \frac{R}{\omega\cos\alpha}\left[\frac{\pi}{3}\cos(\theta+60°)+\sin\alpha+\left(\frac{\pi}{180}\right)(\theta-\alpha-30°)\cos\alpha\right]. \qquad (61)$$

Although $\theta$ is a function of $\alpha$ as given by (43), substituting it into (61) would only serve to make it more unwieldy, so we leave it in its present form [3], [4].

## E. SUMMARY OF CALCULATIONS FOR $L_{crit}$

To summarize, we have the following equations for $L_{crit}$:

$$L_{crit} = \frac{R\tan\alpha}{\omega}\left(1-\frac{\pi\sqrt{3}}{6}\right) \text{ for } \alpha \geq 10.08° \qquad (62)$$

and

$$L_{crit} = \frac{R}{\omega\cos\alpha}\left[\frac{\pi}{3}\cos(\theta+60°)+\sin\alpha+\left(\frac{\pi}{180}\right)(\theta-\alpha-30°)\cos\alpha\right] \qquad (63)$$

for $\alpha \leq 10.08°$, where

$$\theta = \sin^{-1}\left(\frac{3}{\pi}\cos\alpha\right)-60° . \qquad (64)$$

From Figure 14, the critical inductance for the 6-pulse rectifier circuit of Figure 9 can be seen, assuming a unity resistance and a frequency of 60 Hz. An important conclusion is that as $\alpha$ increases, $L_{crit}$ increases at an increasing rate. This is the key reason that circuit

designers of controlled rectifiers desire to keep $\alpha$ relatively small—the size, weight, and cost of the inductor cannot be ignored.

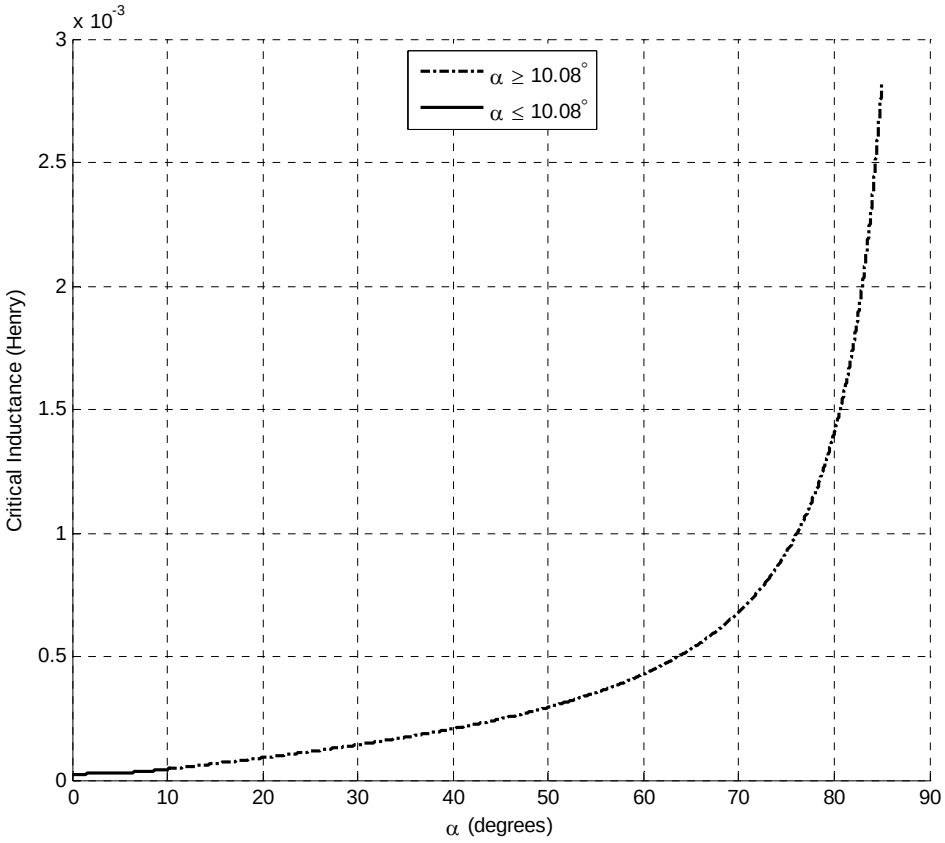


Figure 14. Critical inductance plot for a controlled 6-pulse rectifier with unity resistance operating at 60 Hz.

## F. CRITICAL INDUCTANCE FOR A CONTROLLED P-PULSE RECTIFIER

One way to increase the pulse count of this type of rectifier is by stacking 6-pulse rectifiers in series—for instance, two 6-pulse rectifiers could be connected together to make one 12-pulse rectifier. While this has several benefits, an important one is that it decreases the

value of $L_{crit}$. To prove this, one could certainly go back and tediously derive the necessary equations, solve for $L_{crit}$, and plot it. Indeed, that is exactly what was done for the 12-, 18-, and 24-pulse rectifier circuit configurations, the workings of which have been spared from this thesis. The purpose of this labor was to uncover a possible pattern. This work was not done in vain; a clear pattern exists. There are equations to calculate $L_{crit}$ for a controlled p-pulse rectifier. These equations are derived in the same manner as before, only this time with some clever substitutions. First, let $p$ equal the pulse count. Then, let the lower integration limit $\theta_L$ be expressed in degrees as

$$\theta_L = 90° - \left(\frac{180°}{p}\right), \tag{65}$$

and the upper integration limit $\theta_U$, also in degrees, be

$$\theta_U = 90° + \left(\frac{180°}{p}\right), \tag{66}$$

thereby, making both functions of pulse count. Next, let $A = \cos\theta_L$, $B = \sin\theta_L$, $C = \cos\theta_U$, and $D = \sin\theta_U$; therefore, $C = -A$ and $D = B$.

### 1. Average Load Voltage Calculation

With our new substitutions, the expression for the average load voltage from (1) now becomes

$$V_{C(avg)} = \frac{p}{2\pi}\int_{\alpha+\theta_L}^{\alpha+\theta_U} V_m \sin\gamma d\gamma, \tag{67}$$

which, when integrated, yields

$$V_{C(avg)} = -\frac{pV_m}{2\pi}\left[\cos(\alpha+\theta_U)-\cos(\alpha+\theta_L)\right]. \quad (68)$$

By applying $\cos(a+b)=\cos(a)\cos(b)-\sin(a)\sin(b)$ to (68), we get

$$V_{C(avg)} = -\frac{pV_m}{2\pi}\left[C\cos(\alpha)-D\sin(\alpha)-A\cos(\alpha)+B\sin(\alpha)\right], \quad (69)$$

which simplifies to

$$V_{C(avg)} = \frac{ApV_m}{\pi}\cos\alpha\ . \quad (70)$$

### 2. Procedure to Solve for the Boundary Angle $\alpha_b$ as the Transition Point Between Sub-modes of CCM

By beginning with (6), but this time substituting $\omega t_1 = \alpha_b + \theta_L$ and our new expression for average capacitor voltage from (70), we have

$$V_m \sin\left(\alpha_b+\theta_L\right) = \frac{ApV_m}{\pi}\cos\alpha_b\ . \quad (71)$$

By applying the trigonometric identity $\sin(a+b)=\sin(a)\cos(b)+\cos(a)\sin(b)$, we produce

$$V_m\left[\sin\left(\alpha_b\right)\cos\left(\theta_L\right)+\cos\left(\alpha_b\right)\sin\left(\theta_L\right)\right] = \frac{ApV_m}{\pi}\cos\alpha_b, \quad (72)$$

which can be rewritten as

$$A\sin\left(\alpha_b\right)+B\cos\left(\alpha_b\right) = \frac{Ap}{\pi}\cos\alpha_b\ . \quad (73)$$

Grouping similar terms, yields

$$A\sin\left(\alpha_b\right) = \left(\frac{Ap}{\pi}-B\right)\cos\alpha_b, \quad (74)$$

which can then be reduced, leaving

$$\tan(\alpha_b) = \left(\frac{p}{\pi} - \frac{B}{A}\right). \tag{75}$$

Therefore, we have

$$\alpha_b = \tan^{-1}\left(\frac{p}{\pi} - \frac{B}{A}\right). \tag{76}$$

### 3. Procedure to Solve for the Critical Inductance for a Firing Angle > $\alpha_b$

Starting with (13), we use the same original substitutions, with the exception of our new expression for $V_{C(avg)}$, and obtain

$$V_m \sin(\omega t) = L\frac{di_L}{dt} + \frac{ApV_m}{\pi}\cos\alpha\ , \tag{77}$$

which, after we solve for $di_L / dt$, integrate, and simplify as before, we get

$$i_L(t) = \frac{V_m}{\omega L}\left[\cos(\omega t_1) - \cos(\omega t) + \left(\frac{Ap}{\pi}\right)(\omega t_1 - \omega t)\cos\alpha\right]. \tag{78}$$

By substituting $\omega t_1 = \alpha + \theta_L$ in (78), we get

$$i_L(t) = \frac{V_m}{\omega L}\left[\cos(\alpha + \theta_L) - \cos(\omega t) + \left(\frac{Ap}{\pi}\right)\left(\frac{\alpha\pi}{180} + \frac{\theta_L\pi}{180} - \omega t\right)\cos\alpha\right]. \tag{79}$$

Calculating $I_{avg}$ by substituting (79) into (21), we get

$$I_{avg} = \frac{pV_m}{2\pi\omega L}\int_{\alpha+\theta_L}^{\alpha+\theta_U}\left[\begin{array}{l}\cos(\alpha+\theta_L) - \cos(\omega t) \\ +\left(\frac{Ap}{\pi}\right)\left(\frac{\alpha\pi}{180} + \frac{\theta_L\pi}{180} - \omega t\right)\cos\alpha\end{array}\right] d(\omega t)\ . \tag{80}$$

Breaking up the integral into similar parts as before, we have:

$$X_1 = \cos(\alpha + \theta_L) \int_{\alpha+\theta_L}^{\alpha+\theta_U} d(\omega t), \tag{81}$$

$$X_2 = \int_{\alpha+\theta_L}^{\alpha+\theta_U} [-\cos(\omega t)] d(\omega t), \tag{82}$$

and

$$X_3 = \frac{Ap\cos\alpha}{\pi} \int_{\alpha+\theta_L}^{\alpha+\theta_U} \left( \frac{\alpha\pi}{180} + \frac{\theta_L \pi}{180} - \omega t \right) d(\omega t) . \tag{83}$$

Starting with $X_1$ and integrating (81), we get

$$X_1 = \left[ \omega t \cos(\alpha + \theta_L) \right]_{\omega t=\alpha+\theta_L}^{\omega t=\alpha+\theta_U}, \tag{84}$$

which, when evaluated, becomes

$$X_1 = \left( \frac{\pi}{180} \right) (\theta_U - \theta_L) \cos(\alpha + \theta_L) . \tag{85}$$

We apply $\cos(a+b) = \cos(a)\cos(b) - \sin(a)\sin(b)$ to (85), yielding

$$X_1 = \left( \frac{\pi}{180} \right) (\theta_U - \theta_L) \left[ \cos(\alpha)\cos(\theta_L) - \sin(\alpha)\sin(\theta_L) \right], \tag{86}$$

which can be rewritten as

$$X_1 = \left( \frac{2\pi}{p} \right) \left[ A\cos(\alpha) - B\sin(\alpha) \right] . \tag{87}$$

Continuing with $X_2$ and integrating (82), we get

$$X_2 = \left[ -\sin(\omega t) \right]_{\omega t=\alpha+\theta_L}^{\omega t=\alpha+\theta_U}, \tag{88}$$

which, when evaluated, becomes

$$X_2 = \sin(\alpha + \theta_L) - \sin(\alpha + \theta_U)\,. \tag{89}$$

By applying $\sin(a+b) = \sin(a)\cos(b) + \cos(a)\sin(b)$ to (89), we get

$$\begin{aligned} X_2 &= \sin(\alpha)\cos(\theta_L) + \cos(\alpha)\sin(\theta_L) \\ &-\left[\sin(\alpha)\cos(\theta_U) + \cos(\alpha)\sin(\theta_U)\right] \end{aligned}\,, \tag{90}$$

which simplifies to

$$X_2 = 2A\sin\alpha\,. \tag{91}$$

Finishing with $X_3$ and integrating (83), we get

$$X_3 = \left(\frac{Ap\cos\alpha}{\pi}\right)\left[\left(\frac{\alpha\pi}{180} + \frac{\theta_L\pi}{180}\right)\omega t - \frac{(\omega t)^2}{2}\right]_{\omega t=\alpha+\theta_L}^{\omega t=\alpha+\theta_U}\,, \tag{92}$$

which, when evaluated, becomes

$$X_3 = \left(\frac{Ap\cos\alpha}{\pi}\right)\left[\begin{aligned} &\left(\frac{\alpha\pi}{180} + \frac{\theta_L\pi}{180}\right)(\theta_U - \theta_L)\left(\frac{\pi}{180}\right) \\ &-\frac{1}{2}\left\{\left(\frac{\alpha\pi}{180} + \frac{\theta_U\pi}{180}\right)^2 - \left(\frac{\alpha\pi}{180} + \frac{\theta_L\pi}{180}\right)^2\right\} \end{aligned}\right]. \tag{93}$$

Simplifying (93), the result is,

$$X_3 = -\frac{2A\pi\cos\alpha}{p}\,. \tag{94}$$

Inserting the resultant expressions from (87), (91), and (94) back into (80), we have

$$I_{avg} = \frac{pV_m}{2\pi\omega L}\left\{\left(\frac{2\pi}{p}\right)\left[A\cos\alpha - B\sin\alpha\right] + 2A\sin\alpha - \frac{2A\pi\cos\alpha}{p}\right\}, \tag{95}$$

which, when simplified, produces

$$I_{avg} = \frac{V_m\sin\alpha}{\pi\omega L}\left(Ap - \pi B\right). \tag{96}$$

Because we have already solved for $V_{C(avg)}$ in (70), we have another expression for $I_{avg}$ using Ohm's Law, as

$$I_{avg} = \frac{ApV_m}{\pi R}\cos\alpha \,. \tag{97}$$

By substituting (97) into (96), we can solve for $L_{crit}$ as

$$L_{crit} = \frac{R\tan\alpha}{\omega}\left(1 - \frac{\pi B}{Ap}\right). \tag{98}$$

### 4. Procedure to Solve for the Critical Inductance for a Firing Angle < $\alpha_b$

Starting with (41), we substitute our new expressions for $V_{C(avg)}$ and $\omega t_3$ to obtain

$$V_m \sin\left(\theta + \theta_L\right) = \frac{ApV_m}{\pi}\cos\alpha \tag{99}$$

which can be solved for $\theta$ as

$$\theta = \sin^{-1}\left(\frac{Ap}{\pi}\cos\alpha\right) - \theta_L \,. \tag{100}$$

Once again, we can make an additional verification at the boundary between sub-modes. For the instantaneous source voltage $v_s(t) = V_m \sin(\omega t_3)$ and an average capacitor voltage as previously solved for in (70), we have the equality

$$V_m \sin\left(\omega t_3\right) = \frac{ApV_m}{\pi}\cos\alpha_b \,. \tag{101}$$

By substituting $\omega t_3 = \theta_b + \theta_L$ into (101), we have

$$V_m \sin\left(\theta_b + \theta_L\right) = \frac{ApV_m}{\pi}\cos\alpha_b \,, \tag{102}$$

which can be solved for $\theta_b$ as

$$\theta_b = \sin^{-1}\left(\frac{Ap}{\pi}\cos\alpha_b\right) - \theta_L \quad . \tag{103}$$

Next, we go back to the KVL from (77), solve for $di_L(t)/dt$, and set up the integral as we did in (47), and we obtain

$$i_L(t) = \frac{V_m}{L}\int_{t3}^{t}\left[\sin(\omega t) - \frac{Ap}{\pi}\cos\alpha\right]dt \quad . \tag{104}$$

After integration, we have

$$i_L(t) = \frac{V_m}{L}\left[\frac{-\cos(\omega t)}{\omega} - \frac{Apt\cos\alpha}{\pi}\right]_{t_3}^{t}, \tag{105}$$

and after evaluating (105) and factoring out $1/\omega$, we obtain

$$i_L(t) = \frac{V_m}{\omega L}\left[-\cos(\omega t) - \frac{Ap\omega t\cos\alpha}{\pi} - \left(-\cos(\omega t_3) - \frac{Ap\omega t_3\cos\alpha}{\pi}\right)\right]. \tag{106}$$

By rearranging (106), we get

$$i_L(t) = \frac{V_m}{\omega L}\left[\cos(\omega t_3) - \cos(\omega t) + \left(\frac{Ap}{\pi}\right)(\omega t_3 - \omega t)\cos\alpha\right]. \tag{107}$$

By substituting $\omega t_3 = \theta + \theta_L$ in (107), we get

$$i_L(t) = \frac{V_m}{\omega L}\left[\cos(\theta + \theta_L) - \cos(\omega t) + \left(\frac{Ap}{\pi}\right)\left(\frac{\theta\pi}{180} + \frac{\theta_L\pi}{180} - \omega t\right)\cos\alpha\right]. \tag{108}$$

To calculate the average load current, we again refer to (21). By Substituting (108) into (21), we get

$$I_{avg} = \frac{pV_m}{2\pi\omega L}\int_{\alpha+\theta_L}^{\alpha+\theta_U}\left[\cos(\theta + \theta_L) - \cos(\omega t) + \frac{Ap}{\pi}\left(\frac{\theta\pi}{180} + \frac{\theta_L\pi}{180} - \omega t\right)\cos\alpha\right]d(\omega t) \quad . \tag{109}$$

Because of the complexity of (109), it is again broken into three parts. Let

$$X_1 = \cos(\theta + \theta_L) \int_{\alpha+\theta_L}^{\alpha+\theta_U} d(\omega t)\,, \tag{110}$$

$X_2 = X_2$ from (82), and

$$X_3 = \frac{Ap\cos\alpha}{\pi} \int_{\alpha+\theta_L}^{\alpha+\theta_U} \left( \frac{\theta\pi}{180} + \frac{\theta_L\pi}{180} - \omega t \right) d(\omega t)\,. \tag{111}$$

Starting with $X_1$ and integrating (110), we obtain

$$X_1 = \left[ \omega t \cos(\theta + \theta_L) \right]_{\omega t=\alpha+\theta_L}^{\omega t=\alpha+\theta_U}, \tag{112}$$

which, when evaluated, becomes

$$X_1 = \left( \frac{\pi}{180} \right) (\theta_U - \theta_L) \cos(\theta + \theta_L), \tag{113}$$

which can be rewritten as

$$X_1 = \left( \frac{2\pi}{p} \right) \cos(\theta + \theta_L)\,. \tag{114}$$

Because $X_2$ is the same as the previous $X_2$, its result is given in (91). Finishing with $X_3$ and integrating (111), we obtain

$$X_3 = \left( \frac{Ap\cos\alpha}{\pi} \right) \left[ \left( \frac{\theta\pi}{180} + \frac{\theta_L\pi}{180} \right) \omega t - \frac{(\omega t)^2}{2} \right]_{\omega t=\alpha+\theta_L}^{\omega t=\alpha+\theta_U}, \tag{115}$$

which, when evaluated, becomes

$$X_3 = \left( \frac{Ap\cos\alpha}{\pi} \right) \left[ \begin{array}{l} \left( \frac{\theta\pi}{180} + \frac{\theta_L\pi}{180} \right) (\theta_U - \theta_L) \left( \frac{\pi}{180} \right) \\ -\frac{1}{2} \left\{ \left( \frac{\alpha\pi}{180} + \frac{\theta_U\pi}{180} \right)^2 - \left( \frac{\alpha\pi}{180} + \frac{\theta_L\pi}{180} \right)^2 \right\} \end{array} \right]. \tag{116}$$

By simplifying (116), the result is

$$X_3 = 2A\left(\frac{\theta\pi}{180} - \frac{\alpha\pi}{180} - \frac{\pi}{p}\right)\cos\alpha\,. \tag{117}$$

By inserting the results from (114), (91), and (117) back into (109), we have

$$I_{avg} = \frac{pV_m}{\pi\omega L}\left[\left(\frac{\pi}{p}\right)\cos\left(\theta+\theta_L\right) + A\sin\alpha + A\left(\frac{\theta\pi}{180} - \frac{\alpha\pi}{180} - \frac{\pi}{p}\right)\cos\alpha\right]. \tag{118}$$

By using (97), we can substitute it into (118) and solve for $L_{crit}$ as

$$L_{crit} = \frac{R}{\omega A\cos\alpha}\left[\left(\frac{\pi}{p}\right)\cos\left(\theta+\theta_L\right) + A\sin\alpha + A\left(\frac{\theta\pi}{180} - \frac{\alpha\pi}{180} - \frac{\pi}{p}\right)\cos\alpha\right]. \tag{119}$$

Although $\theta$ is a function of $\alpha$ as given by (100), substituting it into (119) would only serve to make it more unwieldy, so we leave it in its present form.

## 5. Summary of Calculations for $L_{crit}$

To summarize, we have the following equations for $L_{crit}$:

$$L_{crit} = \frac{R\tan\alpha}{\omega}\left(1 - \frac{\pi B}{Ap}\right) \quad \text{for} \quad \alpha \geq \alpha_b \tag{120}$$

and

$$L_{crit} = \frac{R}{\omega A\cos\alpha}\left[\left(\frac{\pi}{p}\right)\cos\left(\theta+\theta_L\right) + A\sin\alpha + A\left(\frac{\theta\pi}{180} - \frac{\alpha\pi}{180} - \frac{\pi}{p}\right)\cos\alpha\right] \tag{121}$$

for $\alpha \leq \alpha_b$, where

$$\alpha_b = \tan^{-1}\left(\frac{p}{\pi} - \frac{B}{A}\right), \tag{122}$$

$$\theta = \sin^{-1}\left(\frac{Ap}{\pi}\cos\alpha\right) - \theta_L\,, \tag{123}$$

$$A = \cos\theta_L \,, \tag{124}$$

and

$$B = \sin\theta_L \,. \tag{125}$$

From Figure 13, critical inductances for a 6-, 12-, 18-, 24-, and 96-pulse rectifier can be seen, assuming a unity resistance and a frequency of 60 Hz. As before, as $\alpha$ increases for each rectifier, $L_{crit}$ increases at an increasing rate. Another important conclusion from Figure 13 is that as pulse count increases, $L_{crit}$ decreases at a decreasing rate. This is most obvious when comparing a 6-pulse rectifier to a 12-pulse rectifier, where there is a large reduction in $L_{crit}$, and then continuing to an 18-pulse rectifier, where the percent difference in $L_{crit}$ is less substantial. To clearly illustrate the concept of diminishing returns, the jump from a 24-pulse rectifier to a 96-pulse rectifier was purposely plotted to show just how little reduction in $L_{crit}$ is obtained by dramatically increasing pulse count. Finally, as pulse count increases, $\alpha_b$ decreases, making the equation for $L_{crit}$ for $\alpha < \alpha_b$ less relevant, especially for high pulse count rectifiers.

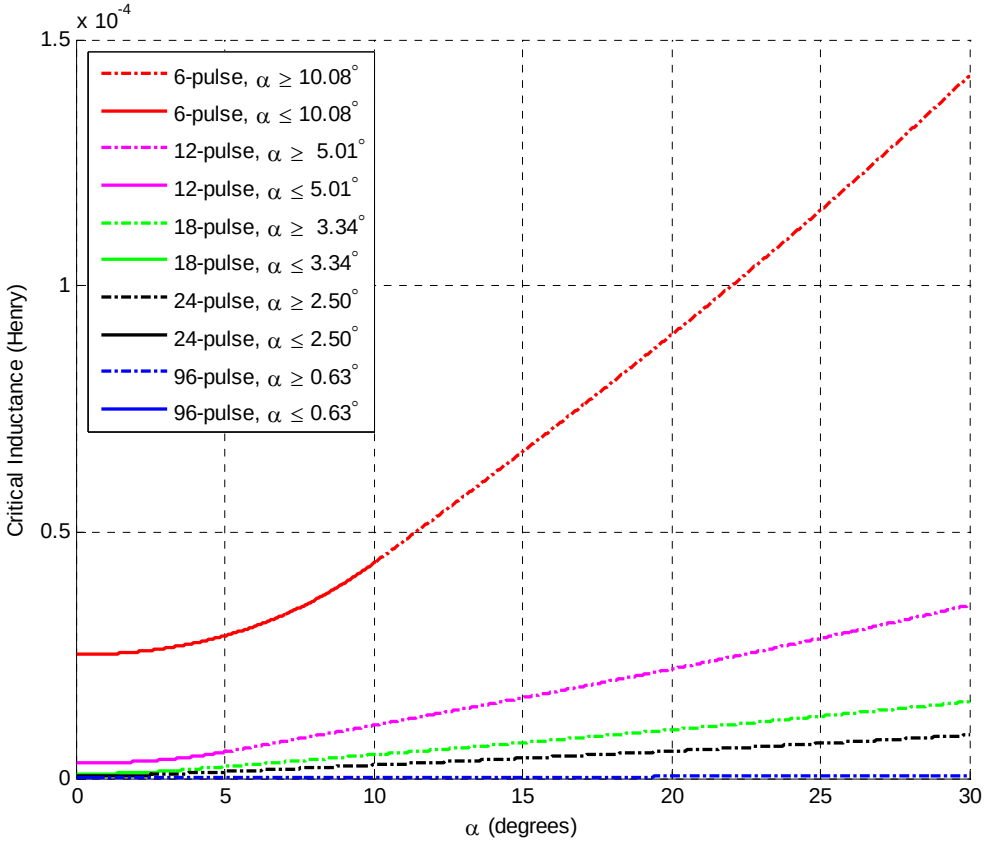


Figure 15. Critical inductance plot for controlled p-pulse rectifiers with unity resistance operating at 60 Hz.

Critical inductance values for the $L_{crit}$ plots of Figure 15 are provided in Table 1, starting at a firing angle of 0° and ending at 80°, in 10° increments. A firing angle of 90° would result in an infinite critical inductance, so the upper bound is not inclusive of 90°.

Table 1. Critical inductance (Henry) for selected firing angles for the controlled p-pulse rectifiers of Figure 15.

| | firing angle alpha (degrees) | | | | | | | | |
|---|---|---|---|---|---|---|---|---|---|
| pulse-count | 0 | 10 | 20 | 30 | 40 | 50 | 60 | 70 | 80 |
| 6 | 2.51E-05 | 4.35E-05 | 8.99E-05 | 1.43E-04 | 2.07E-04 | 2.94E-04 | 4.28E-04 | 6.79E-04 | 1.40E-03 |
| 12 | 3.07E-06 | 1.07E-05 | 2.22E-05 | 3.51E-05 | 5.11E-05 | 7.26E-05 | 1.05E-04 | 1.67E-04 | 3.45E-04 |
| 18 | 9.07E-07 | 4.76E-06 | 9.82E-06 | 1.56E-05 | 2.26E-05 | 3.22E-05 | 4.67E-05 | 7.42E-05 | 1.53E-04 |
| 24 | 3.82E-07 | 2.67E-06 | 5.52E-06 | 8.76E-06 | 1.27E-05 | 1.81E-05 | 2.63E-05 | 4.17E-05 | 8.60E-05 |
| 96 | 5.96E-09 | 1.67E-07 | 3.45E-07 | 5.47E-07 | 7.95E-07 | 1.13E-06 | 1.64E-06 | 2.60E-06 | 5.37E-06 |

A much more useful table would be one that shows a relative comparison between the absolute $L_{crit}$ values of different controlled p-pulse rectifiers, such as Table 2. In Table 2, the 6-pulse controlled rectifier is treated as the basis to which the other p-pulse controlled rectifiers are compared. The $L_{crit}$ ratios become fixed percentages beyond the boundary angle for each controlled rectifier.

Table 2. Critical inductance as a percentage of 6-pulse critical inductance for selected firing angles for the controlled p-pulse rectifiers of Figure 15.

| | firing angle alpha (degrees) | | | | | | | | |
|---|---|---|---|---|---|---|---|---|---|
| pulse-count | 0 | 10 | 20 | 30 | 40 | 50 | 60 | 70 | 80 |
| 6 | 100% | 100% | 100% | 100% | 100% | 100% | 100% | 100% | 100% |
| 12 | 12% | 25% | 25% | 25% | 25% | 25% | 25% | 25% | 25% |
| 18 | 4% | 11% | 11% | 11% | 11% | 11% | 11% | 11% | 11% |
| 24 | 2% | 6% | 6% | 6% | 6% | 6% | 6% | 6% | 6% |
| 96 | <1% | <1% | <1% | <1% | <1% | <1% | <1% | <1% | <1% |

THIS PAGE INTENTIONALLY LEFT BLANK

# IV. DC OUTPUT VOLTAGE RIPPLE

The discussion of critical inductance began with the assumption that the instantaneous capacitor voltage was approximately equal to the average capacitor voltage (which was equal to the average load voltage). While it was useful then to conceptually think of the capacitor as being infinitely big and causing $v_C(t)$ to be constant, we know this is not the case. The load voltage will have some amount of ripple, but it will be mitigated by the capacitor during its charge and discharge periods.

## A. OUTPUT VOLTAGE RIPPLE FOR A CONTROLLED RECTIFIER WITH A RESISTIVE LOAD

While the concentration of this thesis is not specifically about phase controlled rectifiers with purely resistive loads, it is a good starting place to understand about output voltage ripple. The circuit of Figure 16 is an example of a controlled three-phase (6-pulse) rectifier with only a resistive load. However, let us consider it to be a controlled p-pulse rectifier for the proceeding output ripple voltage analysis.

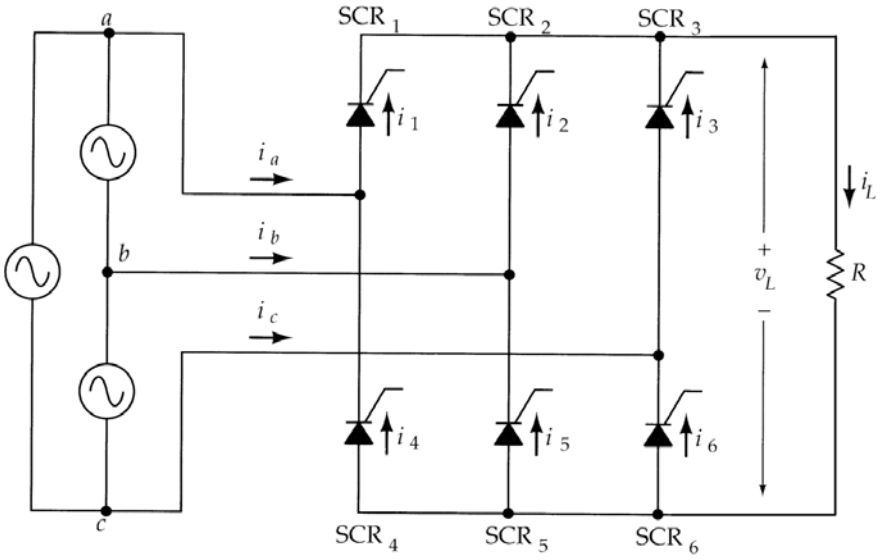


Figure 16. Circuit diagram of a controlled three-phase rectifier with a resistive load. From [4].

From [3] and [4], for $\alpha \le \theta_L$, the instantaneous load voltage is always positive or zero, and its average load voltage is synonymous to (70) and is given by

$$V_{avg} = \frac{ApV_m}{\pi}\cos\alpha \quad . \tag{126}$$

For $\alpha \ge \theta_L$, the instantaneous load voltage becomes negative in parts of the cycle and is expressed as

$$V_{avg} = \frac{p}{2\pi}\int_{\alpha+\theta_L}^{180^\circ} V_m \sin\gamma d\gamma \ , \tag{127}$$

where the upper integration limit is replaced with 180° to limit the instantaneous load voltage to either zero or positive values. Integrating and evaluating (127), we get

$$V_{avg} = \frac{V_m p}{2\pi}\left[1+\cos(\alpha+\theta_L)\right] \quad . \tag{128}$$

From [4], the root mean square (RMS) value of the load voltage is obtained by applying the definition of RMS, given by

$$V_{RMS} = \sqrt{\frac{1}{T}\int_0^T \left[v_s(t)\right]^2 dt} \quad . \tag{129}$$

Starting with the first case, we have

$$V_{RMS} = \sqrt{\frac{pV_m{}^2}{2\pi}\int_{\alpha+\theta_L}^{\alpha+\theta_U} \sin^2\gamma\, d\gamma} \quad . \tag{130}$$

By applying the trigonometric identity $\sin^2\theta = \left[1-\cos\left(2\theta\right)\right]/2$ to (130) and integrating, we get

$$V_{RMS} = \sqrt{\frac{pV_m{}^2}{8\pi}\left[2\gamma - \sin\left(2\gamma\right)\right]_{\gamma=\alpha+\theta_L}^{\gamma=\alpha+\theta_U}} \quad , \tag{131}$$

which, when evaluated, becomes

$$V_{RMS} = \sqrt{\frac{pV_m{}^2}{8\pi}\left\{\frac{4\pi}{p} - \left[\sin\left(2\alpha+2\theta_U\right) - \sin\left(2\alpha+2\theta_L\right)\right]\right\}} \quad . \tag{132}$$

By applying $\sin(a+b) = \sin\left(a\right)\cos\left(b\right) + \cos\left(a\right)\sin\left(b\right)$, we have

$$V_{RMS} = \sqrt{\frac{pV_m{}^2}{8\pi}\left[\begin{array}{l}\frac{4\pi}{p} + \sin\left(2\alpha\right)\cos\left(2\theta_L\right) + \cos\left(2\alpha\right)\sin\left(2\theta_L\right) \\ -\sin\left(2\alpha\right)\cos\left(2\theta_U\right) - \cos\left(2\alpha\right)\sin\left(2\theta_U\right)\end{array}\right]} \quad . \tag{133}$$

Next, let $E = \cos(2\theta_L)$, $F = \sin(2\theta_L)$, $G = \cos(2\theta_U)$, and $H = \sin(2\theta_U)$; therefore, $H = -F$ and $G = E$. Then, (133) reduces to

$$V_{RMS} = \frac{V_m}{\sqrt{2}}\sqrt{1 + \frac{Fp\cos\left(2\alpha\right)}{2\pi}} \quad . \tag{134}$$

Continuing with the second case, we have

$$V_{RMS} = \sqrt{\frac{pV_m{}^2}{2\pi} \int_{\alpha+\theta_L}^{180^\circ} \sin^2 \gamma d\gamma} \quad . \tag{135}$$

We again apply $\sin^2\theta = \left[1-\cos(2\theta)\right]/2$ to this result and integrate to obtain

$$V_{RMS} = \sqrt{\frac{pV_m{}^2}{8\pi}\left[2\gamma - \sin(2\gamma)\right]_{\gamma=\alpha+\theta_L}^{\gamma=180^\circ}} \quad , \tag{136}$$

which, when evaluated, becomes

$$V_{RMS} = \sqrt{\frac{pV_m{}^2}{8\pi}\left[\pi - \frac{\alpha\pi}{90} + \frac{2\pi}{p} + \sin(2\alpha + 2\theta_L)\right]} \quad . \tag{137}$$

By again applying $\sin(a+b) = \sin(a)\cos(b) + \cos(a)\sin(b)$, we have

$$V_{RMS} = \sqrt{\frac{pV_m{}^2}{8\pi}\left[\begin{array}{l} 2\pi - \frac{\alpha\pi}{90} - \pi + \frac{2\pi}{p} \\ +\sin(2\alpha)\cos(2\theta_L) + \cos(2\alpha)\sin(2\theta_L) \end{array}\right]} \quad . \tag{138}$$

Next, let $E = \cos(2\theta_L)$ and $F = \sin(2\theta_L)$. By substituting these into (138) and rearranging, we get

$$V_{RMS} = \frac{V_m}{\sqrt{2}}\sqrt{\frac{2+p}{4} - \frac{\alpha p}{360} + \frac{Ep\sin(2\alpha)}{4\pi} + \frac{Fp\cos(2\alpha)}{4\pi}} \quad . \tag{139}$$

Now we can compute the RMS ripple voltage $V_{RMS-ripple}$ for each case as

$$V_{RMS-ripple} = \sqrt{V_{RMS}^2 - V_{avg}^2} \quad . \tag{140}$$

For the first case ($\alpha \le \theta_L$), we substitute (134) and (126) into (140) to obtain

$$V_{RMS-ripple} = V_m \sqrt{\frac{1}{2}\left(1 + \frac{Fp\cos(2\alpha)}{2\pi}\right) - \frac{A^2 p^2}{\pi^2}\cos^2\alpha}\,, \tag{141}$$

while for the second case ($\alpha \geq \theta_L$), we substitute (139) and (128) into (140) to obtain

$$V_{RMS-ripple} = V_m \sqrt{\frac{1}{2}\left(\frac{2+p}{4} - \frac{\alpha p}{360} + \frac{Ep\sin(2\alpha)}{4\pi} + \frac{Fp\cos(2\alpha)}{4\pi}\right) - \frac{p^2}{4\pi^2}\left[1+\cos(\alpha+\theta_L)\right]^2}\,. \tag{142}$$

Computing the peak-to-peak ripple voltage $V_{pp-ripple}$ and the peak-to-peak ripple voltage as a percentage of the average output voltage $\%V_{pp/avg}$ are slightly more involved because there are actually three separate regions we must evaluate. The first two regions are actually sub-regions of the aforementioned first case, while the final region correlates with the second case from earlier. For the first region, given by $\alpha \leq (\theta_U - \theta_L)/2$, the maximum voltage is $V_m$, and the minimum voltage is $V_m \sin(\alpha + \theta_U)$. Therefore, $V_{pp-ripple_1}$ is their difference,

$$V_{pp-ripple_1} = V_m\left[1 - \sin(\alpha + \theta_U)\right], \tag{143}$$

which can be written in terms of $p$ as

$$V_{pp-ripple_1} = V_m\left[1 - \sin\left(\alpha + 90° + \frac{180°}{p}\right)\right]. \tag{144}$$

The peak-to-peak ripple voltage as a percentage of the average output voltage is given by

$$\%V_{pp/avg} = \left(\frac{V_{pp-ripple}}{V_{avg}}\right)100\%\,. \tag{145}$$

By substituting (144) and (126) into (145), we get

$$\%V_{pp/avg_1} = \left( \frac{1-\sin\left(\alpha+90°+\frac{180°}{p}\right)}{\frac{Ap}{\pi}\cos\alpha} \right) 100\% \quad . \tag{146}$$

The second region is given by $(\theta_U - \theta_L)/2 \le \alpha \le \theta_L$, in which the maximum voltage is $V_m \sin(\alpha+\theta_L)$, while the minimum voltage is $V_m \sin(\alpha+\theta_U)$. Therefore, $V_{pp-ripple_2}$ for this second interval is

$$V_{pp-ripple_2} = V_m\left[\sin(\alpha+\theta_L) - \sin(\alpha+\theta_U)\right], \tag{147}$$

which can be written in terms of $p$ as

$$V_{pp-ripple_2} = V_m\left[\sin\left(\alpha+90°-\frac{180°}{p}\right) - \sin\left(\alpha+90°+\frac{180°}{p}\right)\right]. \tag{148}$$

By substituting (148) and (126) into (145), we get the peak-to-peak ripple voltage as a percentage of the average output voltage

$$\%V_{pp/avg_2} = \left( \frac{\sin\left(\alpha+90°-\frac{180°}{p}\right) - \sin\left(\alpha+90°+\frac{180°}{p}\right)}{\frac{Ap}{\pi}\cos\alpha} \right) 100\% \quad . \tag{149}$$

Finally, the third region is given by $\alpha \ge \theta_L$. In this region, the maximum voltage is $V_m \sin(\alpha+\theta_L)$, and the minimum voltage is zero, making $V_{pp-ripple_3}$ equal to the maximum voltage or

$$V_{pp-ripple_3} = V_m \sin(\alpha+\theta_L), \tag{150}$$

which can be written in terms of $p$ as

$$V_{pp-ripple_3} = V_m \sin\left(\alpha + 90° - \frac{180°}{p}\right). \quad (151)$$

By substituting (151) and (128) into (145), we get the peak-to-peak ripple voltage as a percentage of the average output voltage

$$\%V_{pp/avg_3} = \left(\frac{\sin\left(\alpha + 90° - \frac{180°}{p}\right)}{\frac{p}{2\pi}\left[1 + \cos(\alpha + \theta_L)\right]}\right) 100\% . \quad (152)$$

The results of both cases for a 6-pulse rectifier with $V_m$ equal to 1.0 V and a purely resistive load are summarized in Figures 17 and 18. Initially, as $\alpha$ increases, the difference between the RMS load voltage and the average load voltage increases, making the square root of the difference of their squares grow, causing the RMS load voltage ripple to steadily increase. However, as $\alpha$ continues beyond 60°, the square root of the difference of their squares begins to decrease, causing the RMS load voltage ripple to peak and also begin to decrease. The peak-to-peak ripple load voltage rapidly increases until reaching a subtle inflection point at $\alpha = 30°$ and then increases less rapidly until reaching a maximum at $\alpha = 60°$, where it begins to rapidly decrease.

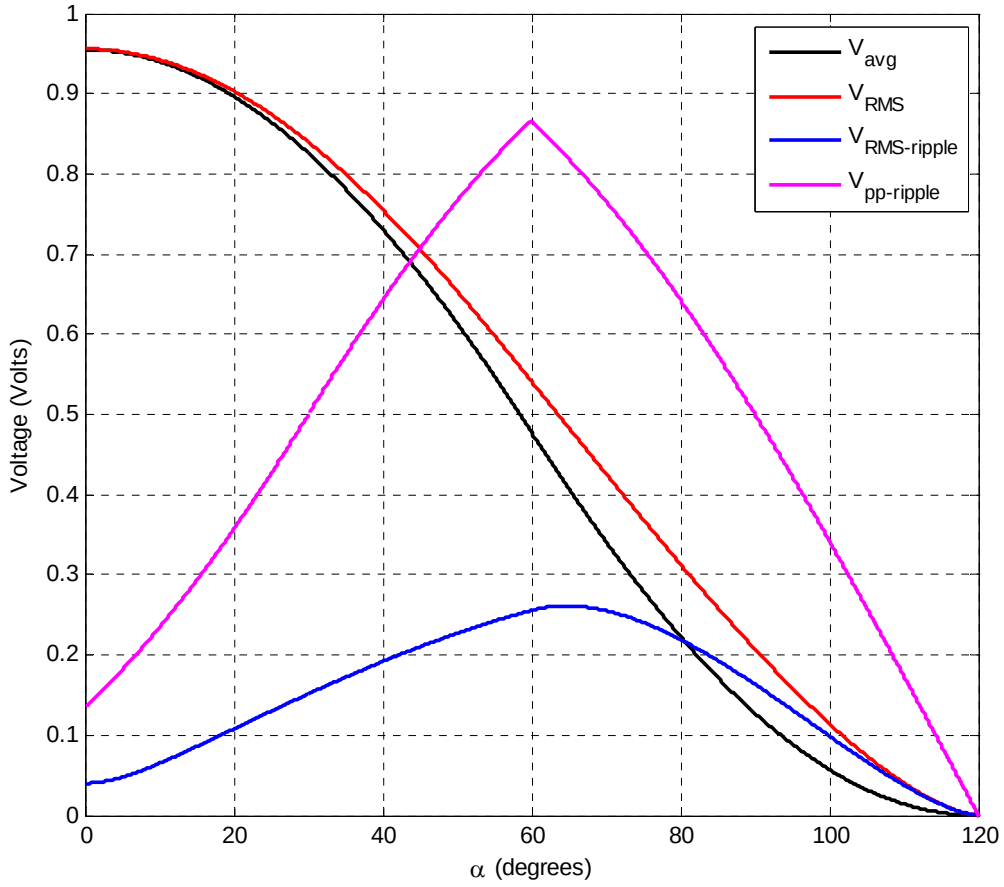


Figure 17. Average voltage, RMS voltage, RMS ripple voltage, and peak-to-peak ripple voltage for a 6-pulse rectifier circuit with a unity $V_m$ and a purely resistive load.

The peak-to-peak ripple voltage as a percentage of the average output voltage increases as $\alpha$ increases to 60° (the transition at 30° is virtually undetectable) because $V_{avg}$ is fairly high and decreasing while $V_{pp-ripple}$ is low but growing quickly. Beyond 60°, $\%V_{pp/avg}$ increases at a tremendous rate

due to $V_{avg}$ decreasing at a faster rate than $V_{pp-ripple}$. This illustrates another reason why circuit designers prefer to keep $\alpha$ fairly small.

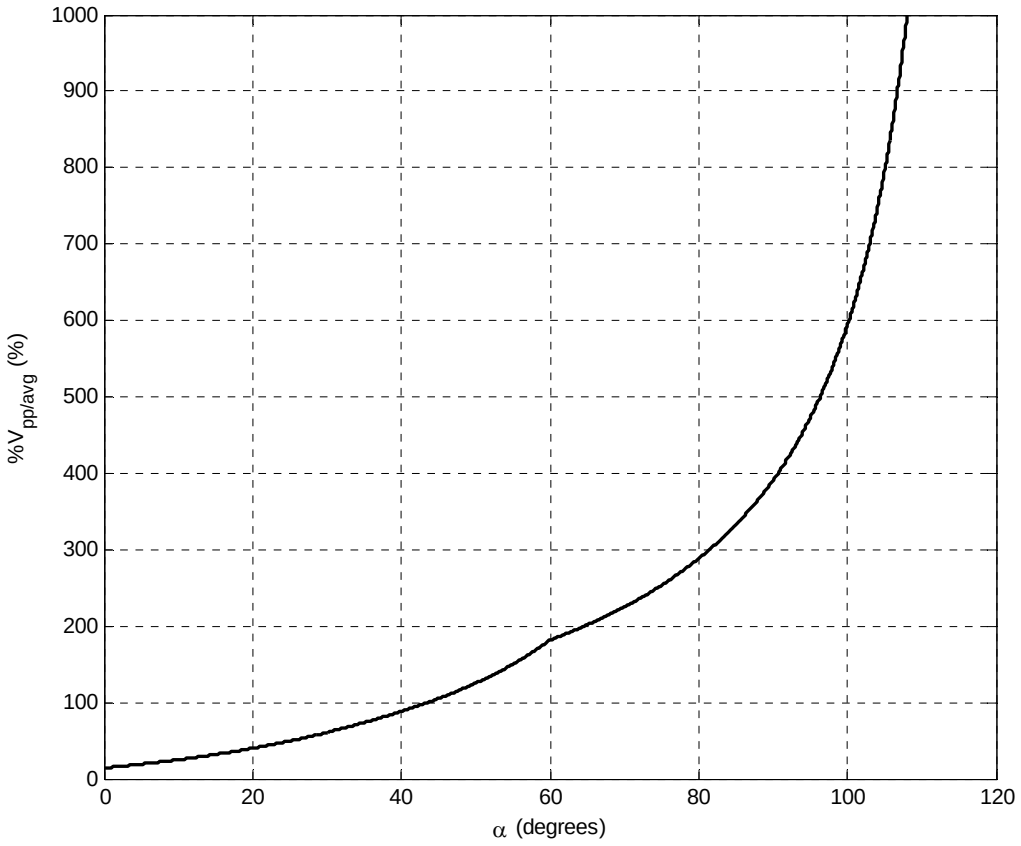


Figure 18. Peak-to-peak ripple voltage as a percentage of the average output voltage for a 6-pulse rectifier circuit with a unity $V_m$ and a purely resistive load.

In order to demonstrate how increasing pulse count improves the peak-to-peak ripple voltage as a percentage of the average output voltage for these types of rectifiers, $\%V_{pp/avg}$ has been plotted for several p-pulse rectifier circuits in Figure 19. The plot exhibits very similar

behavior to Figure 15 in that increasing pulse count yields better results (with rapidly diminishing returns), while increasing $\alpha$ worsens the results. While not shown in Figure 19, further increasing $\alpha$ beyond $\theta_L$ (or much beyond 30°, for that matter) is purely academic as $\%V_{pp/avg}$ very rapidly reaches exorbitant amounts. This also illustrates why a rectifier with a purely resistive load is an unlikely candidate for a rectifier which necessitates a low $\%V_{pp/avg}$ as it will require a high pulse count (increased hardware complexity, cost, and space).

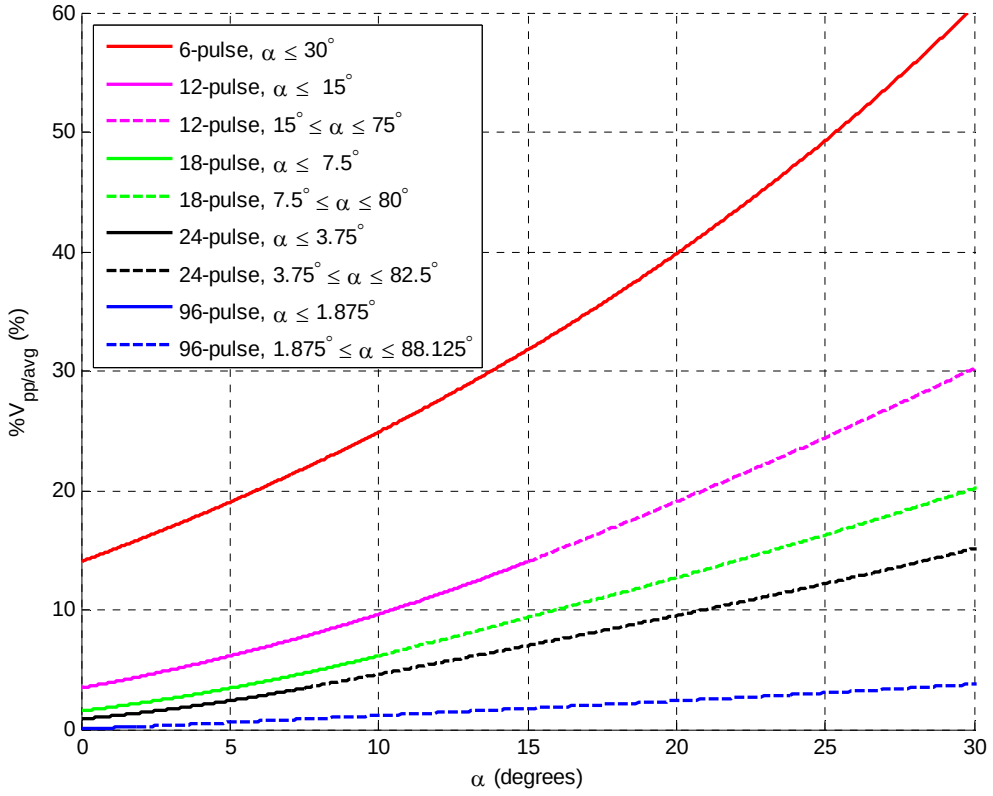


Figure 19. Peak-to-peak ripple voltage as a percentage of the average output voltage for p-pulse rectifier circuits with unity $V_m$ and purely resistive loads.

To help in understanding some of the items associated with angles for the p-pulse rectifiers with purely resistive loads, a quick reference summary is provided in Table 3. For instance, for a 12-pulse rectifier with a purely resistive load, its first pulse starts at 75° and ends at 105°, making its pulse width 30° (their difference); its three regions of varying peak-to-peak voltage (and, hence, differing $\%V_{pp/avg}$) are the intervals of $\alpha$ from 0° to 15°, 15° to 75°, and 75° to 105°.

Table 3. Angular characteristics of some p-pulse controlled rectifiers with purely resistive loads.

| | $\theta_L$ | $\theta_U$ | pulse-width | $\alpha_{limit\ 1}$ | $\alpha_{limit\ 2}$ | $\alpha_{upper\ limit}$ |
|---|---|---|---|---|---|---|
| pulse-count | (degrees) | (degrees) | (degrees) | (degrees) | (degrees) | (degrees) |
| 6 | 60 | 120 | 60 | 30 | 60 | 120 |
| 12 | 75 | 105 | 30 | 15 | 75 | 105 |
| 18 | 80 | 100 | 20 | 10 | 80 | 100 |
| 24 | 82.5 | 97.5 | 15 | 7.5 | 82.5 | 97.5 |
| 96 | 88.125 | 91.875 | 3.75 | 1.875 | 88.125 | 91.875 |

Just as Table 1 was developed to provide $L_{crit}$ for selected values of $\alpha$, Table 4 does the same for $\%V_{pp/avg}$ for the waveforms of Figure 19. Firing angles of 120° for the 6-pulse controlled rectifier and 100° for the 18-pulse controlled rectifier would result in infinite $\%V_{pp/avg}$ because those values of $\alpha$ are the upper limits (and, therefore, not inclusive) for the two rectifiers, in accordance with Table 3.

Table 4. Peak-to-peak ripple voltage as a percentage of the average output voltage for selected firing angles for the controlled p-pulse rectifier waveforms of Figure 19.

| | firing angle alpha (degrees) | | | | | | | | | | | |
|---|---|---|---|---|---|---|---|---|---|---|---|---|
| pulse-count | 0 | 10 | 20 | 30 | 40 | 50 | 60 | 70 | 80 | 90 | 100 | 110 |
| 6 | 14% | 25% | 40% | 60% | 88% | 125% | 181% | 225% | 288% | 391% | 594% | 1197% |
| 12 | 3% | 10% | 19% | 30% | 44% | 62% | 91% | 144% | 236% | 398% | 1199% | |
| 18 | 2% | 6% | 13% | 20% | 29% | 42% | 60% | 96% | 198% | 399% | ∞ | |
| 24 | <1% | 5% | 10% | 15% | 22% | 31% | 45% | 72% | 148% | 399% | | |
| 96 | <1% | 1% | 2% | 4% | 5% | 8% | 11% | 18% | 37% | 400% | | |

While the data presented by Table 4 is somewhat useful for quickly finding the value of $\%V_{pp/avg}$ for a given value of $\alpha$ for a particular p-pulse controlled rectifier with a resistive load, another way to look at the data is by assigning the $\%V_{pp/avg}$ of the 6-pulse controlled rectifier as the basis to which the others are compared. The result is Table 5. For realistic values of $\alpha$, higher pulse count controlled rectifiers clearly possess much less $\%V_{pp/avg}$ than lower pulse count variants.

Table 5. Peak-to-peak ripple voltage as a percentage of the average output voltage as a percentage of 6-pulse $\%V_{pp/avg}$ for selected firing angles for the controlled p-pulse rectifier waveforms of Figure 19.

| | firing angle alpha (degrees) | | | | | | | | | | | |
|---|---|---|---|---|---|---|---|---|---|---|---|---|
| pulse-count | 0 | 10 | 20 | 30 | 40 | 50 | 60 | 70 | 80 | 90 | 100 | 110 |
| 6 | 100% | 100% | 100% | 100% | 100% | 100% | 100% | 100% | 100% | 100% | 100% | 100% |
| 12 | 25% | 39% | 48% | 50% | 50% | 50% | 50% | 64% | 82% | 102% | 202% | |
| 18 | 11% | 25% | 32% | 33% | 33% | 33% | 33% | 43% | 69% | 102% | ∞ | |
| 24 | 6% | 19% | 24% | 25% | 25% | 25% | 25% | 32% | 52% | 102% | | |
| 96 | <1% | 5% | 6% | 6% | 6% | 6% | 6% | 8% | 13% | 102% | | |

## B. OUTPUT VOLTAGE RIPPLE FOR A CONTROLLED RECTIFIER WITH A TWO-POLE *LC* OUTPUT FILTER

Turning back to the circuit of Figure 9, we now desire to calculate the output ripple for the type of circuit we are primarily interested in analyzing. It turns out that the voltage ripple calculations for a controlled rectifier with a two-pole *LC* output filter are actually somewhat simpler than those for the controlled rectifier with a purely resistive load because we are going to assume the inductor is always large enough to maintain a continuous current; therefore, there is only one case to evaluate, not two. Additionally, some of the calculations are the same as for the purely resistive case, so we need not repeat our previous work. To begin from [4], the average capacitor voltage is given by (70), and the RMS load voltage is given by (134). Then, the RMS ripple voltage is given by

$$V_{RMS-ripple} = \sqrt{V_{RMS}^2 - V_{C(avg)}^2} \,. \tag{153}$$

Here we will make a small notation change, letting $V_{DC}$ be equal to $V_{avg}$ and $V_{AC}$ be equal to $V_{RMS-ripple}$ to better illustrate the relationship between RMS, DC, and AC quantities. Additionally, it is important to understand that $V_{AC}$ is applied across the entire load (which includes the resistor, capacitor, and the inductor). Therefore, (153) becomes

$$V_{AC} = \sqrt{V_{RMS}^2 - V_{DC}^2} \tag{154}$$

and (141) becomes

$$V_{AC} = V_m \sqrt{\frac{1}{2}\left(1 + \frac{Fp\cos(2\alpha)}{2\pi}\right) - \frac{A^2 p^2}{\pi^2}\cos^2\alpha} \ . \tag{155}$$

The impedance of the capacitor is

$$Z_C \cong \frac{1}{jp\omega C} \tag{156}$$

and the impedance of the inductor is

$$Z_L \cong jp\omega L \ , \tag{157}$$

where these are considered approximations because $Z_C$ and $Z_L$ are composed of the frequencies $p\omega$, $2p\omega$, $3p\omega$, etc.; however, the dominant frequency is $p\omega$. Next, the impedance of the capacitor in parallel with the resistor is

$$Z_{R\|C} \cong \frac{R}{1 + jp\omega RC} \ , \tag{158}$$

which can be written in terms of real and imaginary parts as

$$Z_{R\|C} \cong \frac{R}{1 + (p\omega RC)^2} - j\frac{p\omega R^2 C}{1 + (p\omega RC)^2} \ . \tag{159}$$

The impedance of $Z_L$ in series with $Z_{R\|C}$ is

$$Z_{total} \cong \frac{R}{1+\left(p\omega RC\right)^2} + j\left[p\omega L - \frac{p\omega R^2 C}{1+\left(p\omega RC\right)^2}\right], \tag{160}$$

which can be rewritten as

$$Z_{total} \cong \frac{R}{1+\left(p\omega RC\right)^2} + j\left[\frac{p\omega L + p^3\omega^3 R^2 LC^2 - p\omega R^2 C}{1+\left(p\omega RC\right)^2}\right]. \tag{161}$$

The magnitude of $Z_{total}$ becomes

$$\left|Z_{total}\right| \cong \sqrt{\left[\frac{R}{1+\left(p\omega RC\right)^2}\right]^2 + \left[\frac{p\omega L + p^3\omega^3 R^2 LC^2 - p\omega R^2 C}{1+\left(p\omega RC\right)^2}\right]^2}. \tag{162}$$

We can now solve for $\left|I_{AC}\right|$ from Ohm's Law as

$$\left|I_{AC}\right| \cong \frac{V_{AC}}{\left|Z_{total}\right|}. \tag{163}$$

By substituting (155) and (162) into (163), we get

$$\left|I_{AC}\right| \cong \frac{V_m\sqrt{\frac{1}{2}\left(1+\frac{Fp\cos\left(2\alpha\right)}{2\pi}\right) - \frac{A^2p^2}{\pi^2}\cos^2\alpha}}{\sqrt{\left[\frac{R}{1+\left(p\omega RC\right)^2}\right]^2 + \left[\frac{p\omega L + p^3\omega^3 R^2 LC^2 - p\omega R^2 C}{1+\left(p\omega RC\right)^2}\right]^2}}. \tag{164}$$

Therefore, the capacitor RMS voltage $V_{C(RMS)}$ is given by

$$V_{C(RMS)} \cong \left|I_{AC}\right|\left|Z_C\right| \tag{165}$$

and the capacitor peak-to-peak ripple voltage is

$$V_{C(pp-ripple)} \cong \left(2\sqrt{2}\right)V_{C(RMS)}. \tag{166}$$

Here, it is important to note another approximation that has taken place. We have made the assumption that $V_{C(RMS)}$ is a perfect sinusoid such that its peak value is simply equal to $\sqrt{2}V_{C(RMS)}$. Finally, the capacitor peak-to-peak ripple voltage as a percentage of the average output voltage $\%V_{C(pp/avg)}$ is

$$\%V_{C(pp/avg)} \cong \left( \frac{V_{C(pp-ripple)}}{V_{C(avg)}} \right) 100\% , \qquad (167)$$

where $V_{C(avg)}$ is given by (70) and $V_{C(pp-ripple)}$ is given by (166).

One of the things that would be interesting to investigate is how $\%V_{C(pp/avg)}$ behaves as the individual circuit elements (inductor, capacitor, and resistor) are changed one at a time. While the behavior of $\%V_{C(pp/avg)}$ for every circuit is unique depending on its peak line-to-line input voltage $V_m$, pulse count, and the values of the inductor, capacitor, and resistor, we will examine one case with the aid of Figure 20. The particular circuit that generated the waveforms of Figure 20 is a 6-pulse controlled rectifier (in the configuration given by Figure 9) with a $V_m$ of 100 V, a 25 mH inductor, a 50 $\mu$F capacitor, and a 10$\Omega$ resistor. Through some initial trial and error with different resistance values, it was discovered that $\%V_{C(pp/avg)}$ was very insensitive to changes in the resistance, so it was excluded from further sensitivity analysis. The initial values of the inductor and capacitor are as previously mentioned and are designated as $L_0$ and $C_0$ in the legend of Figure 20.

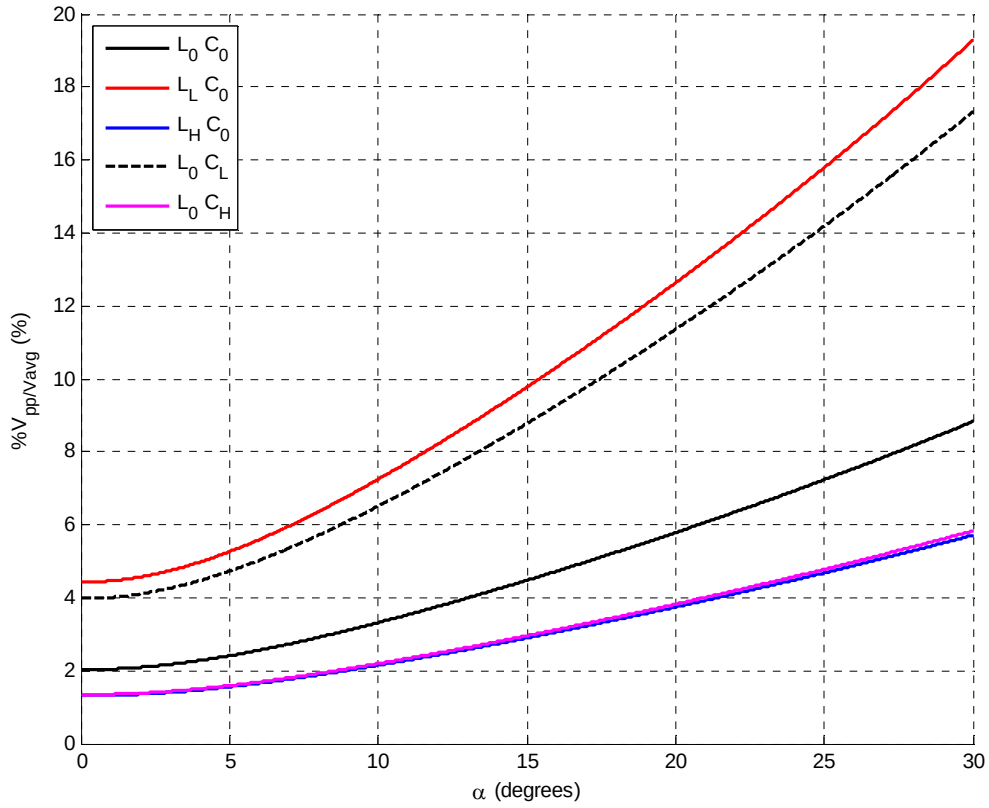


Figure 20. Capacitor peak-to-peak ripple voltage as a percentage of the average output voltage for a 6-pulse controlled rectifier with a two-pole *LC* output filter.

Somewhat arbitrarily, it was decided to increase and decrease $L_0$ and $C_0$ by fifty percent to observe the effect on $\%V_{C(pp/avg)}$ (care had to be taken to ensure the circuit was still in CCM for the reduced inductor value). The larger inductor and capacitor are designated as $L_H$ and $C_H$ in the legend of Figure 20, while the reduced components are $L_L$ and $C_L$, respectively. Interestingly, the combination of a reduced inductor and initial capacitor (worst $\%V_{C(pp/avg)}$) produced close results to the initial inductor and reduced

capacitor pair, while the larger inductor and initial capacitor produced nearly identical results to the combination of the initial inductor and bigger capacitor—both of which could be said to have the best $\%V_{C(pp/avg)}$.

In order to see how increasing pulse count affects $\%V_{C(pp/avg)}$, $\%V_{C(pp/avg)}$ was plotted in Figure 21 for a 6-, 12-, 18-, 24-, and 96-pulse controlled rectifier with a two-pole *LC* output filter using the same initial component values and $V_m$ as before.

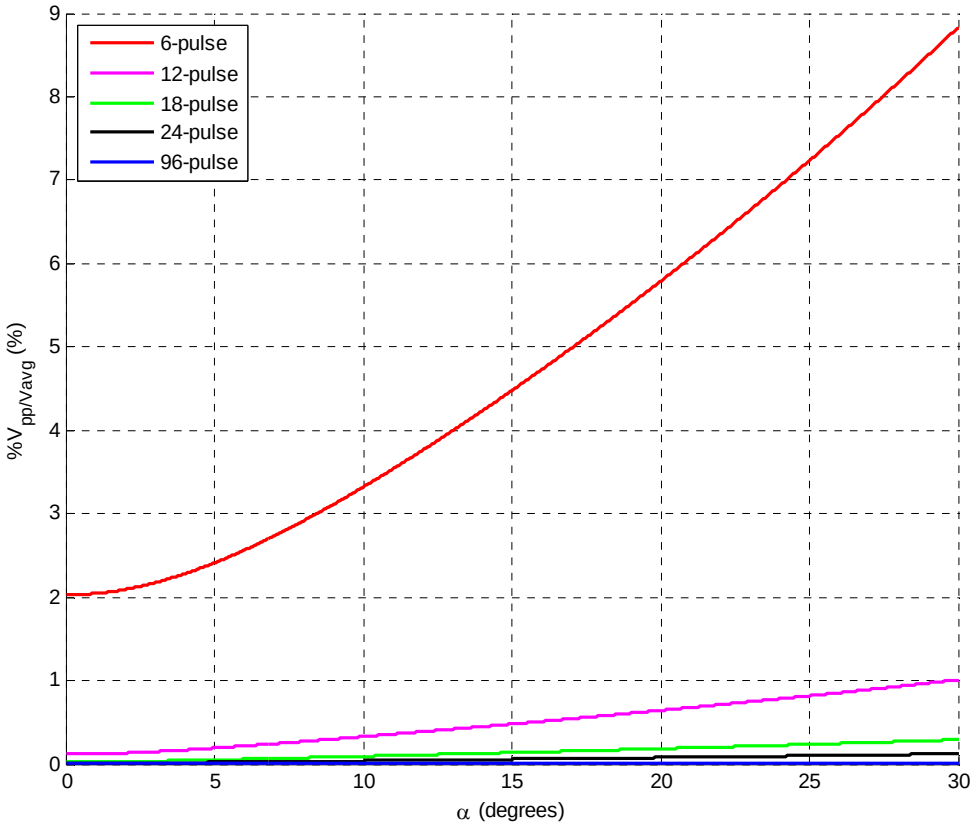


Figure 21. Capacitor peak-to-peak ripple voltage as a percentage of the average output voltage for a 6-, 12-, 18-, 24-, and 96-pulse controlled rectifier with a two-pole *LC* output filter.

Much like the plots of Figures 15 and 19, tremendous improvement is noted in increasing from a 6–pulse to a 12-pulse controlled circuit, but further increasing pulse count results in less of an improvement.

The values of $\%V_{C(pp/avg)}$ for selected values of $\alpha$ for the waveforms of Figure 21 are collected in tabular form in Table 6. The capacitor peak-to-peak ripple voltage as a percentage of the average output voltage approaches infinity at the firing angle limit of 90° because $V_{C(avg)}$ is zero at 90°; hence, the firing angle limit is exclusive of 90°.

Table 6. Capacitor peak-to-peak ripple voltage as a percentage of the average output voltage for selected firing angles for the controlled p-pulse rectifier waveforms of Figure 21.

| | firing angle alpha (degrees) | | | | | | | | |
|---|---|---|---|---|---|---|---|---|---|
| pulse-count | 0 | 10 | 20 | 30 | 40 | 50 | 60 | 70 | 80 |
| 6 | 2% | 3% | 6% | 9% | 13% | 18% | 26% | 41% | 84% |
| 12 | <1% | <1% | <1% | 1% | 1% | 2% | 3% | 5% | 10% |
| 18 | <1% | <1% | <1% | <1% | <1% | <1% | <1% | 1% | 3% |
| 24 | <1% | <1% | <1% | <1% | <1% | <1% | <1% | <1% | 1% |
| 96 | <1% | <1% | <1% | <1% | <1% | <1% | <1% | <1% | <1% |

As stated previously, every circuit of this type is unique and will produce differing $\%V_{C(pp/avg)}$ depending on the parameters of the controlled rectifier with a two-pole *LC* output filter; therefore, Table 6 has limited utility. However, if we employ the technique we have previously used and treat $\%V_{C(pp/avg)}$ for the 6-pulse controlled rectifier as the basis to which the other rectifiers are compared, we

generate Table 7. As opposed to Table 6, which deals in absolutes, the relationships in Table 7 are always valid no matter what the controlled rectifier circuit parameters and value of $V_m$ are (so long as the circuit remains in CCM).

Table 7. Capacitor peak-to-peak ripple voltage as a percentage of the average output voltage as a percentage of 6-pulse $\%V_{C(pp/avg)}$ for selected firing angles for the controlled p-pulse rectifier waveforms of Figure 21.

| | firing angle alpha (degrees) | | | | | | | | |
|---|---|---|---|---|---|---|---|---|---|
| pulse-count | 0 | 10 | 20 | 30 | 40 | 50 | 60 | 70 | 80 |
| 6 | 100% | 100% | 100% | 100% | 100% | 100% | 100% | 100% | 100% |
| 12 | 5.8% | 9.9% | 11.1% | 11.4% | 11.6% | 11.6% | 11.6% | 11.7% | 11.7% |
| 18 | 1.1% | 2.8% | 3.2% | 3.3% | 3.4% | 3.4% | 3.4% | 3.4% | 3.4% |
| 24 | <1% | 1.1% | 1.3% | 1.4% | 1.4% | 1.4% | 1.4% | 1.4% | 1.4% |
| 96 | <1% | <1% | <1% | <1% | <1% | <1% | <1% | <1% | <1% |

# V. HARMONICS

## A. BACKGROUND

Harmonics have existed on power systems from the time of the very first generators. At that time, the harmonic components were so small that their effects on systems were negligible. This was due to the lack of non-linear loads before the 1960s [12]. However, in recent years, there has been a significant increase in the installation and use of power electronics equipment onboard ships and at offshore installations. The operation of this equipment can, and has in many cases, significantly degraded the ship or offshore installation electrical power quality to such an extent that corrective measures have to be implemented in order to reduce the resultant adverse effects on the electrical plant and equipment. The quality and security of voltage supplies are important to the safety of any vessel and its crew and to the protection of the marine environment. Any failure or malfunction of equipment such as propulsion or navigation systems can result in an accident at sea or close ashore with dire consequences. What we are talking about is harmonic distortion of voltage supplies caused by the operation of electronic devices which draw non-linear (i.e., non-sinusoidal in nature) currents from the voltage supplies. These very same pieces of non-linear equipment can also be adversely affected by harmonic currents and the subsequent voltage distortion they produce, as can the majority of linear equipment (particularly generators, AC motors and transformers) [13].

## B. COMMON PROBLEMS ASSOCIATED WITH HARMONICS

Power converters are considered the primary source of undesired harmonics. These AC/DC power converters are extensively used in various applications like power supplies, DC motor drives, front-end converters in adjustable-speed AC drives, high voltage DC transmission, switched-mode power systems, fluorescent lights (with electronic ballasts), utility interfaces with non-conventional energy sources, in-process technology like welding, power supplies for telecommunications systems, aerospace, and military environments. Traditionally, AC/DC power conversion has been dominated by diode or phase controlled rectifiers which act as non-linear loads on power systems and draw input currents that are rich in harmonics and have poor supply power factor, thereby creating the power quality problem for the distribution network and for other electrical systems in the same vicinity of the rectifier. Some common problems associated with the production of these harmonics include:

- Large reactive power drawn by rectifiers from the power system which requires that the distribution equipment handle large power, thus, increasing its volt-ampere ratings;
- Voltage drops at the buses;
- Higher input current harmonics resulting in the distorted line current which tends to distort the line voltage waveform. This often creates problems in the reliable operation of sensitive equipment operating on the same bus;
- Increased losses in the equipment such as transformers and motors connected to the utility;
- Electromagnetic interference with any nearby communications circuits;

- Excessive neutral current, resulting in overheated neutrals. The currents of triplen harmonics, especially odd harmonics ($3^{rd}$, 9th 15th, etc.) are actually additive in the neutral of three-phase, wye-connected circuits;
- Measuring equipment and meters reading incorrectly, including induction disc-type Watt-hour meters and averaging type current meters;
- Blown fuses on power factor correction capacitors due to high voltages and currents from resonance with line impedance and capacitor bank failures;
- Mal-operation of equipment such as computers, telephone systems, and electronic controllers;
- Nuisance operation of protective devices including false tripping of relays and failure of uninterruptible power supplies to transfer properly, especially if the controls incorporate zero-crossing sensing circuits; and
- Damaging dielectric heating in cables [14].

## C. VISUAL REPRESENTATIONS OF HARMONICS

Before delving directly into the mathematics and equations dealing with harmonics, it is useful to go a bit deeper into what is meant by a load being either linear or non-linear. A linear load will draw current that is proportional to the applied voltage, as in Figure 22 [13].

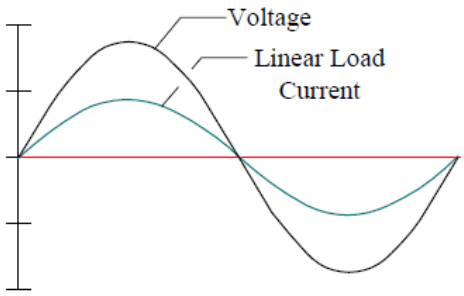


Figure 22. Voltage and current waveforms for a linear load. From [13].

It stands to reason then, that a non-linear load will draw a current that does not flow in proportion to the applied voltage [15]. One such example of a non-linear load is the load current profile for a three-phase AC drive shown in Figure 23.

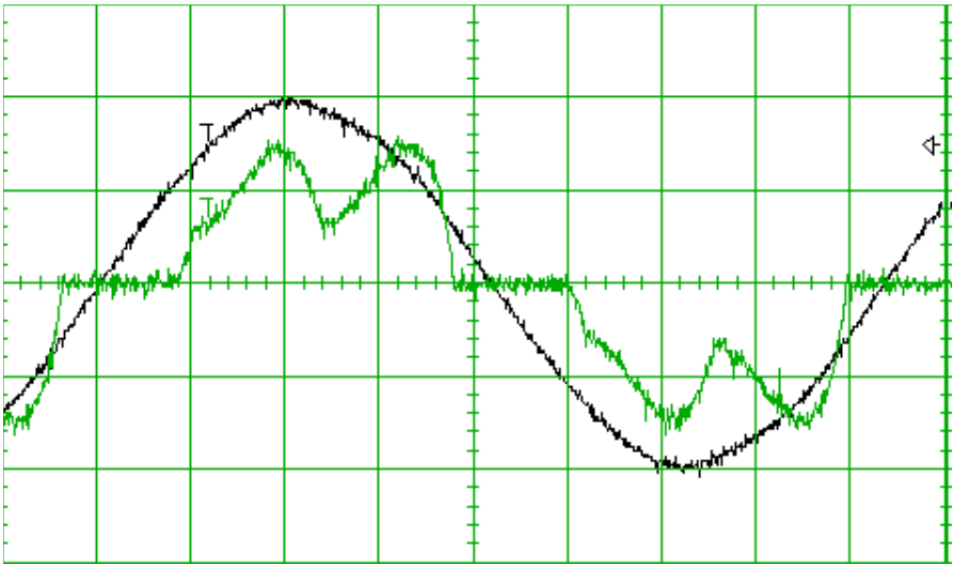

Figure 23. Input line to neutral voltage (in black) and input current (in green) of phase A for a three-phase AC drive. From [15].

Around the 1830s, a French mathematician named Fourier discovered that a distorted waveform—like the current waveform shown in Figure 23—can be represented as a series of sine waves, each an integer number multiple of the fundamental frequency and each with a specific magnitude. For example, for a 60 Hz system, the fundamental frequency is 60 Hz and the 5th harmonic would be five times 60 Hz or 300 Hz [15]. When all harmonics are added to the fundamental, a waveform known as a complex wave is formed. A simple example of a complex wave consisting of the

fundamental and 3rd harmonic is shown in Figure 24. The complex wave is clearly the algebraic summation of the other two waves [13].

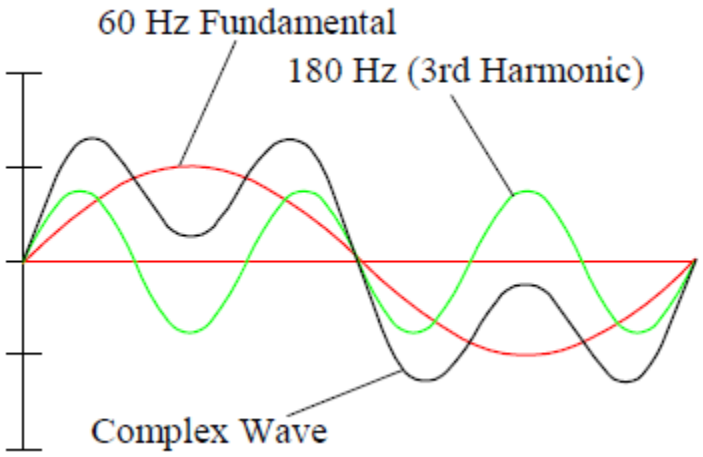


Figure 24. Construction of a complex wave from the fundamental and 3rd harmonic. From [13].

The collective sum of the fundamental and each harmonic is called a Fourier series. This series is often viewed as a spectrum analysis where the fundamental frequency and each harmonic component are displayed graphically in a bar chart format as shown in Figure 25. The total current is the square root of the sum of the squares of the individual harmonic components. One general thing we can say regarding the harmonic content of something is by simply looking at the wave shape. The more it looks like a sine wave, the lower the harmonic content [15].

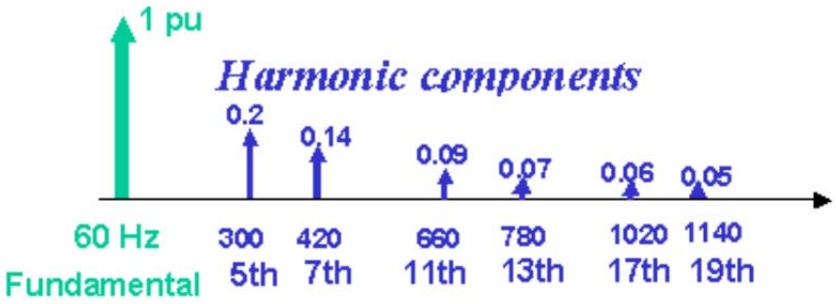


Figure 25. Harmonic spectrum analysis. From [15].

## D. FOURIER SERIES AND TOTAL HARMONIC DISTORTION

From [16], in general, any non-sinusoidal waveform $f(t)$ repeating with an angular frequency $\omega$ can be expressed as

$$f(t) = F_0 + \sum_{h=1}^{\infty} f_h(t) = \frac{1}{2}a_0 + \sum_{h=1}^{\infty}\left\{a_h \cos(h\omega t) + b_h \sin(h\omega t)\right\}, \qquad (168)$$

where $h$ is the harmonic number and $F_0 = a_0/2$ is the average value. Additionally, we have

$$a_h = \frac{1}{\pi}\int_0^{2\pi} f(t)\cos(h\omega t)d(\omega t) \qquad (169)$$

and

$$b_h = \frac{1}{\pi}\int_0^{2\pi} f(t)\sin(h\omega t)d(\omega t), \qquad (170)$$

in which $h = 0,...,\infty$. From (168) and (169), we can solve for the average value $F_0$ (taking note that $\omega = 2\pi/T$) as

$$F_0 = \frac{1}{2}a_0 = \frac{1}{2\pi}\int_0^{2\pi} f(t)d(\omega t) = \frac{1}{T}\int_0^{T} f(t)dt \quad . \qquad (171)$$

Oftentimes, AC waveforms have a zero average value. Moreover, by the use of waveform symmetry, it is often

possible to simplify the calculations of $a_h$ and $b_h$ in (169) and (170). A list of the types of symmetry, requirements, and formulas for $a_h$ and $b_h$ is provided in Table 8.

Table 8. Use of symmetry in Fourier analysis. From [16].

| *Symmetry* | *Condition Required* | $a_h$ and $b_h$ |
|---|---|---|
| Even | $f(-t) = f(t)$ | $b_h = 0 \quad a_h = \frac{2}{\pi}\int_0^{\pi} f(t)\cos(h\omega t)\, d(\omega t)$ |
| Odd | $f(-t) = -f(t)$ | $a_h = 0 \quad b_h = \frac{2}{\pi}\int_0^{\pi} f(t)\sin(h\omega t)\, d(\omega t)$ |
| Half-wave | $f(t) = -f(t + \frac{1}{2}T)$ | $a_h = b_h = 0$ for even $h$<br>$a_h = \frac{2}{\pi}\int_0^{\pi} f(t)\cos(h\omega t)\, d(\omega t)$ for odd $h$<br>$b_h = \frac{2}{\pi}\int_0^{\pi} f(t)\sin(h\omega t)\, d(\omega t)$ for odd $h$ |
| Even quarter-wave | Even and half-wave | $b_h = 0$ for all $h$<br>$a_h = \begin{cases} \frac{4}{\pi}\int_0^{\pi/2} f(t)\cos(h\omega t)\, d(\omega t) & \text{for odd } h \\ 0 & \text{for even } h \end{cases}$ |
| Odd quarter-wave | Odd and half-wave | $a_h = 0$ for all $h$<br>$b_h = \begin{cases} \frac{4}{\pi}\int_0^{\pi/2} f(t)\sin(h\omega t)\, d(\omega t) & \text{for odd } h \\ 0 & \text{for even } h \end{cases}$ |

For simplicity, let us now assume that we have a purely sinusoidal utility input voltage at the fundamental frequency (with $\omega_1 = \omega$ and $f_1 = f$) as $v_s(t) = \sqrt{2}V_s \sin\omega_1 t$. Then, from [16], the input current in steady state is the sum of its Fourier (harmonic) components, given by

$$i_s(t) = i_{s1}(t) + \sum_{h\neq 1} i_{sh}(t)\,, \tag{172}$$

where we have assumed there is no DC component in $i_s$, $i_{s1}$ is the fundamental (line frequency $f_1$) component, and $i_{sh}$ is the component at the $h$ harmonic frequency $f_h (= hf_1)$. The amount of distortion in the current waveform is quantified by means of an index termed the THD. The distortion part of the current $i_{dis}$ is given by

$$i_{dis}(t) = i_s(t) - i_{s1}(t) = \sum_{h \neq 1} i_{sh}(t) \,. \tag{173}$$

In terms of RMS values, we have

$$I_{dis} = \sqrt{I_s^2 - I_{s1}^2} = \sqrt{\sum_{h \neq 1} I_{sh}^2} \,, \tag{174}$$

where the RMS value of $i_s(t)$ has been determined by

$$I_s = \sqrt{\frac{1}{T}\int_0^T [i_s(t)]^2 dt} \,. \tag{175}$$

Finally, the THD of the current is defined as

$$\%THD_i = 100\% \left( \frac{I_{dis}}{I_{s1}} \right) = 100\% \left( \frac{\sqrt{I_s^2 - I_{s1}^2}}{I_{s1}} \right). \tag{176}$$

## E. REDUCTION OF HARMONICS BY INCREASING PULSE NUMBER

One of the most important benefits gained by increasing the pulse count of a controlled rectifier is a reduction in harmonic content. Without diving into the detailed mathematics about why this is the case, suffice it to say that when multiple properly phase shifted converters are connected in series or parallel, harmonic cancellation occurs such that the line currents drawn by a p-pulse converter system have a harmonic content given by

$$h = kp \pm 1, \tag{177}$$

where $k = 1,2,3\ldots$ [6]. Additionally, from [16], the RMS values of the harmonic components are inversely proportional to their harmonic order as

$$I_{sh} = \frac{I_{s1}}{h}. \tag{178}$$

From (177) and (178), it is easy to understand that higher pulse count systems will have smaller harmonics that are further away from the fundamental component.

It is natural to consider a 6-pulse controlled rectifier system as the basic building block from which higher pulse count systems are constructed. In order to achieve the desired harmonic elimination using stacked 6-pulse rectifiers, the required phase shift between individual rectifiers is given as phase shift $\phi$ equals 60° divided by the number of 6-pulse converters [16]. For example, a 12-pulse converter would be made from two 6-pulse converters, and 60°/2=30°; therefore, the required phase shift between the two 6-pulse converters is 30°. One realization of such a system is shown in Figure 26. The system consists of two bridge rectifiers connected so that the DC outputs are in series and the two voltages add. The AC inputs to the two bridges are isolated by two transformers that are connected wye-delta and delta-delta, respectively. The transformers are connected to take advantage of the differing phase shifts of the two connections [3].

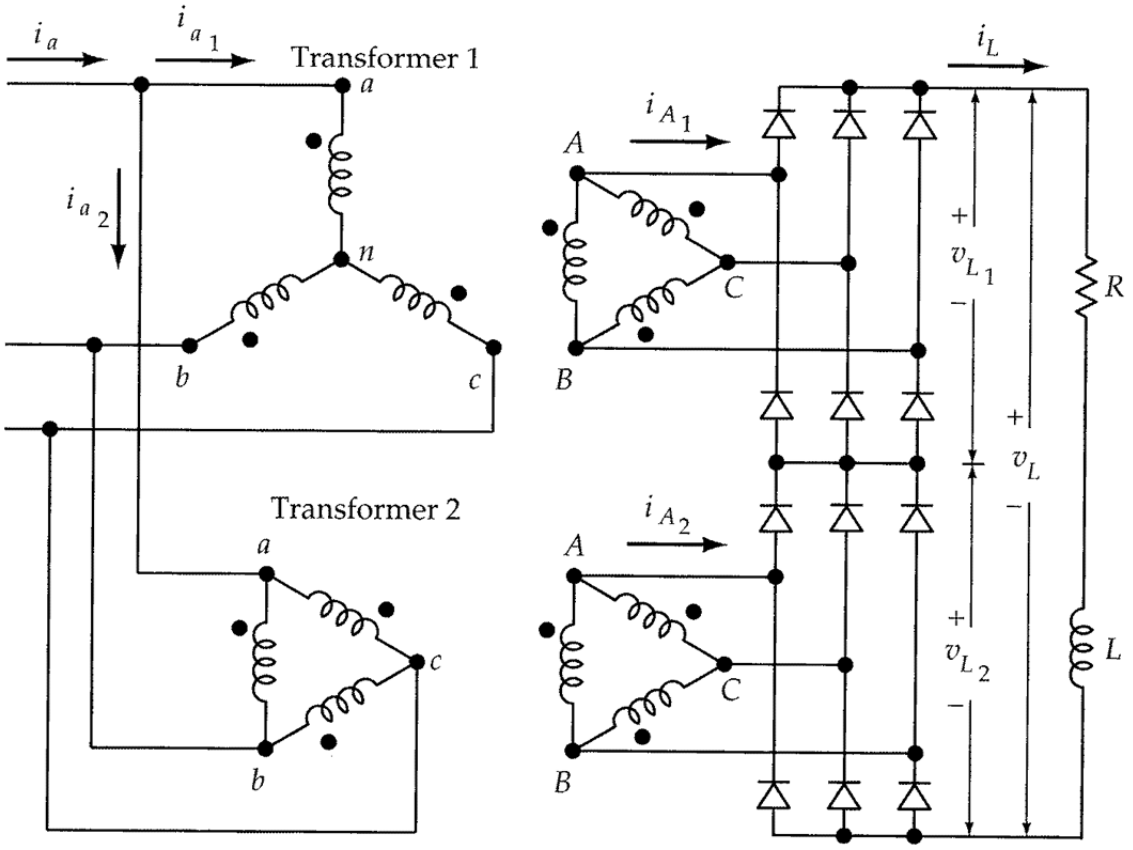


Figure 26. Series circuit arrangement for a 12-pulse rectifier using a wye-delta and delta-delta connected transformer to achieve the necessary 30° phase shift between 6-pulse rectifier units. From [3].

While it was relatively simple to realize the 12-pulse rectifier by taking advantage of the 30° phase shift that naturally occurs for a wye-delta transformer, how would we go about achieving other phase shifts? For example, for an 18- and 24-pulse count rectifier, we would require phase shifts of 20° and 15°, respectively. One such device that can easily accomplish this is called the zig-zag transformer [17].

# VI. SIMULINK® SIMULATIONS

In order to validate the relationship between pulse count and harmonic content (including THD), simulations for a 6-, 12-, 18-, and 24-pulse controlled rectifier with a two-pole *LC* output filter were conducted using Simulink®, specifically looking at the harmonic content of the phase A input line current $i_{ap}$. Additionally, it was desired to observe the behavior of the harmonics and $\%THD_i$ as $\alpha$ was varied.

## A. CIRCUIT PARAMETERS COMMON TO ALL SIMULATION MODELS

The fixed step-size for all simulations was 10 μs using the Runge-Kutta (ode4) solver; total simulation time was 1.0 s.

The voltage source was a three-phase 60 Hz ramp source with a 2,980 V/s slope, going from zero to effectively 150 V (RMS, line-to-line) in 0.05 s. The use of a ramp source rather than a step source allows for faster steady-state results. This voltage source was chosen to match that of an example problem from [4].

The transformers were zigzag phase shifting transformers with the following common parameters:

- Secondary winding (abc) connection: Y,
- Nominal power: 1 MVA,
- Nominal frequency: 60 Hz,
- Primary nominal voltage $V_p$: 150 V (RMS, line-to-line),
- Winding 1 resistance $R_1$: 0,

- Winding 1 inductance $L_1$: 0,
- Winding 2 resistance $R_2$: 0,
- Winding 2 inductance $L_2$: 0,
- Winding 3 resistance $R_3$: 0,
- Winding 3 inductance $L_3$: 0,
- Magnetizing branch resistance $R_m$: 10 kΩ, and
- Magnetizing branch inductance $L_m$: “inf.”

The main circuit component values were as follows:

- Inductor: 23.375 mH,
- Capacitor: 200 μF, and
- Resistor: 19.3 Ω.

These values were also chosen to match those of the same example problem from [4].

For the discrete synchronized 6-pulse generators, a pulse width of 10° was used with double-pulsing disabled.

For the 6-pulse controlled rectifier module, an inductance of 1 pH was added to each branch feeding into the universal bridges.

The universal bridges had the following common parameters:

- Number of bridge arms: 3,
- Snubber resistance $R_s$: 100 Ω,
- Snubber capacitance $C_s$: 0.1 μF,
- Power electronic device: thyristors,
- On-resistance $R_{on}$: 1 mΩ,
- On-inductance $L_{on}$: 0, and
- Forward voltage $V_f$: 1 mV.

The Simulink® schematic for the internal view of the 6-pulse controlled rectifier module common to all of the p-pulse simulation models is shown in Figure 27.

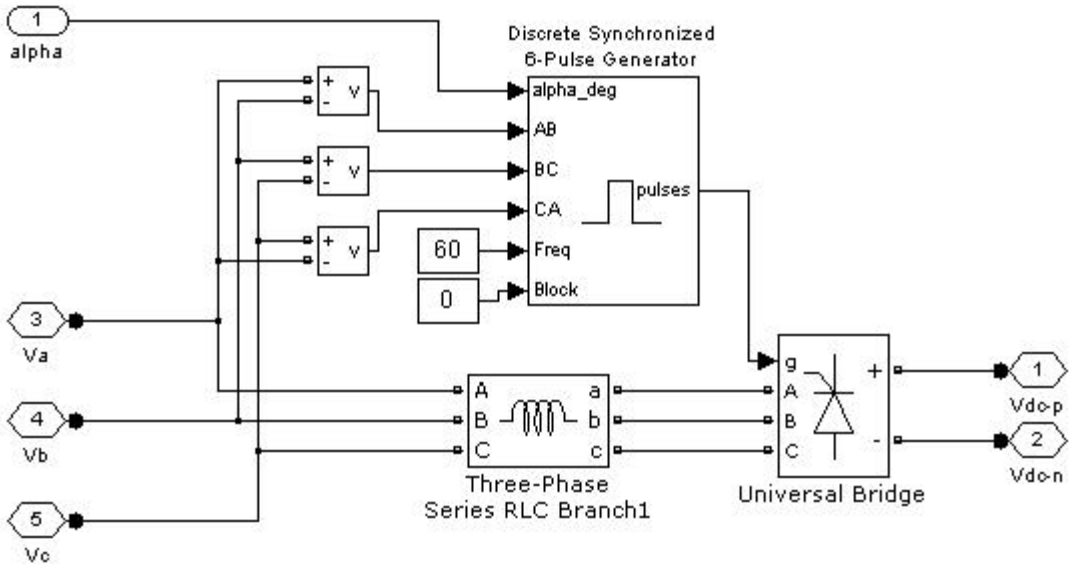


Figure 27. Simulink® schematic of internal view of 6-pulse controlled rectifier module.

## B. DATA COLLECTION

As stated previously, the data of interest was the harmonic content of $i_{ap}$ as $\alpha$ varied. Because it was desirable to observe how individual harmonics (normalized to the fundamental) and $\%THD_i$ varied with respect to $\alpha$, it was decided to evaluate the first ten non-zero harmonics (not including the fundamental) for each p-pulse rectifier. The first ten non-zero harmonics for the simulated p-pulse rectifiers are shown in Table 9.

Table 9. Harmonic numbers for the first ten non-zero harmonics (not including the fundamental) for some p-pulse rectifiers.

| 6-pulse | 12-pulse | 18-pulse | 24-pulse |
|---|---|---|---|
| 5 | 11 | 17 | 23 |
| 7 | 13 | 19 | 25 |
| 11 | 23 | 35 | 47 |
| 13 | 25 | 37 | 49 |
| 17 | 35 | 53 | 71 |
| 19 | 37 | 55 | 73 |
| 23 | 47 | 71 | 95 |
| 25 | 49 | 73 | 97 |
| 29 | 59 | 89 | 119 |
| 31 | 61 | 91 | 121 |

In order to obtain the RMS values of the individual harmonics, a string of eleven Fourier analyser blocks was used in series with gain blocks set at $\sqrt{2}/2$, specifying the fundamental frequency (60 Hz) and harmonic number of interest for each Fourier analyser block. Additionally, to obtain $\%THD_i$, a total harmonic distortion block in series with a gain block equal to 100 was used, again specifying the fundamental frequency of 60 Hz. The Simulink® schematic symbology depicting this is shown in Figure 28.

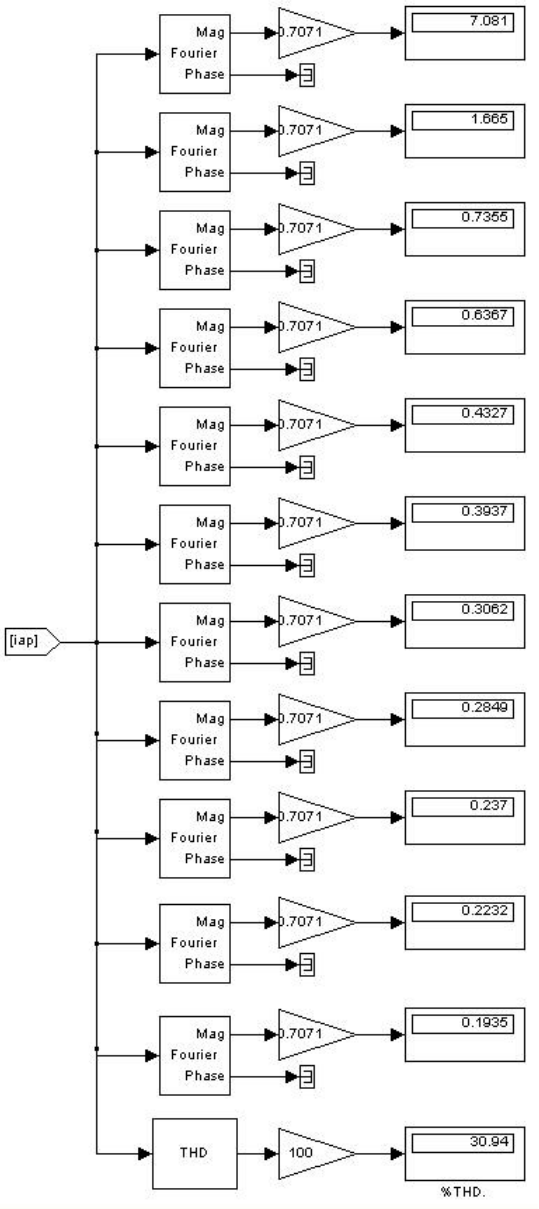


Figure 28. Obtaining the RMS values for the fundamental and first ten non-zero harmonics and $\%THD_i$ from Simulink®.

Because it was initially thought that the harmonics and $\%THD_i$ would change faster at lower values of $\alpha$ (erroneously, in this particular case), the initial step-size for $\alpha$ was chosen to be 3°, starting at $\alpha = 0°$ and going

up to $\alpha = 30°$, then increasing step-size to 10°, and continuing up to $\alpha = 80°$. It was not possible to go up to $\alpha = 90°$ (or even $\alpha = 80°$ for all controlled rectifiers) since $L_{crit}$ would approach infinity, and the controlled rectifier would no longer be in CCM.

The ten harmonics for each $\alpha$ were then normalized to the fundamental by dividing the RMS value of each harmonic by the RMS value of the fundamental. The normalized harmonics were then plotted versus $\alpha$ for each p-pulse controlled rectifier. Additionally, the $\%THD_i$ for all four of the p-pulse controlled rectifiers was plotted versus $\alpha$.

## C. CONTROLLED 6-PULSE RECTIFIER SIMULATION

The controlled 6-pulse rectifier Simulink® model is shown in Figure 29.

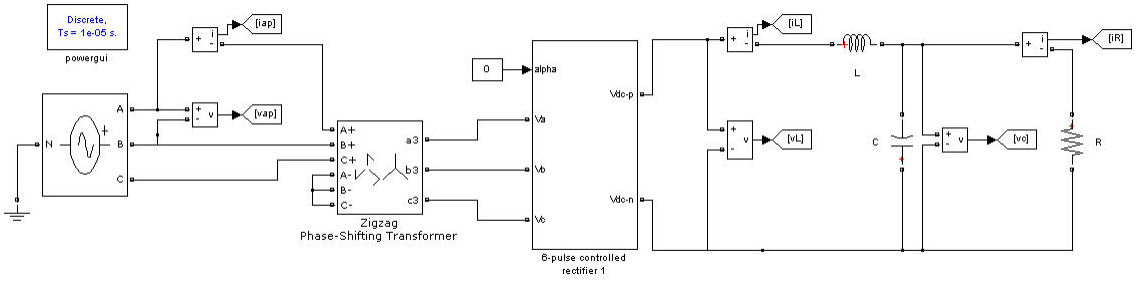


Figure 29. Simulink® model for a controlled 6-pulse rectifier with a two-pole *LC* output filter.

Although a transformer is not necessary for the controlled 6-pulse rectifier (because no other phase shifts beyond those that already exist for the three-phase source are required), a zigzag phase shifting transformer was used to

provide isolation. The secondary nominal voltage $V_3$ and phase shift $\phi$ were 150 V (RMS, line-to-line) and 1X10–$^6$ degrees (because 0° is not permitted), respectively.

The first ten normalized harmonics are plotted versus $\alpha$ in Figure 30. The 6-pulse controlled rectifier did not have enough inductance at $\alpha = 80°$ to remain in CCM. Interestingly, the first normalized non-zero harmonic ($h_5$) increases with $\alpha$ (which causes $\%THD_i$ to worsen), but the second non-zero harmonic ($h_7$) decreases with $\alpha$; the remaining eight normalized harmonics appear to only decrease very slightly as $\alpha$ increases.

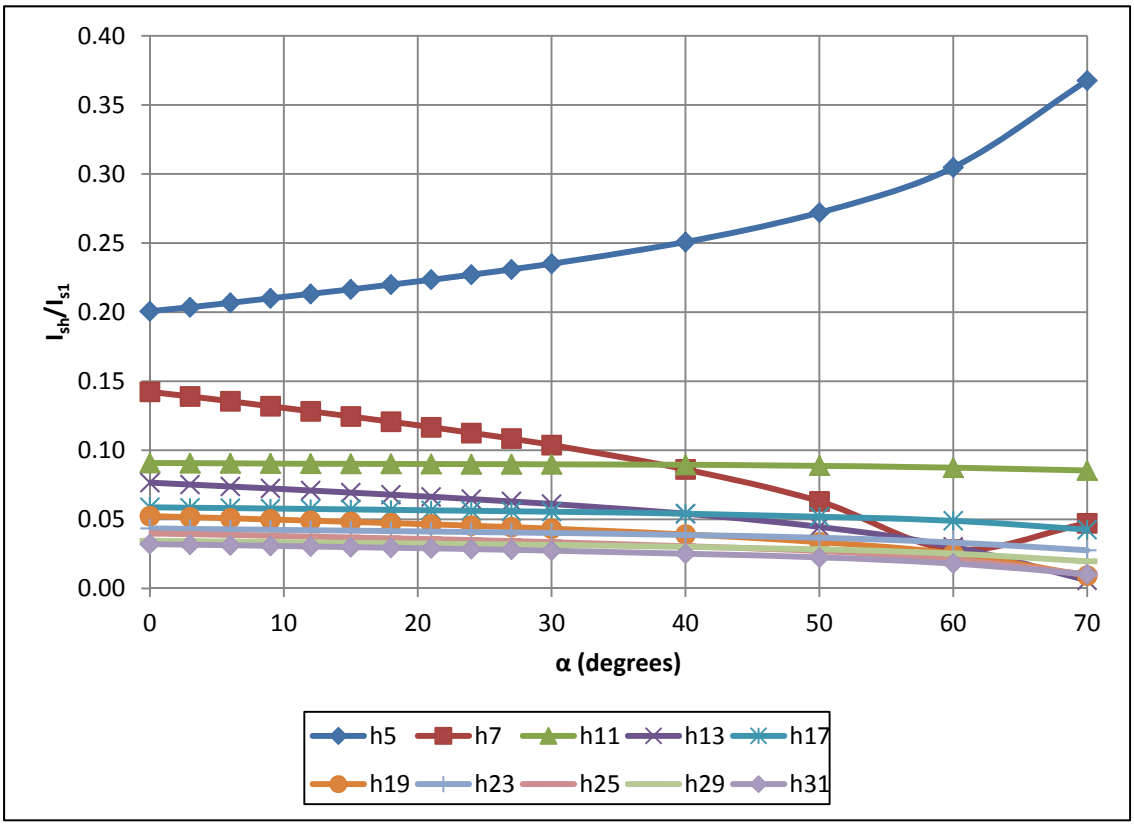


Figure 30. First ten non-zero normalized harmonics versus $\alpha$ for a 6–pulse controlled rectifier with a two-pole *LC* output filter.

## D. CONTROLLED 12-PULSE RECTIFIER SIMULATION

The controlled 12-pulse rectifier Simulink® model is shown in Figure 31.

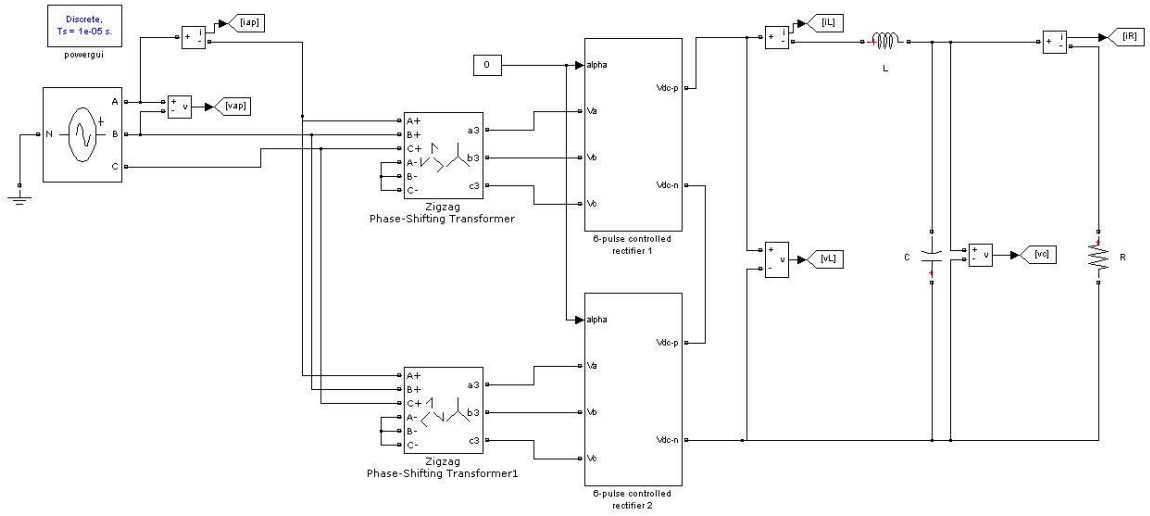


Figure 31. Simulink® model for a controlled 12-pulse rectifier with a two-pole *LC* output filter.

The secondary nominal voltage $V_3$ for both the upper and lower zigzag phase shifting transformer were 75 V (RMS, line-to-line) while the phase shift $\phi$ was 15° for the upper transformer and -15° for the lower transformer. The reason the secondary nominal voltages are the same and are half of what they were for the 6-pulse case is because it is desirable to maintain the same overall rectifier output side voltage. Recall that since the two 6-pulse controlled rectifiers are connected in series, their output voltages are additive. The $\pm 15°$ phase shifts create the necessary 30° phase difference between the two 6-pulse controlled rectifiers to ensure proper harmonic cancellation.

The first ten normalized harmonics are plotted versus $\alpha$ in Figure 32. The normalized harmonics of the 12-pulse controlled rectifier displayed fairly similar behavior to those of the 6-pulse controlled rectifier, although, they are smaller, as predicted by (177) and (178).

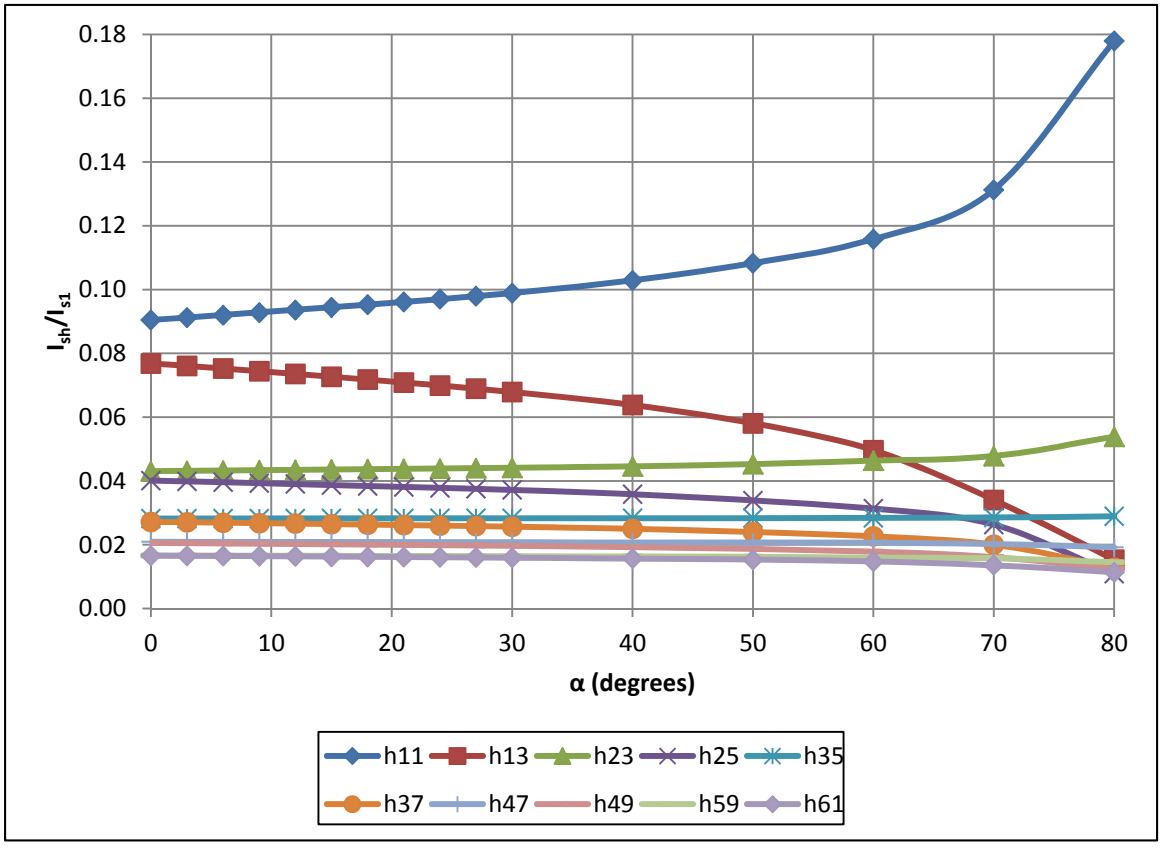


Figure 32. First ten non-zero normalized harmonics versus $\alpha$ for a 12–pulse controlled rectifier with a two-pole *LC* output filter.

## E. CONTROLLED 18-PULSE RECTIFIER SIMULATION

The controlled 18-pulse rectifier Simulink® model is shown in Figure 33.

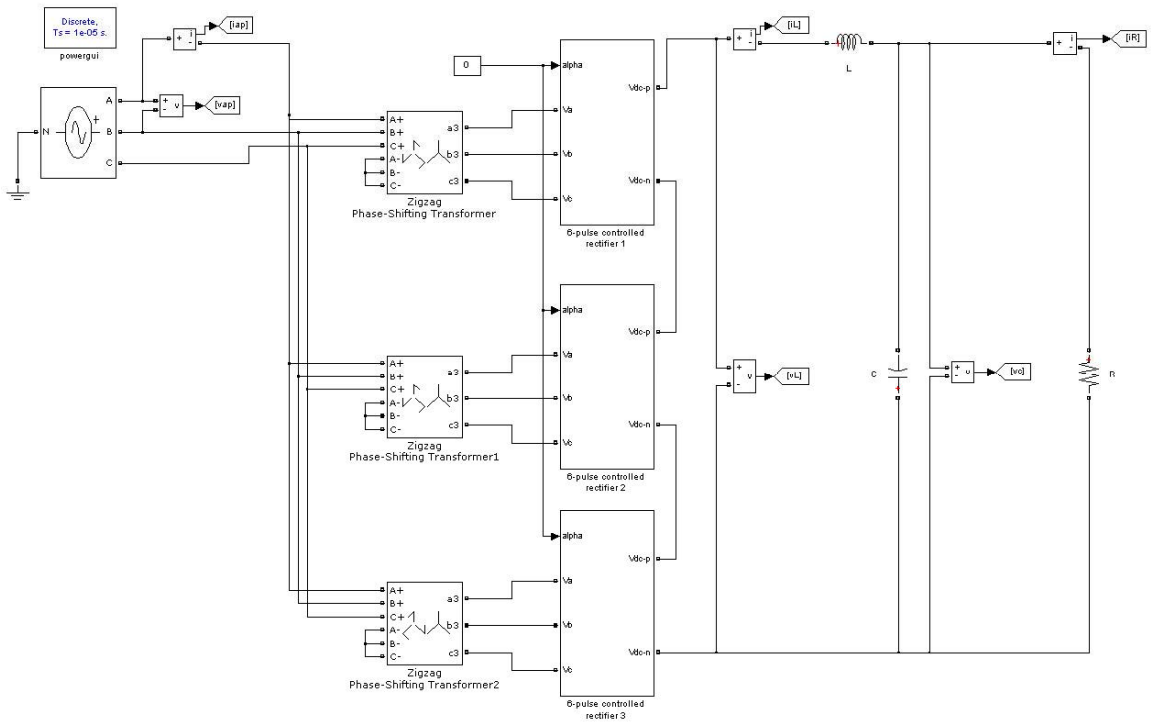


Figure 33. Simulink® model for a controlled 18-pulse rectifier with a two-pole *LC* output filter.

The secondary nominal voltage $V_3$ for all three zigzag phase shifting transformer was 50 V (RMS, line-to-line) while the phase shift $\phi$ was 20° for the upper transformer, 1X10–$^6$ degrees (because 0° is not permitted) for the middle transformer, and -20° for the lower transformer. The reason the secondary nominal voltages are the same is for the same reason as before. The $\pm 20°$ and 0° (effectively) phase shifts create the necessary 20° phase differences between the three 6-pulse controlled rectifiers to ensure proper harmonic cancellation.

The first ten normalized harmonics are plotted versus $\alpha$ in Figure 34. The normalized harmonics of the 18-pulse

controlled rectifier displayed similar behavior to those of the other two controlled rectifiers, although, they are smaller, again as predicted.

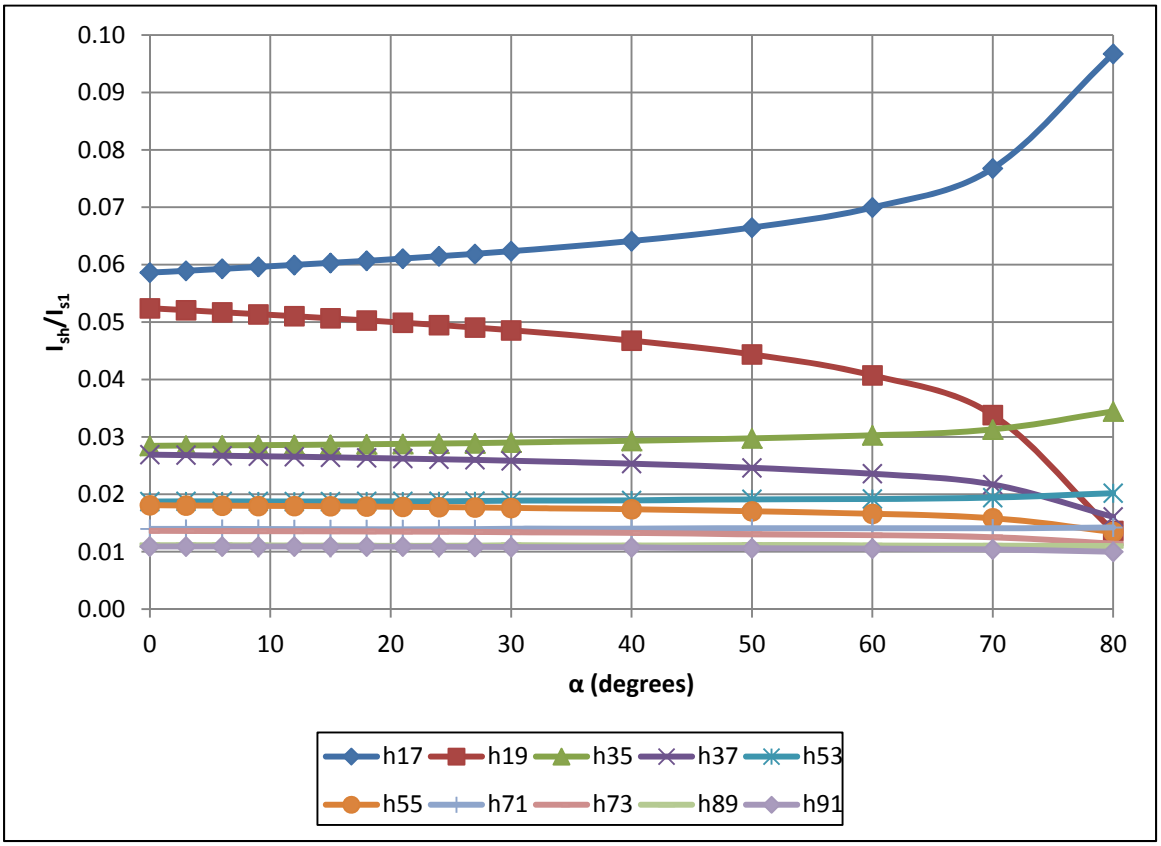


Figure 34. First ten non-zero normalized harmonics versus $\alpha$ for an 18–pulse controlled rectifier with a two-pole *LC* output filter.

## F. CONTROLLED 24-PULSE RECTIFIER SIMULATION

The controlled 24-pulse rectifier Simulink® model is shown in Figure 35.

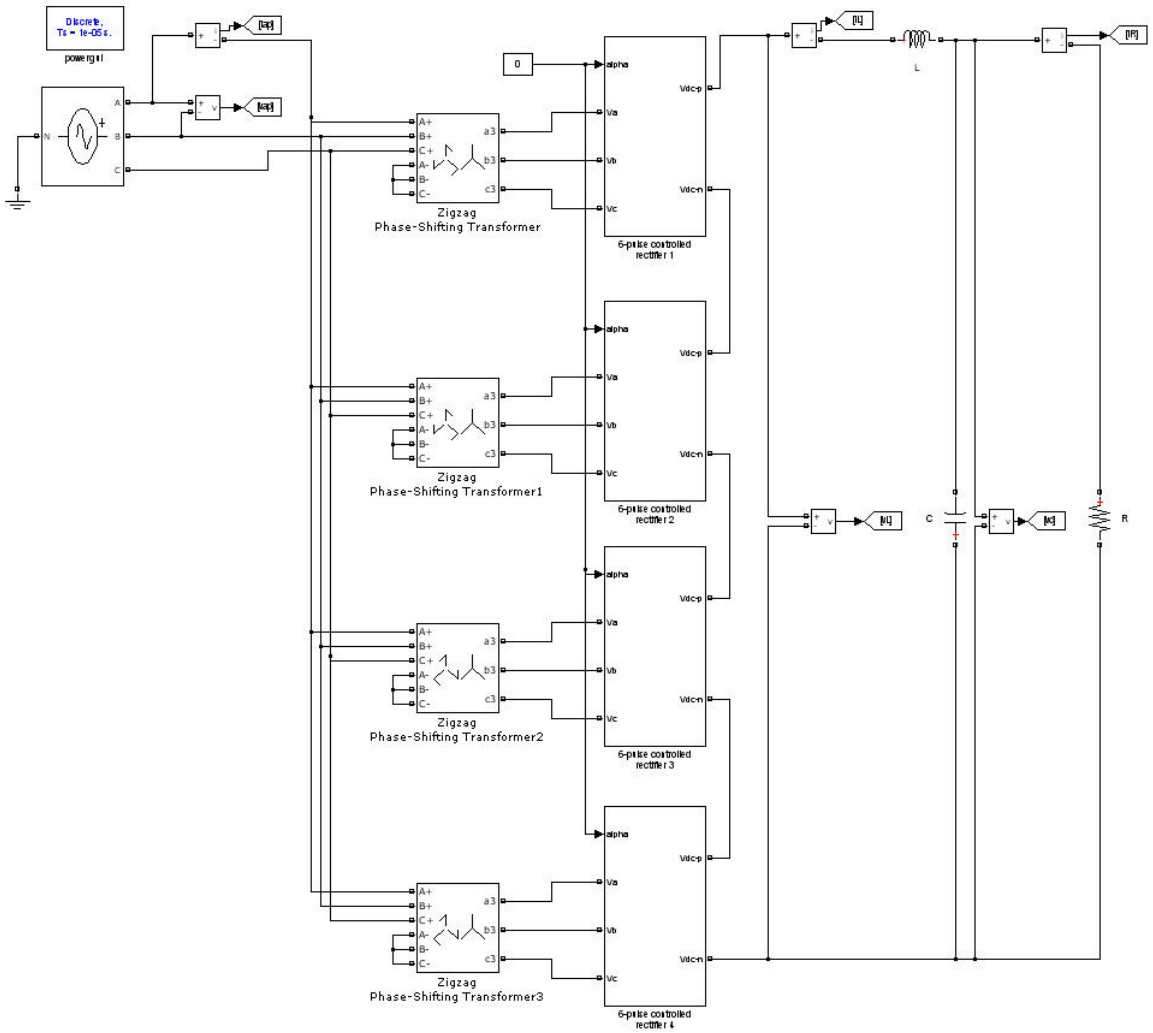


Figure 35. Simulink® model for a controlled 24-pulse rectifier with a two-pole *LC* output filter.

The secondary nominal voltage $V_3$ for all four zigzag phase shifting transformer was 37.5 V (RMS, line-to-line) while the phase shift $\phi$ was 22.5° for the top transformer, 7.5° for the second transformer, -7.5° for the third transformer, and -22.5° for the bottom transformer. The phase shifts of $\pm 22.5°$ and $\pm 7.5°$ create the necessary 15° phase differences between the four 6-pulse controlled rectifiers to ensure proper harmonic cancellation.

The first ten normalized harmonics are plotted versus $\alpha$ in Figure 36. It is no surprise that the normalized harmonics of the 24-pulse controlled rectifier displayed similar behavior to those of the other three controlled rectifiers, although, they are once again smaller, just as predicted.

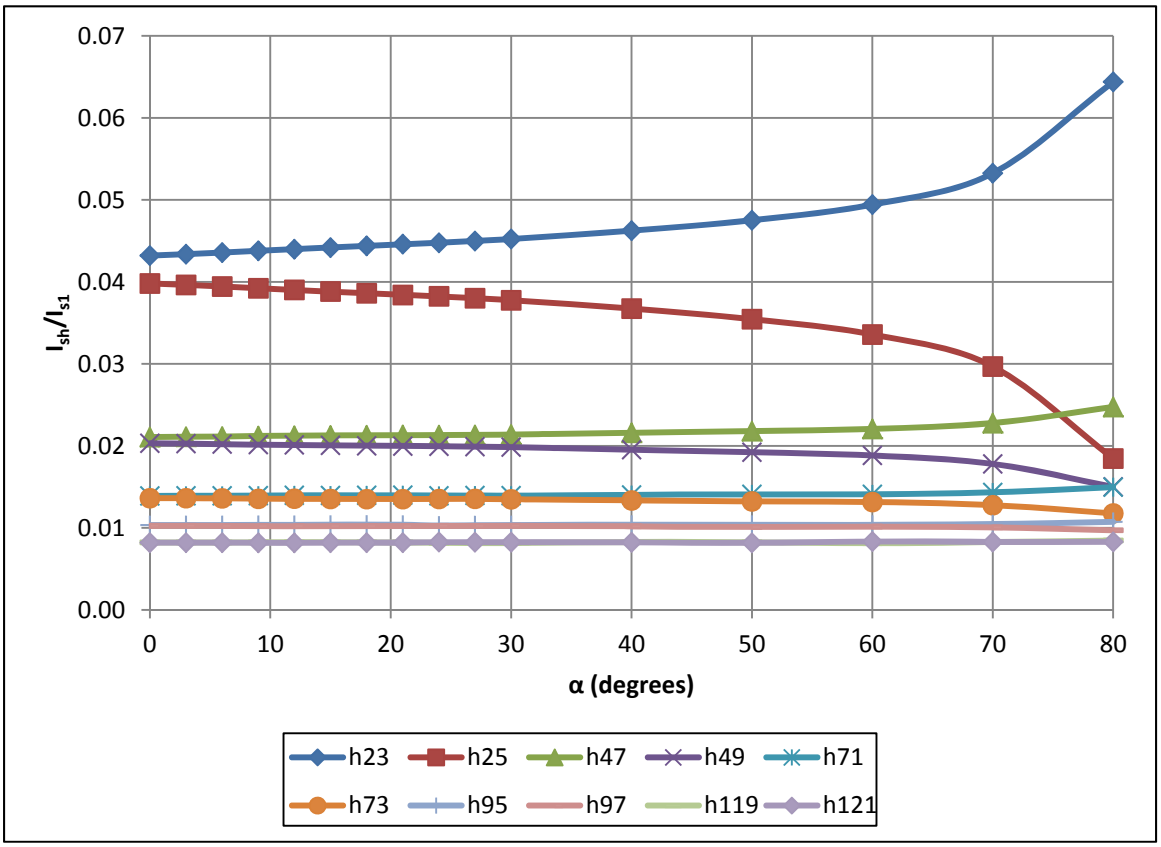


Figure 36. First ten non-zero normalized harmonics versus $\alpha$ for a 24–pulse controlled rectifier with a two-pole $LC$ output filter.

## G. SIMULATION RESULTS FOR $\%THD_i$

The $\%THD_i$ versus $\alpha$ for p–pulse controlled rectifiers with a two-pole $LC$ output filter is shown in Figure 37.

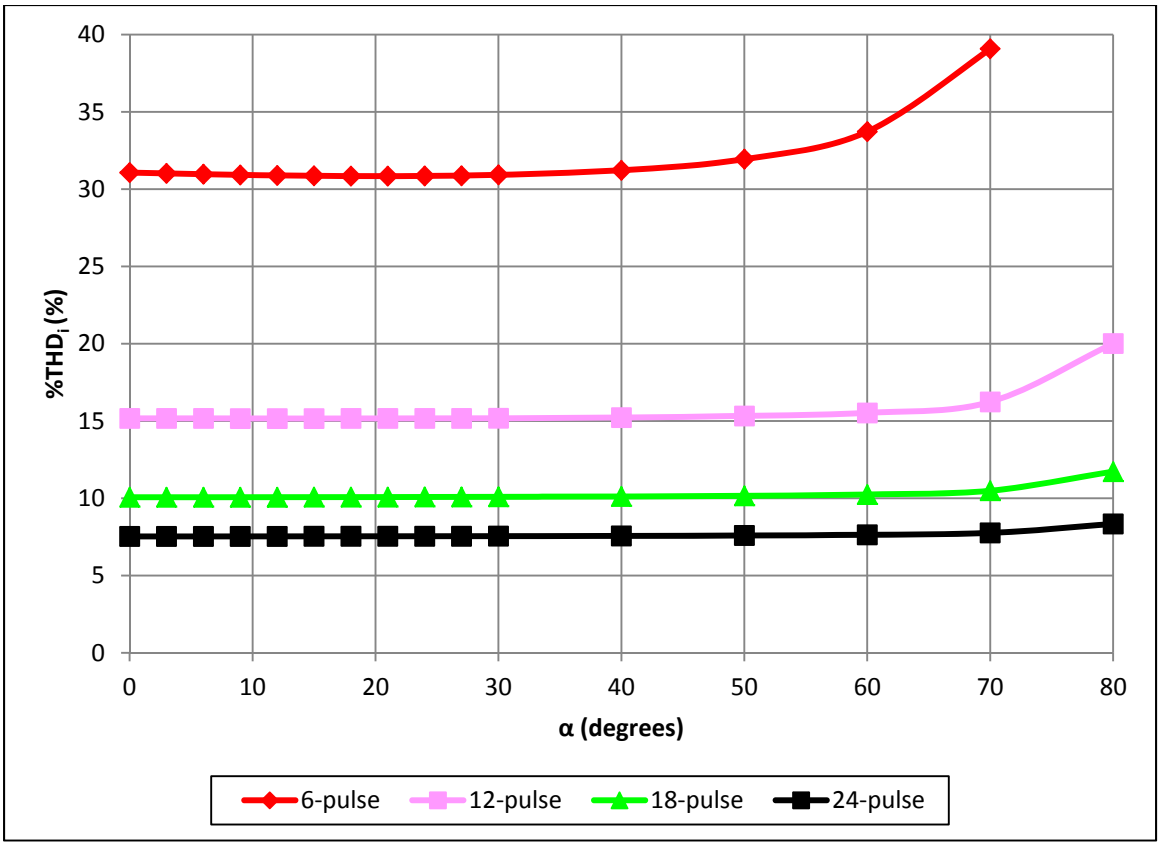


Figure 37. Percent total harmonic distortion in $i_{ap}$ versus $\alpha$ for p–pulse controlled rectifiers with a two-pole *LC* output filter.

The data clearly show that a higher pulse count produces a lower $\%THD_i$, with the 24-pulse controlled rectifier the clear winner. However, an incorrect conclusion that might be drawn from Figure 37 is that $\%THD_i$ does not vary much with $\alpha$; in fact, it appears as if $\%THD_i$ only gets slightly worse for very high values of $\alpha$. The real reason that $\%THD_i$ does not appreciably worsen as $\alpha$ increases is because the value of the inductor chosen for the simulations was very large (23.375 mH). The point is that $\%THD_i$ and $L_{crit}$ are both related to $\alpha$ in much the same way. That is, Figure 37 is related to Figure 15. If we had

instead initially selected a much smaller inductor that would still ensure CCM for the 6-pulse controlled rectifier up to $\alpha = 30°$ ($\cong$ 3 mH), we would more than likely see $\%THD_i$ increase for much smaller values of $\alpha$, particularly for the 6-pulse controlled rectifier and less so for the other higher pulse-count controlled rectifiers because of the reduction in $L_{crit}$ as pulse count increases.

THIS PAGE INTENTIONALLY LEFT BLANK

# VII. CONCLUSIONS

## A. SUMMARY OF RESULTS

### 1. Critical Inductance

The critical inductance as a function of $\alpha$ was calculated for a p-pulse controlled rectifier with a two-pole *LC* output filter. Plotting $L_{crit}$ for several multi-pulse controlled rectifiers demonstrated how it increased as $\alpha$ increased and that higher pulse count controlled rectifiers have a lower $L_{crit}$ than lower pulse count controlled rectifiers for a given value of $\alpha$. Additionally, $L_{crit}$ as a percentage of $L_{crit}$ for a 6-pulse controlled rectifier was calculated for selected values of $\alpha$ (0° to 90°, in 10° increments) for a 6-, 12-, 18-, 24-, and 96-pulse controlled rectifier. This clearly illustrated how the greatest reduction in $L_{crit}$ occurs in increasing from a 6-pulse to a 12-pulse controlled rectifier and that, while further increasing pulse count does reduce $L_{crit}$, the reduction is less.

### 2. DC Output Voltage Ripple

The peak-to-peak ripple voltage as a percentage of the average output voltage as a function of $\alpha$ was calculated for a p-pulse controlled rectifier with a purely resistive load. Plotting $\%V_{pp/avg}$ for several multi-pulse controlled rectifiers demonstrated how it increased as $\alpha$ increased and that higher pulse count controlled rectifiers have a lower $\%V_{pp/avg}$ than lower pulse count controlled rectifiers for a

given value of $\alpha$. Additionally, $\%V_{pp/avg}$ as a percentage of $\%V_{pp/avg}$ for a 6-pulse controlled rectifier was calculated for selected values of $\alpha$ (0° to 90°+, in 10° increments) for a 6-, 12-, 18-, 24-, and 96-pulse controlled rectifier. This clearly illustrated how the greatest reduction in $\%V_{pp/avg}$ occurs in increasing from a 6-pulse to a 12-pulse controlled rectifier and that, while further increasing pulse count does reduce $\%V_{pp/avg}$, the reduction is less.

The peak-to-peak ripple voltage as a percentage of the average output voltage as a function of $\alpha$ was also calculated for a p-pulse controlled rectifier with a two-pole *LC* output filter. Plotting $\%V_{pp/avg}$ for several multi-pulse controlled rectifiers demonstrated how it increased as $\alpha$ increased and that higher pulse count controlled rectifiers have a lower $\%V_{pp/avg}$ than lower pulse count controlled rectifiers for a given value of $\alpha$. Additionally, $\%V_{pp/avg}$ as a percentage of $\%V_{pp/avg}$ for a 6-pulse controlled rectifier was calculated for selected values of $\alpha$ (0° to 90°, in 10° increments) for a 6-, 12-, 18-, 24-, and 96-pulse controlled rectifier. This clearly illustrated how the greatest reduction in $\%V_{pp/avg}$ occurs in increasing from a 6-pulse to a 12-pulse controlled rectifier and that, while further increasing pulse count does reduce $\%V_{pp/avg}$, the reduction is less.

### 3. Harmonics and Total Harmonic Distortion

Simulations were conducted using Simulink® for a 6-, 12-, 18-, and 24-pulse controlled rectifier with a two-pole *LC* output filter, specifically investigating the behavior

of the first ten non-zero harmonics (normalized to the fundamental) and $\%THD_i$ of $i_{ap}$ for specific values of $\alpha$. Plotting the harmonics of each p-pulse controlled rectifier validated that the harmonics for higher pulse count controlled rectifiers are smaller than those for lower pulse count controlled rectifiers. Additionally, it revealed that the first harmonic increased as $\alpha$ increased, while the second harmonic decreased as $\alpha$ increased. The remaining eight harmonics did not show significant change as $\alpha$ varied.

Plotting $\%THD_i$ for the p-pulse controlled rectifiers confirmed that it increased as $\alpha$ increased (though it was reasoned that it would show a more definitive increase as $\alpha$ increased if a smaller inductor had been used) and that higher pulse count controlled rectifiers have a lower $\%THD_i$ than lower pulse count controlled rectifiers for a given value of $\alpha$. This also illustrated how the greatest reduction in $\%THD_i$ occurs in increasing from a 6-pulse to a 12-pulse controlled rectifier and that, while further increasing pulse count does reduce $\%THD_i$, it results in diminishing returns.

## B. RECOMMENDATIONS FOR FUTURE WORK

### 1. Discontinuous Conduction Mode

When the inductor in a multi-pulse phase controlled rectifier with a two-pole *LC* output filter is less than the value of $L_{crit}$, the inductor current is no longer continuous, and the equations, tables, and figures of Chapters III and IV no longer apply. Although operation of a controlled

rectifier in discontinuous conduction mode is not generally considered desirable, it is still a possible mode for the rectifier, and the model is not complete without it.

### 2. Size and Weight Considerations

While it is clear that a higher pulse count controlled rectifier produces better results than one with a lower pulse count, it can only do so at the cost of greater system complexity (and hence, less system reliability) and with more power electronic components. Power SCRs, inductors, capacitors, and especially low frequency transformers are bulky and heavy; this must be considered in real systems designed to operate on Navy ships with space and weight limitations. One useful study would be to use actual space and weight characteristics of the power electronic components for these controlled rectifiers and to determine the optimal pulse count system that would satisfy the electrical requirements and be within size and weight constraints for the intended Navy ship platform.

### 3. Parallel Vice Series Connection of Multi-Pulse Controlled Rectifiers

Only the series (vice parallel) connection of multiple controlled rectifiers in order to increase pulse count was considered in this thesis. With a series connection, the output voltage of the system is the summation of the individual output voltages of each rectifier, whereas, with a parallel connection, the output current of the system is the summation of the individual output currents of each rectifier. However, connecting rectifiers in parallel is more complex due to fluctuations in DC voltages which cause circulating currents to flow. To remedy this, these types

of systems typically require the use of an interphase transformer which absorbs the differences in the DC voltages between individual rectifiers. A useful study would be the evaluation of differences between the two topologies as a result of the added interphase transformer.

### 4. The Effect of $\alpha$ on Total Harmonic Distortion

In general, increasing $\alpha$ will cause the THD of a controlled rectifier system to worsen. However, a theoretical mathematical model for how THD behaves as a function of $\alpha$ similar to how $L_{crit}$ behaves as $\alpha$ changes for a p-pulse controlled rectifier with a two-pole *LC* output filter (as in Chapter III) would be beneficial.

### 5. A Better Solution for the Output Voltage Ripple for a Controlled Rectifier with a Two-Pole *LC* Output Filter

In Chapter IV, approximations were introduced in the determination of the output voltage ripple for a controlled rectifier with a two-pole *LC* output filter. This had to do with the fact that $|I_{AC}|$ was calculated from $V_{AC}$ and the overall load impedance $|Z_{total}|$ only at the frequency $p\omega$. While $p\omega$ is the dominant frequency, load impedances at frequency multiples of $p\omega$ also exist. A more accurate estimate of $|I_{AC}|$ can be obtained by using the principle of superposition to solve for $|I_{AC}|$ using several values of $|Z_{total}|$ at frequency multiples of $p\omega$ and adding them together. While this will provide a better estimate of $|I_{AC}|$, which will in turn result in a more accurate value for $V_{C(RMS)}$, the fact remains that

$V_{C(RMS)}$ is not perfectly sinusoidal, and $V_{C(pp-ripple)}$ and $\%V_{C(pp/avg)}$ will still be approximations, although, somewhat better than before. It would still be interesting to determine the error caused by this approximation.

# APPENDIX. MATLAB® CODE

## A. BASIC LINE-TO-LINE VOLTAGE WAVEFORM PLOT FOR A HYPOTHETICAL THREE-PHASE CIRCUIT

```
clc
clear

f=60;
w=2*pi*f;
t=linspace(0, 3/pi, 1000);
Vab = sind(w*t);
Vbc = sind(w*t-120);
Vca = sind(w*t-240);
Vba=-Vab;
Vcb=-Vbc;
Vac=-Vca;

hold on
plot(w*t, Vab, 'b', w*t, Vbc, 'g', w*t, Vca, 'r', 'LineWidth', 2)
axis([0,360,-1,1])
xlabel('angle (degrees)')
ylabel('Voltage (Volts)')
legend('V_a_b', 'V_b_c', 'V_c_a')
grid on
hold off
```

## B. LINE-TO-LINE VOLTAGE WAVEFORM PLOT SHOWING SIX PULSES FOR A HYPOTHETICAL THREE-PHASE CIRCUIT

```
clc
clear

f=60;
w=2*pi*f;
t=linspace(0, 3/pi, 1000);
Vab = sind(w*t);
Vbc = sind(w*t-120);
Vca = sind(w*t-240);
Vba=-Vab;
Vcb=-Vbc;
Vac=-Vca;

hold on
plot(w*t, Vab, 'b', w*t, Vbc, 'g', w*t, Vca, 'r', 'LineWidth', 2)
plot(w*t, Vba, 'c', w*t, Vcb, 'k', w*t, Vac, 'm', 'LineWidth', 2)
axis([0,360,-1,1])
xlabel('angle (degrees)')
ylabel('Voltage (Volts)')
legend('V_a_b', 'V_b_c', 'V_c_a', 'V_b_a', 'V_c_b', 'V_a_c')
grid on
hold off
```

## C. CRITICAL INDUCTANCE CALCULATION AND PLOT FOR A CONTROLLED 6-PULSE RECTIFIER

```
clear
clc

p = 6; % p = pulse count; i.e., p = 6 for 6-pulse controlled rectifier
lil = 90-(360/(2*p)); % lil = lower integration limit for start of a
pulse
A = cosd(lil); % constant to make math cleaner/neater
B = sind(lil); % constant to make math cleaner/neater
alpha_u = 85; % upper limit in degrees of firing angle alpha
num_points = 5e5; % number of points for alpha
alpha_b_r = atan((p/pi)-(B/A)); % boundary angle alpha in radians that
     % defines transition point between submodes of continuous
conduction
alpha_b_d = alpha_b_r*180/pi; % boundary angle alpha in degrees
w = 2*pi*60; % radian frequency for 60Hz
R = 1; % unit resistance chosen for ease of comparison

% code for angles greater than the boundary angle
alpha_d = linspace(alpha_b_d, alpha_u, num_points); % range of alpha
    % in degrees for Lcrit1
Lcrit1 = ((R*tand(alpha_d))/w)*(1-((pi*B)/(p*A))); % critical
inductance
    % for angles greater than the boundary angle
hold on
plot(alpha_d, Lcrit1, 'k-.', 'LineWidth', 2)

% code for angles less than the boundary angle
alpha_d = linspace(0, alpha_b_d, num_points); % range of alpha
    % in degrees for Lcrit2
alpha_r = alpha_d*pi/180; % alpha in radians
theta_d = asind((p*A*cosd(alpha_d))/pi) - lil; % angle in degrees at
which
    % the inductor current will be minimum for this submode
theta_r = theta_d*pi/180; % theta in radians
Lcrit2 = (R./(p*A*w.*cosd(alpha_d))).*...
    (pi.*cosd(theta_d+lil)+...
    (p*A.*sind(alpha_d))+...
    ((p.*theta_r-p.*alpha_r-pi)*A.*cosd(alpha_d)));
plot(alpha_d, Lcrit2, 'k', 'LineWidth', 2)

% title('Critical Inductance vs. \alpha for a 6 Pulse Controlled
Rectifier')
xlabel('\alpha (degrees)')
ylabel('Critical Inductance (Henry)')
legend('\alpha \geq 10.08^\circ', '\alpha \leq 10.08^\circ',...
    'location', 'North')
grid on
hold off
```

## D. CRITICAL INDUCTANCE CALCULATIONS AND PLOT FOR CONTROLLED 6-, 12-, 18-, 24-, AND 96-PULSE RECTIFIERS

```
clear
clc

hold on

alpha_u = 30; % upper limit in degrees of firing angle alpha
num_points = 5e5; % number of points for alpha

%% 6 pulse

p = 6; % p = pulse count; i.e., p = 6 for 6-pulse controlled rectifier
lil = 90-(360/(2*p)); % lil = lower integration limit for start of a
pulse
A = cosd(lil); % constant to make math cleaner/neater
B = sind(lil); % constant to make math cleaner/neater
alpha_b_r = atan((p/pi)-(B/A)); % boundary angle alpha in radians that
     % defines transition point between submodes of continuous
conduction
alpha_b_d = alpha_b_r*180/pi; % boundary angle alpha in degrees
w = 2*pi*60; % radian frequency for 60Hz
R = 1; % unit resistance chosen for ease of comparison

% code for angles greater than the boundary angle
alpha_d = linspace(alpha_b_d, alpha_u, num_points); % range of alpha
    % in degrees for Lcrit1
Lcrit1 = ((R*tand(alpha_d))/w)*(1-((pi*B)/(p*A))); % critical
inductance
    % for angles greater than the boundary angle
plot(alpha_d, Lcrit1, 'r-.', 'LineWidth', 2)

% code for angles less than the boundary angle
alpha_d = linspace(0, alpha_b_d, num_points); % range of alpha
    % in degrees for Lcrit2
alpha_r = alpha_d*pi/180; % alpha in radians
theta_d = asind((p*A*cosd(alpha_d))/pi) - lil; % angle in degrees at
which
    % the inductor current will be minimum for this submode
theta_r = theta_d*pi/180; % theta in radians
Lcrit2 = (R./(p*A*w.*cosd(alpha_d))).*...
    (pi.*cosd(theta_d+lil)+...
    (p*A.*sind(alpha_d))+...
    ((p.*theta_r-p.*alpha_r-pi)*A.*cosd(alpha_d)));
plot(alpha_d, Lcrit2, 'r', 'LineWidth', 2)

%% 12 pulse

p = 12; % p = pulse count; i.e., p = 6 for 6-pulse controlled rectifier
lil = 90-(360/(2*p)); % lil = lower integration limit for start of a
pulse
A = cosd(lil); % constant to make math cleaner/neater
```

```
B = sind(lil); % constant to make math cleaner/neater
alpha_b_r = atan((p/pi)-(B/A)); % boundary angle alpha in radians that
     % defines transition point between submodes of continuous
conduction
alpha_b_d = alpha_b_r*180/pi; % boundary angle alpha in degrees
w = 2*pi*60; % radian frequency for 60Hz
R = 1; % unit resistance chosen for ease of comparison

% code for angles greater than the boundary angle
alpha_d = linspace(alpha_b_d, alpha_u, num_points); % range of alpha
    % in degrees for Lcrit1
Lcrit3 = ((R*tand(alpha_d))/w)*(1-((pi*B)/(p*A))); % critical
inductance
    % for angles greater than the boundary angle
plot(alpha_d, Lcrit3, 'm-.', 'LineWidth', 2)

% code for angles less than the boundary angle
alpha_d = linspace(0, alpha_b_d, num_points); % range of alpha
    % in degrees for Lcrit2
alpha_r = alpha_d*pi/180; % alpha in radians
theta_d = asind((p*A*cosd(alpha_d))/pi) - lil; % angle in degrees at
which
    % the inductor current will be minimum for this submode
theta_r = theta_d*pi/180; % theta in radians
Lcrit4 = (R./(p*A*w.*cosd(alpha_d))).*...
    (pi.*cosd(theta_d+lil)+...
    (p*A.*sind(alpha_d))+...
    ((p.*theta_r-p.*alpha_r-pi)*A.*cosd(alpha_d)));
plot(alpha_d, Lcrit4, 'm', 'LineWidth', 2)

%% 18 pulse

p = 18; % p = pulse count; i.e., p = 6 for 6-pulse controlled rectifier
lil = 90-(360/(2*p)); % lil = lower integration limit for start of a
pulse
A = cosd(lil); % constant to make math cleaner/neater
B = sind(lil); % constant to make math cleaner/neater
alpha_b_r = atan((p/pi)-(B/A)); % boundary angle alpha in radians that
     % defines transition point between submodes of continuous
conduction
alpha_b_d = alpha_b_r*180/pi; % boundary angle alpha in degrees
w = 2*pi*60; % radian frequency for 60Hz
R = 1; % unit resistance chosen for ease of comparison

% code for angles greater than the boundary angle
alpha_d = linspace(alpha_b_d, alpha_u, num_points); % range of alpha
    % in degrees for Lcrit1
Lcrit5 = ((R*tand(alpha_d))/w)*(1-((pi*B)/(p*A))); % critical
inductance
    % for angles greater than the boundary angle
plot(alpha_d, Lcrit5, 'g-.', 'LineWidth', 2)

% code for angles less than the boundary angle
alpha_d = linspace(0, alpha_b_d, num_points); % range of alpha
```

```
    % in degrees for Lcrit2
alpha_r = alpha_d*pi/180; % alpha in radians
theta_d = asind((p*A*cosd(alpha_d))/pi) - lil; % angle in degrees at
which
    % the inductor current will be minimum for this submode
theta_r = theta_d*pi/180; % theta in radians
Lcrit6 = (R./(p*A*w.*cosd(alpha_d))).*...
    (pi.*cosd(theta_d+lil)+...
    (p*A.*sind(alpha_d))+...
    ((p.*theta_r-p.*alpha_r-pi)*A.*cosd(alpha_d)));
plot(alpha_d, Lcrit6, 'g', 'LineWidth', 2)

%% 24 pulse

p = 24; % p = pulse count; i.e., p = 6 for 6-pulse controlled rectifier
lil = 90-(360/(2*p)); % lil = lower integration limit for start of a
pulse
A = cosd(lil); % constant to make math cleaner/neater
B = sind(lil); % constant to make math cleaner/neater
alpha_b_r = atan((p/pi)-(B/A)); % boundary angle alpha in radians that
     % defines transition point between submodes of continuous
conduction
alpha_b_d = alpha_b_r*180/pi; % boundary angle alpha in degrees
w = 2*pi*60; % radian frequency for 60Hz
R = 1; % unit resistance chosen for ease of comparison

% code for angles greater than the boundary angle
alpha_d = linspace(alpha_b_d, alpha_u, num_points); % range of alpha
    % in degrees for Lcrit1
Lcrit7 = ((R*tand(alpha_d))/w)*(1-((pi*B)/(p*A))); % critical
inductance
    % for angles greater than the boundary angle
plot(alpha_d, Lcrit7, 'k-.', 'LineWidth', 2)

% code for angles less than the boundary angle
alpha_d = linspace(0, alpha_b_d, num_points); % range of alpha
    % in degrees for Lcrit2
alpha_r = alpha_d*pi/180; % alpha in radians
theta_d = asind((p*A*cosd(alpha_d))/pi) - lil; % angle in degrees at
which
    % the inductor current will be minimum for this submode
theta_r = theta_d*pi/180; % theta in radians
Lcrit8 = (R./(p*A*w.*cosd(alpha_d))).*...
    (pi.*cosd(theta_d+lil)+...
    (p*A.*sind(alpha_d))+...
    ((p.*theta_r-p.*alpha_r-pi)*A.*cosd(alpha_d)));
plot(alpha_d, Lcrit8, 'k', 'LineWidth', 2)

%% 96 pulse

p = 96; % p = pulse count; i.e., p = 6 for 6-pulse controlled rectifier
lil = 90-(360/(2*p)); % lil = lower integration limit for start of a
pulse
A = cosd(lil); % constant to make math cleaner/neater
```

```
B = sind(lil); % constant to make math cleaner/neater
alpha_b_r = atan((p/pi)-(B/A)); % boundary angle alpha in radians that
     % defines transition point between submodes of continuous
conduction
alpha_b_d = alpha_b_r*180/pi; % boundary angle alpha in degrees
w = 2*pi*60; % radian frequency for 60Hz
R = 1; % unit resistance chosen for ease of comparison

% code for angles greater than the boundary angle
alpha_d = linspace(alpha_b_d, alpha_u, num_points); % range of alpha
    % in degrees for Lcrit1
Lcrit9 = ((R*tand(alpha_d))/w)*(1-((pi*B)/(p*A))); % critical
inductance
    % for angles greater than the boundary angle
plot(alpha_d, Lcrit9, 'b-.', 'LineWidth', 2)

% code for angles less than the boundary angle
alpha_d = linspace(0, alpha_b_d, num_points); % range of alpha
    % in degrees for Lcrit2
alpha_r = alpha_d*pi/180; % alpha in radians
theta_d = asind((p*A*cosd(alpha_d))/pi) - lil; % angle in degrees at
which
    % the inductor current will be minimum for this submode
theta_r = theta_d*pi/180; % theta in radians
Lcrit10 = (R./(p*A*w.*cosd(alpha_d))).*...
    (pi.*cosd(theta_d+lil)+...
    (p*A.*sind(alpha_d))+...
    ((p.*theta_r-p.*alpha_r-pi)*A.*cosd(alpha_d)));
plot(alpha_d, Lcrit10, 'b', 'LineWidth', 2)

%% Plot Formatting

grid on
%%title('Critical Inductance vs. \alpha for an n-Pulse Controlled
Rectifier')
xlabel('\alpha (degrees)')
ylabel('Critical Inductance (Henry)')
legend('6-pulse, \alpha \geq 10.08^\circ', '6-pulse, \alpha \leq
10.08^\circ',...
       '12-pulse, \alpha \geq  5.01^\circ', '12-pulse, \alpha \leq
5.01^\circ',...
       '18-pulse, \alpha \geq  3.34^\circ', '18-pulse, \alpha \leq
3.34^\circ',...
       '24-pulse, \alpha \geq 2.50^\circ', '24-pulse, \alpha \leq
2.50^\circ',...
       '96-pulse, \alpha \geq 0.63^\circ', '96-pulse, \alpha \leq
0.63^\circ',...
       'location', 'Northwest')
hold off
```

## E. VOLTAGE RIPPLE CALCULATIONS AND PLOT FOR A CONTROLLED 6-PULSE RECTIFIER WITH A RESISTIVE LOAD

```
clear
```

```
clc

%% 6-pulse

p = 6; % p = pulse count; i.e., p = 6 for 6-pulse controlled rectifier
Vm = 1;
lil = 90-(180/p); % lil = lower integration limit for start of a pulse
uil = 90+(180/p); % uil = upper integration limit for start of a pulse
A = cosd(lil); % constant to make math cleaner/neater
E = cosd(2*lil);
F = sind(2*lil);
alpha_b1_d = (uil-lil)/2; % first boundary angle in degrees
alpha_b2_d = lil; % second boundary angle in degrees
num_points = 1000; % number of points for alpha

% code for alpha < boundary angle 1
alpha_d = linspace(0, alpha_b1_d, num_points); % range of alpha in
degrees
Vavg1 = (A*Vm*p*cosd(alpha_d))/pi;
Vrms1 = (Vm/sqrt(2))*sqrt(1 + ((F*p*cosd(2*alpha_d))/(2*pi)));
Vrms_ripple1 = sqrt(Vrms1.^2 - Vavg1.^2);
Vpp_ripple1 = Vm*(1-sind(alpha_d + uil));
Vpp_by_Vavg_percent1 = (Vpp_ripple1 ./ Vavg1)*100;
figure(1)
plot(alpha_d, Vavg1, 'k',...
     alpha_d, Vrms1, 'r',...
     alpha_d, Vrms_ripple1, 'b',...
     alpha_d, Vpp_ripple1, 'm', 'LineWidth', 2)
xlabel('\alpha (degrees)')
ylabel('Voltage (Volts)')
legend('V_a_v_g', 'V_R_M_S', 'V_R_M_S_-_r_i_p_p_l_e', 'V_p_p_-
_r_i_p_p_l_e', 'location', 'NorthEast')
grid on
hold on
figure(2)
plot(alpha_d, Vpp_by_Vavg_percent1, 'k', 'LineWidth', 2)
xlabel('\alpha (degrees)')
ylabel('%V_p_p_/_a_v_g (%)')
grid on
axis([0 uil 0 1000])
hold on

% code for boundary angle 1 < alpha < boundary angle 2
alpha_d = linspace(alpha_b1_d, alpha_b2_d, num_points); % range of
alpha in degrees
Vavg2 = (A*Vm*p*cosd(alpha_d))/pi;
Vrms2 = (Vm/sqrt(2))*sqrt(1 + ((F*p*cosd(2*alpha_d))/(2*pi)));
Vrms_ripple2 = sqrt(Vrms2.^2 - Vavg2.^2);
Vpp_ripple2 = Vm*(sind(alpha_d + lil) - sind(alpha_d + uil));
Vpp_by_Vavg_percent2 = (Vpp_ripple2 ./ Vavg2)*100;
figure(1)
plot(alpha_d, Vavg2, 'k',...
     alpha_d, Vrms2, 'r',...
     alpha_d, Vrms_ripple2, 'b',...
     alpha_d, Vpp_ripple2, 'm', 'LineWidth', 2)
```

```
figure (2)
plot(alpha_d, Vpp_by_Vavg_percent2, 'k', 'LineWidth', 2)

% code for alpha > boundary angle 2
alpha_d = linspace(alpha_b2_d, uil, num_points); % range of alpha in
degrees
Vavg3 = ((Vm*p)/(2*pi))*(1 + cosd(alpha_d + lil));
Vrms3 = (Vm/sqrt(2))*sqrt(((2+p)/4)-((alpha_d*p)/360)+...
        ((E*p*sind(2*alpha_d))/(4*pi))+((F*p*cosd(2*alpha_d))/(4*pi)));
Vrms_ripple3 = sqrt(Vrms3.^2 - Vavg3.^2);
Vpp_ripple3 = Vm*sind(alpha_d + lil);
Vpp_by_Vavg_percent3 = (Vpp_ripple3 ./ Vavg3)*100;
figure(1)
plot(alpha_d, Vavg3, 'k',...
     alpha_d, Vrms3, 'r',...
     alpha_d, Vrms_ripple3, 'b',...
     alpha_d, Vpp_ripple3, 'm', 'LineWidth', 2)
figure (2)
plot(alpha_d, Vpp_by_Vavg_percent3, 'k', 'LineWidth', 2)

hold off
```

## F. VOLTAGE RIPPLE CALCULATIONS AND PLOT FOR A CONTROLLED 6-, 12-, 18-, 24-, AND 96-PULSE RECTIFIER WITH A RESISTIVE LOAD

```
clear
clc

hold on
%% 6-pulse

p = 6; % p = pulse count; i.e., p = 6 for 6-pulse controlled rectifier
Vm = 1;
lil = 90-(180/p); % lil = lower integration limit for start of a pulse
uil = 90+(180/p); % uil = upper integration limit for start of a pulse
A = cosd(lil); % constant to make math cleaner/neater
E = cosd(2*lil);
F = sind(2*lil);
alpha_b1_d = (uil-lil)/2; % first boundary angle in degrees
alpha_b2_d = lil; % second boundary angle in degrees
num_points = 1000; % number of points for alpha

% code for alpha < boundary angle 1
alpha_d = linspace(0, alpha_b1_d, num_points); % range of alpha in
degrees
Vavg1 = (A*Vm*p*cosd(alpha_d))/pi;
Vrms1 = (Vm/sqrt(2))*sqrt(1 + ((F*p*cosd(2*alpha_d))/(2*pi)));
Vrms_ripple1 = sqrt(Vrms1.^2 - Vavg1.^2);
Vpp_ripple1 = Vm*(1-sind(alpha_d + uil));
Vpp_by_Vavg_percent1 = (Vpp_ripple1 ./ Vavg1)*100;
plot(alpha_d, Vpp_by_Vavg_percent1, 'r', 'LineWidth', 2)

% % code for boundary angle 1 < alpha < boundary angle 2
```

```
% alpha_d = linspace(alpha_b1_d, alpha_b2_d, num_points); % range of
alpha in degrees
% Vavg2 = (A*Vm*p*cosd(alpha_d))/pi;
% Vrms2 = (Vm/sqrt(2))*sqrt(1 + ((F*p*cosd(2*alpha_d))/(2*pi)));
% Vrms_ripple2 = sqrt(Vrms2.^2 - Vavg2.^2);
% Vpp_ripple2 = Vm*(sind(alpha_d + lil) - sind(alpha_d + uil));
% Vpp_by_Vavg_percent2 = (Vpp_ripple2 ./ Vavg2)*100;
% plot(alpha_d, Vpp_by_Vavg_percent2, 'r--', 'LineWidth', 2)
%
% % code for alpha > boundary angle 2
% alpha_d = linspace(alpha_b2_d, uil, num_points); % range of alpha in
degrees
% Vavg3 = ((Vm*p)/(2*pi))*(1 + cosd(alpha_d + lil));
% Vrms3 = (Vm/sqrt(2))*sqrt(((2+p)/4)-((alpha_d*p)/360)+...
%
((E*p*sind(2*alpha_d))/(4*pi))+((F*p*cosd(2*alpha_d))/(4*pi)));
% Vrms_ripple3 = sqrt(Vrms3.^2 - Vavg3.^2);
% Vpp_ripple3 = Vm*sind(alpha_d + lil);
% Vpp_by_Vavg_percent3 = (Vpp_ripple3 ./ Vavg3)*100;
% plot(alpha_d, Vpp_by_Vavg_percent3, 'r-.', 'LineWidth', 2)

%% 12-pulse

p = 12; % p = pulse count; i.e., p = 6 for 6-pulse controlled rectifier
Vm = 1;
lil = 90-(180/p); % lil = lower integration limit for start of a pulse
uil = 90+(180/p); % uil = upper integration limit for start of a pulse
A = cosd(lil); % constant to make math cleaner/neater
E = cosd(2*lil);
F = sind(2*lil);
alpha_b1_d = (uil-lil)/2; % first boundary angle in degrees
alpha_b2_d = lil; % second boundary angle in degrees
num_points = 1000; % number of points for alpha

% code for alpha < boundary angle 1
alpha_d = linspace(0, alpha_b1_d, num_points); % range of alpha in
degrees
Vavg1 = (A*Vm*p*cosd(alpha_d))/pi;
Vrms1 = (Vm/sqrt(2))*sqrt(1 + ((F*p*cosd(2*alpha_d))/(2*pi)));
Vrms_ripple1 = sqrt(Vrms1.^2 - Vavg1.^2);
Vpp_ripple1 = Vm*(1-sind(alpha_d + uil));
Vpp_by_Vavg_percent1 = (Vpp_ripple1 ./ Vavg1)*100;
plot(alpha_d, Vpp_by_Vavg_percent1, 'm', 'LineWidth', 2)

% code for boundary angle 1 < alpha < boundary angle 2
alpha_d = linspace(alpha_b1_d, alpha_b2_d, num_points); % range of
alpha in degrees
Vavg2 = (A*Vm*p*cosd(alpha_d))/pi;
Vrms2 = (Vm/sqrt(2))*sqrt(1 + ((F*p*cosd(2*alpha_d))/(2*pi)));
Vrms_ripple2 = sqrt(Vrms2.^2 - Vavg2.^2);
Vpp_ripple2 = Vm*(sind(alpha_d + lil) - sind(alpha_d + uil));
Vpp_by_Vavg_percent2 = (Vpp_ripple2 ./ Vavg2)*100;
plot(alpha_d, Vpp_by_Vavg_percent2, 'm--', 'LineWidth', 2)

% % code for alpha > boundary angle 2
```

```
% alpha_d = linspace(alpha_b2_d, uil, num_points); % range of alpha in
degrees
% Vavg3 = ((Vm*p)/(2*pi))*(1 + cosd(alpha_d + lil));
% Vrms3 = (Vm/sqrt(2))*sqrt(((2+p)/4)-((alpha_d*p)/360)+...
%
((E*p*sind(2*alpha_d))/(4*pi))+((F*p*cosd(2*alpha_d))/(4*pi)));
% Vrms_ripple3 = sqrt(Vrms3.^2 - Vavg3.^2);
% Vpp_ripple3 = Vm*sind(alpha_d + lil);
% Vpp_by_Vavg_percent3 = (Vpp_ripple3 ./ Vavg3)*100;
% plot(alpha_d, Vpp_by_Vavg_percent3, 'm-.', 'LineWidth', 2)

%% 18-pulse

p = 18; % p = pulse count; i.e., p = 6 for 6-pulse controlled rectifier
Vm = 1;
lil = 90-(180/p); % lil = lower integration limit for start of a pulse
uil = 90+(180/p); % uil = upper integration limit for start of a pulse
A = cosd(lil); % constant to make math cleaner/neater
E = cosd(2*lil);
F = sind(2*lil);
alpha_b1_d = (uil-lil)/2; % first boundary angle in degrees
alpha_b2_d = lil; % second boundary angle in degrees
num_points = 1000; % number of points for alpha

% code for alpha < boundary angle 1
alpha_d = linspace(0, alpha_b1_d, num_points); % range of alpha in
degrees
Vavg1 = (A*Vm*p*cosd(alpha_d))/pi;
Vrms1 = (Vm/sqrt(2))*sqrt(1 + ((F*p*cosd(2*alpha_d))/(2*pi)));
Vrms_ripple1 = sqrt(Vrms1.^2 - Vavg1.^2);
Vpp_ripple1 = Vm*(1-sind(alpha_d + uil));
Vpp_by_Vavg_percent1 = (Vpp_ripple1 ./ Vavg1)*100;
plot(alpha_d, Vpp_by_Vavg_percent1, 'g', 'LineWidth', 2)

% code for boundary angle 1 < alpha < boundary angle 2
alpha_d = linspace(alpha_b1_d, alpha_b2_d, num_points); % range of
alpha in degrees
Vavg2 = (A*Vm*p*cosd(alpha_d))/pi;
Vrms2 = (Vm/sqrt(2))*sqrt(1 + ((F*p*cosd(2*alpha_d))/(2*pi)));
Vrms_ripple2 = sqrt(Vrms2.^2 - Vavg2.^2);
Vpp_ripple2 = Vm*(sind(alpha_d + lil) - sind(alpha_d + uil));
Vpp_by_Vavg_percent2 = (Vpp_ripple2 ./ Vavg2)*100;
plot(alpha_d, Vpp_by_Vavg_percent2, 'g--', 'LineWidth', 2)

% % code for alpha > boundary angle 2
% alpha_d = linspace(alpha_b2_d, uil, num_points); % range of alpha in
degrees
% Vavg3 = ((Vm*p)/(2*pi))*(1 + cosd(alpha_d + lil));
% Vrms3 = (Vm/sqrt(2))*sqrt(((2+p)/4)-((alpha_d*p)/360)+...
%
((E*p*sind(2*alpha_d))/(4*pi))+((F*p*cosd(2*alpha_d))/(4*pi)));
% Vrms_ripple3 = sqrt(Vrms3.^2 - Vavg3.^2);
% Vpp_ripple3 = Vm*sind(alpha_d + lil);
% Vpp_by_Vavg_percent3 = (Vpp_ripple3 ./ Vavg3)*100;
% plot(alpha_d, Vpp_by_Vavg_percent3, 'g-.', 'LineWidth', 2)
```

```
%% 24-pulse

p = 24; % p = pulse count; i.e., p = 6 for 6-pulse controlled rectifier
Vm = 1;
lil = 90-(180/p); % lil = lower integration limit for start of a pulse
uil = 90+(180/p); % uil = upper integration limit for start of a pulse
A = cosd(lil); % constant to make math cleaner/neater
E = cosd(2*lil);
F = sind(2*lil);
alpha_b1_d = (uil-lil)/2; % first boundary angle in degrees
alpha_b2_d = lil; % second boundary angle in degrees
num_points = 1000; % number of points for alpha

% code for alpha < boundary angle 1
alpha_d = linspace(0, alpha_b1_d, num_points); % range of alpha in
degrees
Vavg1 = (A*Vm*p*cosd(alpha_d))/pi;
Vrms1 = (Vm/sqrt(2))*sqrt(1 + ((F*p*cosd(2*alpha_d))/(2*pi)));
Vrms_ripple1 = sqrt(Vrms1.^2 - Vavg1.^2);
Vpp_ripple1 = Vm*(1-sind(alpha_d + uil));
Vpp_by_Vavg_percent1 = (Vpp_ripple1 ./ Vavg1)*100;
plot(alpha_d, Vpp_by_Vavg_percent1, 'k', 'LineWidth', 2)

% code for boundary angle 1 < alpha < boundary angle 2
alpha_d = linspace(alpha_b1_d, alpha_b2_d, num_points); % range of
alpha in degrees
Vavg2 = (A*Vm*p*cosd(alpha_d))/pi;
Vrms2 = (Vm/sqrt(2))*sqrt(1 + ((F*p*cosd(2*alpha_d))/(2*pi)));
Vrms_ripple2 = sqrt(Vrms2.^2 - Vavg2.^2);
Vpp_ripple2 = Vm*(sind(alpha_d + lil) - sind(alpha_d + uil));
Vpp_by_Vavg_percent2 = (Vpp_ripple2 ./ Vavg2)*100;
plot(alpha_d, Vpp_by_Vavg_percent2, 'k--', 'LineWidth', 2)

% % code for alpha > boundary angle 2
% alpha_d = linspace(alpha_b2_d, uil, num_points); % range of alpha in
degrees
% Vavg3 = ((Vm*p)/(2*pi))*(1 + cosd(alpha_d + lil));
% Vrms3 = (Vm/sqrt(2))*sqrt(((2+p)/4)-((alpha_d*p)/360)+...
%
((E*p*sind(2*alpha_d))/(4*pi))+((F*p*cosd(2*alpha_d))/(4*pi)));
% Vrms_ripple3 = sqrt(Vrms3.^2 - Vavg3.^2);
% Vpp_ripple3 = Vm*sind(alpha_d + lil);
% Vpp_by_Vavg_percent3 = (Vpp_ripple3 ./ Vavg3)*100;
% plot(alpha_d, Vpp_by_Vavg_percent3, 'k-.', 'LineWidth', 2)

%% 96-pulse

p = 96; % p = pulse count; i.e., p = 6 for 6-pulse controlled rectifier
Vm = 1;
lil = 90-(180/p); % lil = lower integration limit for start of a pulse
uil = 90+(180/p); % uil = upper integration limit for start of a pulse
A = cosd(lil); % constant to make math cleaner/neater
E = cosd(2*lil);
```

```
F = sind(2*lil);
alpha_b1_d = (uil-lil)/2; % first boundary angle in degrees
alpha_b2_d = lil; % second boundary angle in degrees
num_points = 1000; % number of points for alpha

% code for alpha < boundary angle 1
alpha_d = linspace(0, alpha_b1_d, num_points); % range of alpha in
degrees
Vavg1 = (A*Vm*p*cosd(alpha_d))/pi;
Vrms1 = (Vm/sqrt(2))*sqrt(1 + ((F*p*cosd(2*alpha_d))/(2*pi)));
Vrms_ripple1 = sqrt(Vrms1.^2 - Vavg1.^2);
Vpp_ripple1 = Vm*(1-sind(alpha_d + uil));
Vpp_by_Vavg_percent1 = (Vpp_ripple1 ./ Vavg1)*100;
plot(alpha_d, Vpp_by_Vavg_percent1, 'b', 'LineWidth', 2)

% code for boundary angle 1 < alpha < boundary angle 2
alpha_d = linspace(alpha_b1_d, alpha_b2_d, num_points); % range of
alpha in degrees
Vavg2 = (A*Vm*p*cosd(alpha_d))/pi;
Vrms2 = (Vm/sqrt(2))*sqrt(1 + ((F*p*cosd(2*alpha_d))/(2*pi)));
Vrms_ripple2 = sqrt(Vrms2.^2 - Vavg2.^2);
Vpp_ripple2 = Vm*(sind(alpha_d + lil) - sind(alpha_d + uil));
Vpp_by_Vavg_percent2 = (Vpp_ripple2 ./ Vavg2)*100;
plot(alpha_d, Vpp_by_Vavg_percent2, 'b--', 'LineWidth', 2)

% % code for alpha > boundary angle 2
% alpha_d = linspace(alpha_b2_d, uil, num_points); % range of alpha in
degrees
% Vavg3 = ((Vm*p)/(2*pi))*(1 + cosd(alpha_d + lil));
% Vrms3 = (Vm/sqrt(2))*sqrt(((2+p)/4)-((alpha_d*p)/360)+...
%
((E*p*sind(2*alpha_d))/(4*pi))+((F*p*cosd(2*alpha_d))/(4*pi)));
% Vrms_ripple3 = sqrt(Vrms3.^2 - Vavg3.^2);
% Vpp_ripple3 = Vm*sind(alpha_d + lil);
% Vpp_by_Vavg_percent3 = (Vpp_ripple3 ./ Vavg3)*100;
% plot(alpha_d, Vpp_by_Vavg_percent3, 'b-.', 'LineWidth', 2)

%% Plot Formatting

grid on
axis([0 30 0 60])
%title('%V_p_p_/_a_v_g % vs. \alpha for an n-Pulse Controlled Rectifier
with a Purely Resistive Load')
xlabel('\alpha (degrees)')
ylabel('%V_p_p_/_a_v_g (%)')
legend('6-pulse, \alpha \leq 30^\circ',...
       '12-pulse, \alpha \leq  15^\circ', '12-pulse, 15^\circ \leq
\alpha \leq 75^\circ',...
       '18-pulse, \alpha \leq  7.5^\circ', '18-pulse, 7.5^\circ \leq
\alpha \leq 80^\circ',...
       '24-pulse, \alpha \leq 3.75^\circ', '24-pulse, 3.75^\circ \leq
\alpha \leq 82.5^\circ',...
       '96-pulse, \alpha \leq 1.875^\circ', '96-pulse, 1.875^\circ \leq
\alpha \leq 88.125^\circ',...
       'location', 'Northwest')
```

```
% full legend below
% legend('6-pulse, \alpha \leq 30^\circ', '6-pulse, 30^\circ \leq
\alpha \leq 60^\circ', '6-pulse, \alpha \geq 60^\circ',...
%        '12-pulse, \alpha \leq  15^\circ', '12-pulse, 15^\circ \leq
\alpha \leq 75^\circ', '12-pulse, \alpha \geq 75^\circ',...
%        '18-pulse, \alpha \leq  7.5^\circ', '18-pulse, 7.5^\circ \leq
\alpha \leq 80^\circ', '18-pulse, \alpha \geq 80^\circ',...
%        '24-pulse, \alpha \leq 3.75^\circ', '24-pulse, 3.75^\circ \leq
\alpha \leq 82.5^\circ', '24-pulse, \alpha \geq 82.5^\circ',...
%        '96-pulse, \alpha \leq 1.875^\circ', '96-pulse, 1.875^\circ
\leq \alpha \leq 88.125^\circ', '96-pulse, \alpha \geq
88.125^\circ',...
%        'location', 'Northwest')
hold off
```

## G. VOLTAGE RIPPLE CALCULATIONS AND PLOT FOR A CONTROLLED 6-PULSE RECTIFIER WITH A TWO-POLE *LC* OUTPUT FILTER

```
clear
clc

hold on

%% initial constants

alpha_u = 30; % upper limit on firing angle alpha
num_points = 10000; % number of points for alpha
Vm = (100/sqrt(2))*sqrt(2);

L0 = 25e-3; % inductance of load inductor
C0 = 50e-6; % capacitance of load capacitor
R0 = 10; % resistance of load resistor

LL = L0-(.5*L0);
LH = L0+(.5*L0);
CL = C0-(.5*C0);
CH = C0+(.5*C0);

%% 6p_L0_C0

p = 6; % p = pulse count; i.e., p = 6 for 6-pulse controlled rectifier
L = L0; % inductance of load inductor
C = C0; % capacitance of load capacitor
R = R0; % resistance of load resistor
lil = 90-(180/p); % lil = lower integration limit for start of a pulse
uil = 90+(180/p); % uil = upper integration limit for start of a pulse
A = cosd(lil); % constant to make math cleaner/neater
F = sind(2*lil);

Z_C = 1 / (j*120*p*pi*C);
Z_L = j*120*p*pi*L;
Z_R_p_C = (Z_C * R)/(Z_C + R);
```

```
Ztot = Z_L + Z_R_p_C;
mag_Ztot = abs(Ztot);

alpha_d = linspace(0, alpha_u, num_points); % range of alpha in degrees
Vavg = (A*Vm*p*cosd(alpha_d))/pi;
Vrms = (Vm/sqrt(2))*sqrt(1 + ((F*p*cosd(2*alpha_d))/(2*pi)));
Vrms_ripple = sqrt(Vrms.^2 - Vavg.^2);
Vac = Vrms_ripple;
mag_Iac = Vac / mag_Ztot;
VCrms = mag_Iac * abs(Z_C);

Vpp_ripple = VCrms * 2 * sqrt(2);
Vpp_by_Vavg_percent = (Vpp_ripple ./ Vavg)*100;
plot(alpha_d, Vpp_by_Vavg_percent, 'k', 'LineWidth', 2)

%% 6p_LL_C0

p = 6; % p = pulse count; i.e., p = 6 for 6-pulse controlled rectifier
L = LL; % inductance of load inductor
C = C0; % capacitance of load capacitor
R = R0; % resistance of load resistor
lil = 90-(180/p); % lil = lower integration limit for start of a pulse
uil = 90+(180/p); % uil = upper integration limit for start of a pulse
A = cosd(lil); % constant to make math cleaner/neater
F = sind(2*lil);

Z_C = 1 / (j*120*p*pi*C);
Z_L = j*120*p*pi*L;
Z_R_p_C = (Z_C * R)/(Z_C + R);
Ztot = Z_L + Z_R_p_C;
mag_Ztot = abs(Ztot);

alpha_d = linspace(0, alpha_u, num_points); % range of alpha in degrees
Vavg = (A*Vm*p*cosd(alpha_d))/pi;
Vrms = (Vm/sqrt(2))*sqrt(1 + ((F*p*cosd(2*alpha_d))/(2*pi)));
Vrms_ripple = sqrt(Vrms.^2 - Vavg.^2);
Vac = Vrms_ripple;
mag_Iac = Vac / mag_Ztot;
VCrms = mag_Iac * abs(Z_C);

Vpp_ripple = VCrms * 2 * sqrt(2);
Vpp_by_Vavg_percent = (Vpp_ripple ./ Vavg)*100;
plot(alpha_d, Vpp_by_Vavg_percent, 'r', 'LineWidth', 2)

%% 6p_LH_C0

p = 6; % p = pulse count; i.e., p = 6 for 6-pulse controlled rectifier
L = LH; % inductance of load inductor
C = C0; % capacitance of load capacitor
R = R0; % resistance of load resistor
lil = 90-(180/p); % lil = lower integration limit for start of a pulse
uil = 90+(180/p); % uil = upper integration limit for start of a pulse
A = cosd(lil); % constant to make math cleaner/neater
F = sind(2*lil);
```

```
Z_C = 1 / (j*120*p*pi*C);
Z_L = j*120*p*pi*L;
Z_R_p_C = (Z_C * R)/(Z_C + R);
Ztot = Z_L + Z_R_p_C;
mag_Ztot = abs(Ztot);

alpha_d = linspace(0, alpha_u, num_points); % range of alpha in degrees
Vavg = (A*Vm*p*cosd(alpha_d))/pi;
Vrms = (Vm/sqrt(2))*sqrt(1 + ((F*p*cosd(2*alpha_d))/(2*pi)));
Vrms_ripple = sqrt(Vrms.^2 - Vavg.^2);
Vac = Vrms_ripple;
mag_Iac = Vac / mag_Ztot;
VCrms = mag_Iac * abs(Z_C);

Vpp_ripple = VCrms * 2 * sqrt(2);
Vpp_by_Vavg_percent = (Vpp_ripple ./ Vavg)*100;
plot(alpha_d, Vpp_by_Vavg_percent, 'b', 'LineWidth', 2)

%% 6p_L0_CL

p = 6; % p = pulse count; i.e., p = 6 for 6-pulse controlled rectifier
L = L0; % inductance of load inductor
C = CL; % capacitance of load capacitor
R = R0; % resistance of load resistor
lil = 90-(180/p); % lil = lower integration limit for start of a pulse
uil = 90+(180/p); % uil = upper integration limit for start of a pulse
A = cosd(lil); % constant to make math cleaner/neater
F = sind(2*lil);

Z_C = 1 / (j*120*p*pi*C);
Z_L = j*120*p*pi*L;
Z_R_p_C = (Z_C * R)/(Z_C + R);
Ztot = Z_L + Z_R_p_C;
mag_Ztot = abs(Ztot);

alpha_d = linspace(0, alpha_u, num_points); % range of alpha in degrees
Vavg = (A*Vm*p*cosd(alpha_d))/pi;
Vrms = (Vm/sqrt(2))*sqrt(1 + ((F*p*cosd(2*alpha_d))/(2*pi)));
Vrms_ripple = sqrt(Vrms.^2 - Vavg.^2);
Vac = Vrms_ripple;
mag_Iac = Vac / mag_Ztot;
VCrms = mag_Iac * abs(Z_C);

Vpp_ripple = VCrms * 2 * sqrt(2);
Vpp_by_Vavg_percent = (Vpp_ripple ./ Vavg)*100;
plot(alpha_d, Vpp_by_Vavg_percent, 'k--', 'LineWidth', 2)

%% 6p_L0_CH

p = 6; % p = pulse count; i.e., p = 6 for 6-pulse controlled rectifier
L = L0; % inductance of load inductor
C = CH; % capacitance of load capacitor
R = R0; % resistance of load resistor
```

```
lil = 90-(180/p); % lil = lower integration limit for start of a pulse
uil = 90+(180/p); % uil = upper integration limit for start of a pulse
A = cosd(lil); % constant to make math cleaner/neater
F = sind(2*lil);

Z_C = 1 / (j*120*p*pi*C);
Z_L = j*120*p*pi*L;
Z_R_p_C = (Z_C * R)/(Z_C + R);
Ztot = Z_L + Z_R_p_C;
mag_Ztot = abs(Ztot);

alpha_d = linspace(0, alpha_u, num_points); % range of alpha in degrees
Vavg = (A*Vm*p*cosd(alpha_d))/pi;
Vrms = (Vm/sqrt(2))*sqrt(1 + ((F*p*cosd(2*alpha_d))/(2*pi)));
Vrms_ripple = sqrt(Vrms.^2 - Vavg.^2);
Vac = Vrms_ripple;
mag_Iac = Vac / mag_Ztot;
VCrms = mag_Iac * abs(Z_C);

Vpp_ripple = VCrms * 2 * sqrt(2);
Vpp_by_Vavg_percent = (Vpp_ripple ./ Vavg)*100;
plot(alpha_d, Vpp_by_Vavg_percent, 'm', 'LineWidth', 2)

%% Plot Formatting

grid on
axis([0 30 0 20])
%title('Vpp-ripple/Vavg % vs. \alpha for a 6-Pulse Controlled Rectifier
with a Two-Pole LC Output Filter')
xlabel('\alpha (degrees)')
ylabel('%V_p_p_/_V_a_v_g (%)')
legend('L_0 C_0',...
       'L_L C_0',...
       'L_H C_0',...
       'L_0 C_L',...
       'L_0 C_H',...
       'location', 'Northwest')
hold off
```

## H. VOLTAGE RIPPLE CALCULATIONS AND PLOT FOR A CONTROLLED 6-, 12-, 18-, 24-, AND 96-PULSE RECTIFIER WITH A TWO-POLE *LC* OUTPUT FILTER

```
clear
clc

hold on

%% initial constants

alpha_u = 30; % upper limit on firing angle alpha
num_points = 10000; % number of points for alpha
Vm = (100/sqrt(2))*sqrt(2);
```

```
L0 = 25e-3; % inductance of load inductor
C0 = 50e-6; % capacitance of load capacitor
R0 = 10; % resistance of load resistor

%% 6p_L0_C0

p = 6; % p = pulse count; i.e., p = 6 for 6-pulse controlled rectifier
L = L0; % inductance of load inductor
C = C0; % capacitance of load capacitor
R = R0; % resistance of load resistor
lil = 90-(180/p); % lil = lower integration limit for start of a pulse
uil = 90+(180/p); % uil = upper integration limit for start of a pulse
A = cosd(lil); % constant to make math cleaner/neater
F = sind(2*lil);

Z_C = 1 / (j*120*p*pi*C);
Z_L = j*120*p*pi*L;
Z_R_p_C = (Z_C * R)/(Z_C + R);
Ztot = Z_L + Z_R_p_C;
mag_Ztot = abs(Ztot);

alpha_d = linspace(0, alpha_u, num_points); % range of alpha in degrees
Vavg = (A*Vm*p*cosd(alpha_d))/pi;
Vrms = (Vm/sqrt(2))*sqrt(1 + ((F*p*cosd(2*alpha_d))/(2*pi)));
Vrms_ripple = sqrt(Vrms.^2 - Vavg.^2);
Vac = Vrms_ripple;
mag_Iac = Vac / mag_Ztot;
VCrms = mag_Iac * abs(Z_C);

Vpp_ripple = VCrms * 2 * sqrt(2);
Vpp_by_Vavg_percent = (Vpp_ripple ./ Vavg)*100;
plot(alpha_d, Vpp_by_Vavg_percent, 'r', 'LineWidth', 2)

%% 12p_L0_C0

p = 12; % p = pulse count; i.e., p = 6 for 6-pulse controlled rectifier
L = L0; % inductance of load inductor
C = C0; % capacitance of load capacitor
R = R0; % resistance of load resistor
lil = 90-(180/p); % lil = lower integration limit for start of a pulse
uil = 90+(180/p); % uil = upper integration limit for start of a pulse
A = cosd(lil); % constant to make math cleaner/neater
F = sind(2*lil);

Z_C = 1 / (j*120*p*pi*C);
Z_L = j*120*p*pi*L;
Z_R_p_C = (Z_C * R)/(Z_C + R);
Ztot = Z_L + Z_R_p_C;
mag_Ztot = abs(Ztot);

alpha_d = linspace(0, alpha_u, num_points); % range of alpha in degrees
Vavg = (A*Vm*p*cosd(alpha_d))/pi;
Vrms = (Vm/sqrt(2))*sqrt(1 + ((F*p*cosd(2*alpha_d))/(2*pi)));
```

```
Vrms_ripple = sqrt(Vrms.^2 - Vavg.^2);
Vac = Vrms_ripple;
mag_Iac = Vac / mag_Ztot;
VCrms = mag_Iac * abs(Z_C);

Vpp_ripple = VCrms * 2 * sqrt(2);
Vpp_by_Vavg_percent = (Vpp_ripple ./ Vavg)*100;
plot(alpha_d, Vpp_by_Vavg_percent, 'm', 'LineWidth', 2)

%% 18p_L0_C0

p = 18; % p = pulse count; i.e., p = 6 for 6-pulse controlled rectifier
L = L0; % inductance of load inductor
C = C0; % capacitance of load capacitor
R = R0; % resistance of load resistor
lil = 90-(180/p); % lil = lower integration limit for start of a pulse
uil = 90+(180/p); % uil = upper integration limit for start of a pulse
A = cosd(lil); % constant to make math cleaner/neater
F = sind(2*lil);

Z_C = 1 / (j*120*p*pi*C);
Z_L = j*120*p*pi*L;
Z_R_p_C = (Z_C * R)/(Z_C + R);
Ztot = Z_L + Z_R_p_C;
mag_Ztot = abs(Ztot);

alpha_d = linspace(0, alpha_u, num_points); % range of alpha in degrees
Vavg = (A*Vm*p*cosd(alpha_d))/pi;
Vrms = (Vm/sqrt(2))*sqrt(1 + ((F*p*cosd(2*alpha_d))/(2*pi)));
Vrms_ripple = sqrt(Vrms.^2 - Vavg.^2);
Vac = Vrms_ripple;
mag_Iac = Vac / mag_Ztot;
VCrms = mag_Iac * abs(Z_C);

Vpp_ripple = VCrms * 2 * sqrt(2);
Vpp_by_Vavg_percent = (Vpp_ripple ./ Vavg)*100;
plot(alpha_d, Vpp_by_Vavg_percent, 'g', 'LineWidth', 2)

%% 24p_L0_C0

p = 24; % p = pulse count; i.e., p = 6 for 6-pulse controlled rectifier
L = L0; % inductance of load inductor
C = C0; % capacitance of load capacitor
R = R0; % resistance of load resistor
lil = 90-(180/p); % lil = lower integration limit for start of a pulse
uil = 90+(180/p); % uil = upper integration limit for start of a pulse
A = cosd(lil); % constant to make math cleaner/neater
F = sind(2*lil);

Z_C = 1 / (j*120*p*pi*C);
Z_L = j*120*p*pi*L;
Z_R_p_C = (Z_C * R)/(Z_C + R);
Ztot = Z_L + Z_R_p_C;
mag_Ztot = abs(Ztot);
```

```
alpha_d = linspace(0, alpha_u, num_points); % range of alpha in degrees
Vavg = (A*Vm*p*cosd(alpha_d))/pi;
Vrms = (Vm/sqrt(2))*sqrt(1 + ((F*p*cosd(2*alpha_d))/(2*pi)));
Vrms_ripple = sqrt(Vrms.^2 - Vavg.^2);
Vac = Vrms_ripple;
mag_Iac = Vac / mag_Ztot;
VCrms = mag_Iac * abs(Z_C);

Vpp_ripple = VCrms * 2 * sqrt(2);
Vpp_by_Vavg_percent = (Vpp_ripple ./ Vavg)*100;
plot(alpha_d, Vpp_by_Vavg_percent, 'k', 'LineWidth', 2)

%% 96p_L0_C0

p = 96; % p = pulse count; i.e., p = 6 for 6-pulse controlled rectifier
L = L0; % inductance of load inductor
C = C0; % capacitance of load capacitor
R = R0; % resistance of load resistor
lil = 90-(180/p); % lil = lower integration limit for start of a pulse
uil = 90+(180/p); % uil = upper integration limit for start of a pulse
A = cosd(lil); % constant to make math cleaner/neater
F = sind(2*lil);

Z_C = 1 / (j*120*p*pi*C);
Z_L = j*120*p*pi*L;
Z_R_p_C = (Z_C * R)/(Z_C + R);
Ztot = Z_L + Z_R_p_C;
mag_Ztot = abs(Ztot);

alpha_d = linspace(0, alpha_u, num_points); % range of alpha in degrees
Vavg = (A*Vm*p*cosd(alpha_d))/pi;
Vrms = (Vm/sqrt(2))*sqrt(1 + ((F*p*cosd(2*alpha_d))/(2*pi)));
Vrms_ripple = sqrt(Vrms.^2 - Vavg.^2);
Vac = Vrms_ripple;
mag_Iac = Vac / mag_Ztot;
VCrms = mag_Iac * abs(Z_C);

Vpp_ripple = VCrms * 2 * sqrt(2);
Vpp_by_Vavg_percent = (Vpp_ripple ./ Vavg)*100;
plot(alpha_d, Vpp_by_Vavg_percent, 'b', 'LineWidth', 2)

%% Plot Formatting

grid on
axis([0 30 0 9])
%title('Vpp-ripple/Vavg % vs. \alpha for a 6-Pulse Controlled Rectifier
with a Two-Pole LC Output Filter')
xlabel('\alpha (degrees)')
ylabel('%V_p_p_/_V_a_v_g (%)')
legend('6-pulse',...
       '12-pulse',...
       '18-pulse',...
       '24-pulse',...
```

```
        ‘96-pulse’,...
        ‘location’, ‘Northwest’)
hold off
```

# LIST OF REFERENCES


[1] R. W. Ashton *et al.*, “Common commercial-off-the-shelf high power electronic modules for naval applications,” in *American Society of Naval Engineers Reconfiguration and Survivability Symp.*, Atlantic Beach, FL, 2005.

[2] D. C. Ku, “Multi-pulse converters and passive filtering to improve power harmonics in an integrated power system,” M.S. thesis, Dept. Elec. Eng., USNA, Annapolis, MD, 2007.

[3] M. J. Fisher, “Phase-controlled rectifiers,” in *Power Electronics*. Boston: PWS-Kent Publishing Co., ch. 5, pp. 143–255, 1991.

[4] R. W. Ashton, Notes for EC3150 (Solid State Power Conversion), Naval Postgraduate School, unpublished, 2012.

[5] A.N. Arvindan, “24-pulse rectifier topology with 3-phase to four 3-phase transformation by novel interconnection of conventional 3-phase and 1-phase transformers,” in *International Symposium on Parameterized and Exact Computation*, Chennai, India, pp. 973–979, 2010.

[6] F.J. Chivite-Zabalza *et al.*, “Analysis and practical evaluation of an 18-pulse rectifier for aerospace applications,” Goodrich Corp., Birmingham, UK, 2004.

[7] R. Abdollahi and A. Jalilian, “Application of pulse doubling in delta/polygon-connected transformer-based 36-pulse AC-DC converter for power quality improvement,” in *Power Electronics, Drive Systems & Technologies Conf.*, Tehran, Iran, pp. 428–434, 2012.

[8] R. Abdollahi and A. Jalilian, “Application of pulse doubling in star-connected autotransformer based 12-pulse AC-DC converter for power quality improvement,” *Int. J. Elect. Electron. Eng.*, vol 5, no. 4, pp. 280–288, 2011.

[9] M. Peterson and B. Singh, “Multipulse controlled AC–DC converters for harmonic mitigation and reactive power management,” *Institution Eng. Technology Power Electron.*, vol. 2, no. 4, pp. 443–455, 2009.

[10] K. Rajashekara *et al*., “Power electronic devices,” in *The Power Electronics Handbook*, T. L. Skvarenina, Ed. Boca Raton: CRC Press LLC, pp. 18–116, 2002.

[11] R. Visintini, “Rectifiers,” in *Proc. Power Converters for Particle Accelerators Course*, Warrington, UK, pp. 133–183, 2004.

[12] Associated Power Technologies, “Total harmonic distortion and effects in electrical power systems,” Diamond Bar, CA, n.d.

[13] *Guidance Notes on Control of Harmonics in Electrical Power Systems*, American Bureau of Shipping, Houston, TX, 2006.

[14] A. H. Bhat and P. Agarwal, “Improved power quality AC/DC converters,” in *Power Quality*, Rijeka, Croatia: InTech, ch. 14, pp. 271–310, 2011.

[15] T. Maritz, “Straight talk about PWM AC drive harmonic problems and solutions,” Rockwell Automation, Mequon, WI, 2009.

[16] N. Mohan *et al*., *Power Electronics: Converters, Applications, and Design*, 3rd ed. Hoboken: John Wiley & Sons, Inc., 2003.

[17] R. Del Vecchio, “Phase-shifting and zig-zag transformers,” in *Transformer Design Principles With Applications to Core-Form Power Transformers*, 2nd ed. Boca Raton: CRC Press LLC, ch. 7, pp. 155–193, 2010.

# INITIAL DISTRIBUTION LIST

1. Defense Technical Information Center
   Ft. Belvoir, Virginia

2. Dudley Knox Library
   Naval Postgraduate School
   Monterey, California

3. Dr. Clark Robertson
   Naval Postgraduate School
   Monterey, California

4. Dr. Robert Ashton
   Naval Postgraduate School
   Monterey, California

5. Mr. Andrew Parker
   Naval Postgraduate School
   Monterey, California

6. LCDR Kurt Young, USN
   Strategic Systems Programs
   Washington, DC